UNIVERSITY' OF NAPLES "FEDERICO II"
PhD program
Molecular Pathology and Physiopathology

School of Molecular Medicine

XXVII Cycle

Functional organization of chemical senses: central neural processing

Tutor
Ch.mo Prof.
Francesco Di Salle

Candidate
Elena Cantone

PhD Coordinator
Ch.mo Prof.
Vittorio Enrico Avvedimento

ACADEMIC YEAR 2014-2015

UNIVERSITY' OF NAPLES "FEDERICO II"
PhD program
Molecular Pathology and Physiopathology

"Functional Organization Of Chemical Senses: Central Neural Processing"

Elena Cantone

INDEX

ABBREVIATIONS

5-HT serotonin
ACC anterior cingulated cortex
ACh acetylcholine
Ado adenosine
AI anterior insula
Amy amygdale
As-Ac aspartame & acesulfame
BOLD blood oxygenation-level–dependent
BTC basal temporal cortex
CBA cortex-based alignment
CgC cingulate cortex
CN cranial nerves
CrC cerebellar cortex
CrV cerebellar vermis
CS chemical sense
EEG electroencephalography
ENaC amiloride-sensitive epithelial Na channel
FBC fronto-basal cortex
fMRI functional magnetic resonance imaging
FO frontal operculum
FO/AI frontal operculum /anterior insula
GI gastrointestinal
GLM General Linear Model
GPCRs G protein-coupled receptors
hPTC human primary taste cortex
IC insula cortex
IFC inferior frontal cortex
M3 muscarinic receptors
MR magnetic resonance
MEG magnetoencephalography
MFG middle frontal gyrus
MTC mesial temporal cortex
NE norepinephrine
NTS nucleus of the solitary tract
OBC occipito-basal cortex
OC opercular cortex
OFC orbitofrontal cortex
OTC occipito-temporal cortex
PET positron emission tomography
PFC dorsolateral prefrontal cortex
PFC prefrontal cortex
PGFC perigenual frontal cortex
PKDL polycystic kidney disease like receptor

PPHG posterior parahyppocampal gyrus
PTC primary taste cortex
SCrC superior cerebellar cortex
SFG superior frontal gyrus
SGFMC subgenual frontomesial cortex
SI primary somatosensory cortex
SII secondary somatosensory cortex
SPECT single photon emission computed tomography
Th thalamus
TMS Transcranial Magnetic Stimulation
TN trigeminal nerve
TO temporo-occipital
TP temporo-parietal
TR repetition time
TRs taste receptors
TRCs taste receptor cells
VAS Visual Analogue Scale
VLPFC ventrolateral prefrontal cortex
VPMN ventroposterior medial nucleus

ABSTRACT

The sense of taste regulates feeding behavior and guides in the selection of food. Humans perceive 5 basic tastes: sweet, umami (savory taste or amino acids), bitter, sour, and salty, although other taste modalities may be added, including CO2.

Taste reception is orchestrated by distinct populations of selectively tuned cells clustered to form taste buds in the tongue, mouth, and gastrointestinal tract, which express specific receptors for different gustatory stimuli.

Sweet, umami, and bitter are detected by 2 distinct families of G-protein–coupled receptors. By contrast, sour and salty are sensed by ion channels. The polycystic kidney disease channel has been proposed as the acid-sensing machinery detecting the sour taste. CO2 is also detected by sour-sensing cells; however, the taste of carbonation is separated from sour detection. Thus, CO2 taste machinery does not perceive sour taste despite being detected by the same cells.

Even though different tastes act on different sets of taste cells, there is significant cell–cell communication within taste buds.

Despite a growing literature on the peripheral mechanisms for taste, knowledge of the central neural processing of taste is still largely elusive.

In this study, we investigated the cortical representation of taste-related neural responses, the neural mechanisms underlying the perception of taste and the chemotopic organization of taste modalities in the human primary taste cortex (insula). Furthermore, we studied the interference between perceptual mechanisms of different tastants, and in particular the effect of CO2 on the brain processing of sweet stimuli, analyzing its differential effect on sucrose and artificial sweeteners.

We used an experimental setting with Magnetic Resonance echo planar blood oxygenation-level-dependent experiments, while gustatory stimuli were delivered by computer controlled automatic injectors.

We found a detailed chemotopic representation in the human insula where each taste, including CO2, that could be considered a sixth taste, has its own cortical representation.

Our study demonstrated that the interference between different tastants can act as a powerful modulator of the perceptual processes of taste. The presence of CO2 produced a strong overall decrease in the neural processing of sweetness-related signals, while reducing the neural processing of sucrose more than artificial sweeteners. The analysis of the functional organization of the insular cortex unveiled essential steps allowing the perception of taste and regulating feeding and dietary behaviors.

1. BACKGROUND

1.1 Chemical senses

Chemical senses (CS) are nervous mechanisms dedicated to the perception of chemical stimulations and to generate a response to them. Chemoreceptors are specialized receptors sensitive to chemical substances in solution. From an evolutionary perspective, chemical senses (smell, taste and trigeminal) are probably the oldest of our senses and the first to have evolved (Welge-Luessen and Hummel 2013, Hummel and Welge-Luessen 2006). All cellular life forms, from bacteria to humans, are sensitive to chemical information (olfaction, taste or trigeminal perception), whether it comes from potential food, predators, environment, or other members of the same species (Wyatt 2014).

Our knowledge on the neural processing of the three chemical senses has been considerably lagging behind that of our other senses. Indeed, we are still struggling to understand even the more basic steps of how the chemical senses operate (Hummel and Welge-Luessen 2006). Conversely, visual and auditory systems are relatively well understood.

The last twenty-five years have, however, brought notable and rapid advances in our understanding of the basic cerebral processing of the human chemical senses. This progress has largely been owed to the advances in methods of stimulus delivery and an increased interest in the topic. The invention of the modern olfactometer and gustometer devices allowed the use of advanced electroencephalogram recordings (EEG), of positron emission tomography (PET) and, more recently, of functional magnetic resonance imaging (fMRI) (Lundstrom et al. 2011).

Chemical senses differ considerably with regards to role and function from the from the more evolutionary recent senses, such as vision and hearing. For instance, the most important role of the human sense of smell is to modulate our attention toward hazards (e.g., poison\ous fumes and spoiled food) or items with positive connotations (e.g., nutritious food). This guidance is primarily driven by the hedonic value (i.e., pleasantness or unpleasantness of an odorous item [e.g., food]), which, to a large extent, is determined by the individual′s personal experience.

The relatively strong positive or negative emotions often evoked by smell are also shaped by prior experience, and believed to enhance the appropriate behavioral response. Apart from being an important chemical warning system for safety issues and for regulating food intake, the sense of smell is involved in social communication (Stevenson 2010).

An infinite number of volatile chemical compounds can evoke a smell sensation, and a smell is, in many cases, an integrated sensation caused by a combination of such compounds.

Similarly, the sense of taste guides ingestive and avoidance behaviors. As with smell, hedonic value is an important perceptual dimension of taste, with close ties to motivational behavior. Furthermore, taste qualities provide information about the presence of useful or dangerous substances: carbohydrate energy sources in sweetness, sodium in saltiness, and proteins in umami ("meaty," "brothy") perception; and possible danger from acids and toxins in sour and bitter perception, respectively. While olfaction is known to play a social communication role in humans, it is unknown whether taste in humans plays a similar social role (Grammer et al. 2005).

Taste is commonly confused with flavor, the combined sensory experience of olfaction and gustation. Gustatory signals originate in sensory end organs in the oral cavity—taste buds—and are triggered by water-soluble compounds that contact the apical tips of the epithelial cells of taste buds. By contrast, olfactory signals are generated by neurons in a specialized patch of nasal epithelium and are triggered by volatile compounds. Although the peripheral sensory organs for taste and smell are quite distinct, their signals are integrated in the orbitofrontal and other cortical areas to generate flavors and mediate food recognition (Small and Prescott 2005).

Taste is also commonly confused with somatosensory sensations such as the cool of menthol or the heat of chili peppers. Strictly speaking, gustation is the sensory modality generated when chemicals activate oral taste buds and transmit signals to a specific region of the brainstem (the rostral solitary nucleus). Capsaicin (the active compound in chilies) and menthol principally stimulate ion channels in somatosensory nerve fibers (Chaudhari and Roper 2010). They stimulate important interactions between somatosensory trigeminal (cranial nerve V) nerve fibers in the tongue and taste buds, and thus modulate taste (Chaudhari and Roper 2010).

Additional somatosensory modalities such as texture and visual cues such as color also significantly influence the "taste" of foods (Small and Prescott. 2005).

1.2 The "basic" tastes

Taste guides organisms to identify and consume nutrients and avoid toxins and indigestible materials. For humans, this means recognizing and distinguishing sweet, umami, sour, salty, and bitter—the so-called "basic" tastes. There are likely additional qualities such as fatty, CO2, metallic, and others that might also be considered basic tastes.

Each taste quality is believed to represent different nutritional or physiological requirements or potential dietary hazards. Thus, sweet taste signals the presence of carbohydrates that serve as an energy source. Salty taste governs the intake of Na+ and other salts, essential for maintaining the body's water balance and blood circulation. Umami, the taste of l-glutamate and a few other l-amino acids, reflects a food's protein content. Bitter taste is innately aversive and is thought to guard against consuming poisons, many of which taste bitter to humans. Sour taste signals the presence of dietary acids. Because sour taste is generally aversive, we avoid ingesting excess acids and overloading the mechanisms that maintain acid–base balance for the body. Moreover, spoiled foods often are acidic and are thus avoided. However, people learn to tolerate and even seek out certain bitter- and sour-tasting compounds such as caffeine and citric acid (e.g., in sweet-tart citrus fruits), overcoming innate taste responses.

Variations of taste preference may arise from genetic differences in taste receptors and may have important consequences for food selection, nutrition, and health (Drayna 2005, Shigemura et al. 2009).

In addition to its requisite role in feeding, taste in other species plays a role in detecting and identifying hydrocarbons that serve as a pheromonal social communication signal such as in courting and mating (Bray and Amrein 2003).

1.3 Peripheral taste anatomy and physiology

1.3.1 Gustatory papillae

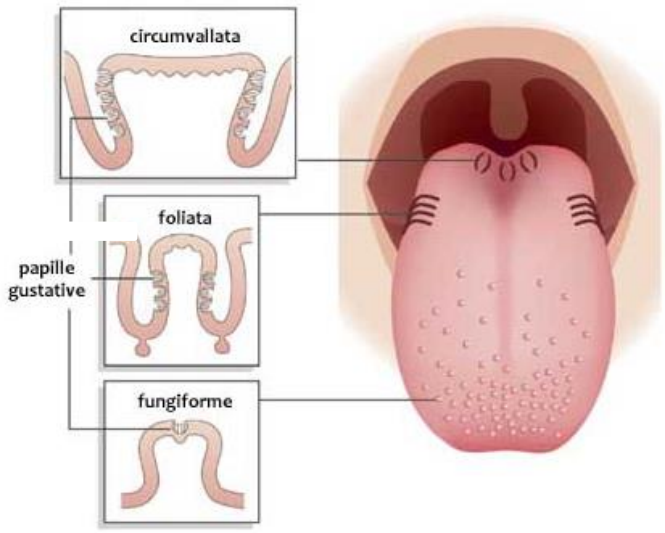

Fig. 1. Gustatory papillae: Most of the taste papillae belong to three types—fungiform, foliate, and vallate—and are located in the tongue (Chandrashekar 2006)

The taste system in mammals includes taste receptor cells (TRCs) organized in multicellular rosette clusters labeled ‘taste buds’ and located within gustatory papillae. Most of the taste papillae belong to three types—fungiform, foliate, and vallate—and are located in the tongue (Fig.1). Although there are subtle regional differences in sensitivity to different compounds over the lingual surface, the oft-quoted concept of a “tongue map” defining distinct zones for sweet, bitter, salty, and sour has largely been discredited (Lindemann1999).

There is also a substantial number of non-lingual taste papillae in the palate, oropharynx, larynx, epiglottis, and the upper esophagus. In humans there are between 2000 and 5000 taste buds distributed on the upper surface of the tongue, palate, and to a lesser extent epiglottis, pharynx, and larynx (Miller 1995). There may be important differences between taste buds in different regions on the tongue and elsewhere, although histologically they appear quite similar.

Taste buds on the anterior tongue surface are embedded in fungiform papilla. These taste buds are innervated by the chorda tympani nerve, a branch of the large facial nerve (N VII). Taste buds on the posterior tongue surface are located in circumvallate papillae. These taste buds are innervated by the glossopharyngeal nerve (N IX) (Fig.2).

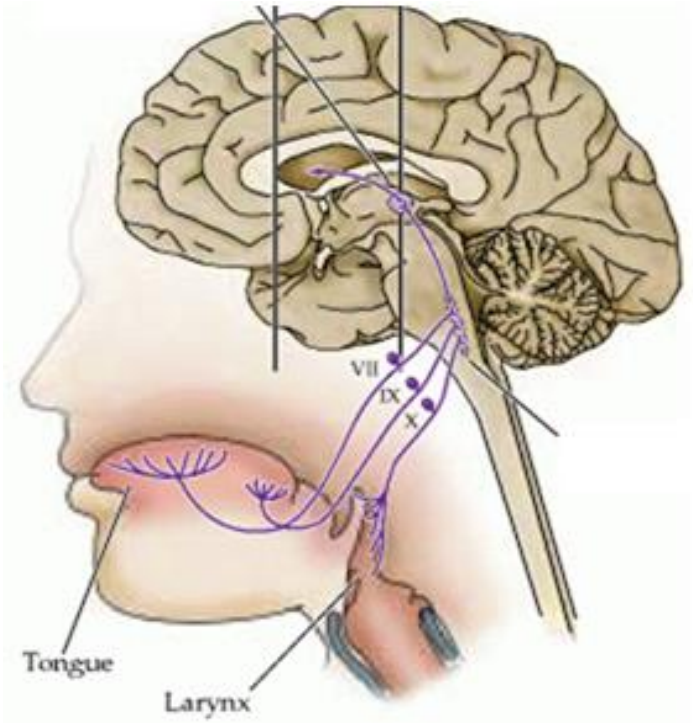

Fig.2. Tongue innervation: *Anterior taste buds are innervated by the chorda tympani nerve, a branch of the large facial nerve (N VII), posterior taste buds are innervated by the glossopharyngeal nerve (N IX), laryngeal taste buds are innervated by the vagus nerve (N X). http://vsuphysio.blogspot.it*

There are also taste buds buried in folds in the lateral sides of the tongue, in the foliate papillae. These taste buds receive innervation from branches of the chorda tympani and glossopharyngeal nerves (Fig.2). Lastly, taste buds in the palate are innervated by the greater superficial petrosal nerve, another branch of the facial nerve (Fig.2). Although taste buds in all regions respond to all five basic tastes, there are differences in their sensitivities to these tastes (Roper 2013). Presumably this reflects differences in the taste cell populations from region to region.

1.3.2 Taste buds

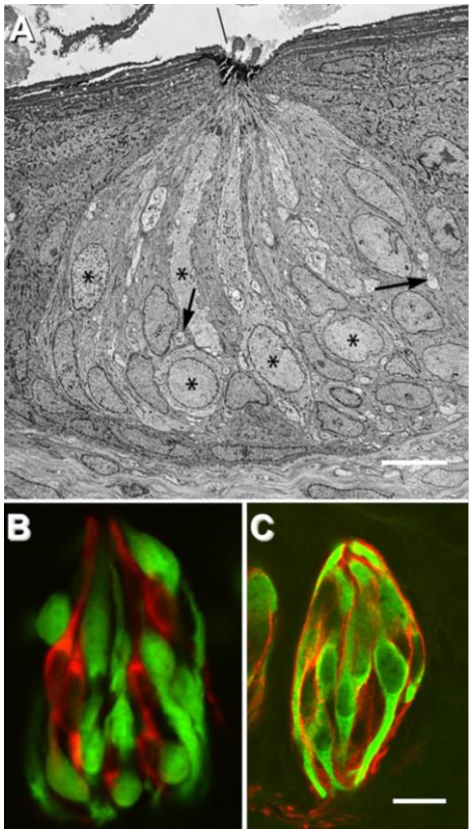

Fig.3.Taste buds: A) nerve profiles (arrows). *Type II cells. B) Type II cells (green). Type III (red). C), Type I (red), Type III (green) (Roper 2013).

Every taste bud is a community of approximately 100 cells. Taste buds are clusters of polarized neuroepithelial cells that form compact, columnar pseudo-stratified "islands" embedded in the surrounding stratified epithelium of the oral cavity (Fig. 3).

Thus, the receptor cells within taste buds are not neural cells. Rather, they are specialized epithelial cells, that share almost all of the same properties as neural cells except that they lack an axon. The elongate cells of taste buds are mature differentiated cells. Their apical tips directly contact the external environment in the oral cavity and thus experience wide fluctuations of tonicity and osmolarity, and the presence of potentially harmful compounds. Hence, taste bud cells, similar to olfactory neurons, comprise a continuously renewing population, quite unlike the sensory receptors for vision and hearing: photoreceptors and hair cells. It is now clear that adult taste buds are derived from local epithelium. At least some precursor cells are common between taste buds and the stratified non-sensory epithelium surrounding them (Okubo et al. 2009). Tight junctions connecting the apical tips of cells are noted in electron micrographs of taste buds from several species (Murray1993). Typical tight

junction components such as claudins and ZO-1 are detected at the apical junctions (Michlig 2007).

Taste buds, like most epithelia, impede the permeation of water and many solutes through their intercellular spaces. Nevertheless, paracellular pathways through taste buds have been demonstrated for certain ionic and nonpolar compounds (Chaudhari and Roper 2010). Indeed, permeation of Na+ into the interstitial spaces within taste buds may contribute to the detection of salty taste (Chaudhari and Roper 2010).

Taste buds cells fall into three major categories, originally defined by their morphological appearances and more recently distinguished by their expression of specific proteins and responses to gustatory stimulation. These cells were termed types I, II, and III, and Basal, a non-polarized, presumably undifferentiated cell, sometimes termed type IV (Chaudhari and Roper 2010).

1.3.3 Taste cells

I. Type I cells (Glial-like): type I cells (Fig.4), the most abundant cells in taste buds, are characterized by extensive lamellar processes that enwrap other taste cells like blankets (Fig. 3: C red), perhaps to further limit the spread of transmitter(s) and prevent local changes in ion concentrations from reaching other regions of the taste bud during taste reception (Chaudhari and Roper 2010). They have electron-dense cytoplasm and elongate, pleomorphic nuclei, and glial-like functions. Type I cells synthesize and deposit a powerful ecto-ATPase on their surface that degrades the transmitter released by other taste cells. Furthermore, they express GLAST, a transporter for glutamate, indicating that they may be involved in glutamate uptake (Lawton et al. 2000) and NTPDase2, a plasma membrane–bound nucleotidase that hydrolyzes extracellular ATP (Bartel et al. 2006). ATP and glutamate serve as neurotransmitters in taste buds (Finger et al. 2005). Thus, type I cells appear to be involved in terminating synaptic transmission and restricting the spread of transmitters, a role performed in the central nervous system by glial cells. Type I cells also express ROMK, a K channel that may be involved in K+ homeostasis within the taste bud (Dvoryanchikov et al. 2009). During prolonged trains of action potentials elicited by intense taste stimulation, type I cells may serve to eliminate K+ that would accumulate in the limited interstitial spaces of the taste bud and lead to diminished excitability of type II and III cells. This is another stereotypic glial function. Patch-clamp studies have suggested that some taste cells, presumably type I, possesses electrophysiological properties, such as inexcitability and high resting K+ conductance, also characteristic of glia (Chaudhari and Roper 2010). Nevertheless, not all type I cells necessarily participate in each of the glial roles described

above. Lastly, type I cells may exhibit ionic currents implicated in salt taste transduction (Vandenbeuch et al. 2008). Despite their being the most abundant cell type in taste buds, the least is known about type I cells.

II. Type II (Receptor) cells (Fig.4): Type II cells feature large ovoid nuclei and electron-lucent cytoplasm (Fig.3: A *, C green). Although they are responsible for detecting sweet, bitter, and umami tastes, each receptor cell responds mainly to a single taste quality. Thus, they are relatively well "tuned" to specific taste stimuli. Furthermore, type II cells do not form conventional synapses and appear to release ATP as a transmitter onto sensory afferent fibers (Fig.3: A arrows) in a non-vesicular fashion through pannexin or connexin hemichannels. At the molecular level, type II cells express G protein-coupled receptors (GPCRs) for sweet, bitter, and umami taste compounds. They also express downstream effectors that couple to the taste GPCRs. Consequently, these cells have been renamed taste receptor cells (Yamamoto and Ishimaru 2013).

III. Type III (Presynaptic) cells (Fig.4): Type III cells have ultrastructural features somewhat intermediate between type I and type II cells. Most importantly, though, differently from type I and II, type III possess synapses (Roper 2013). Accordingly, they have been renamed presynaptic cells. The specific postsynaptic targets at these synapses have not been confidently identified. They may be sensory afferent fibers, but if so, they do not use ATP as a transmitter. Type III cells do not secrete ATP (Roper 2013) but serotonin (5-HT), norepinephrine (NE), and GABA. Consistent with the identification of synapses, type III cells express proteins associated with synaptic transmission, including SNAP 25, voltage-gated Ca2+ channels, biosynthetic enzymes for 5-HT and GABA, and uptake transporters for biogenic amines. When isolated as single cells, presynaptic cells respond to sour stimuli (Roper 2013). In addition to these neuronal properties, presynaptic cells also respond directly to carbonated solutions and are presumably the cells responsible for signaling these sensations (Chandrashekar et al. 2010). Indeed, mice lacking type III cells do not respond to sour taste. However, when studied in intact taste buds, presynaptic cells also are excited by sweet, bitter, and umami stimuli even though they do not possess receptors for those compounds. The explanation is cell–cell communication from receptor to presynaptic cells in situ. ATP secreted by receptor cells during taste activation stimulates presynaptic cells in addition to exciting sensory afferent fibers. As a result, presynaptic cells are indirectly excited by sweet, bitter, and umami compounds and appear to be some form of integrating element in taste bud signaling (Chaudhari and Roper 2010).

IV. Type IV (Basal) cells: This cells are spherical or ovoid cells that do not extend processes into the taste pore and are likely to be undifferentiated or immature taste cells (Chaudhari and Roper 2010). It is not clear whether all basal cells within taste buds represent a common undifferentiated class of cell.

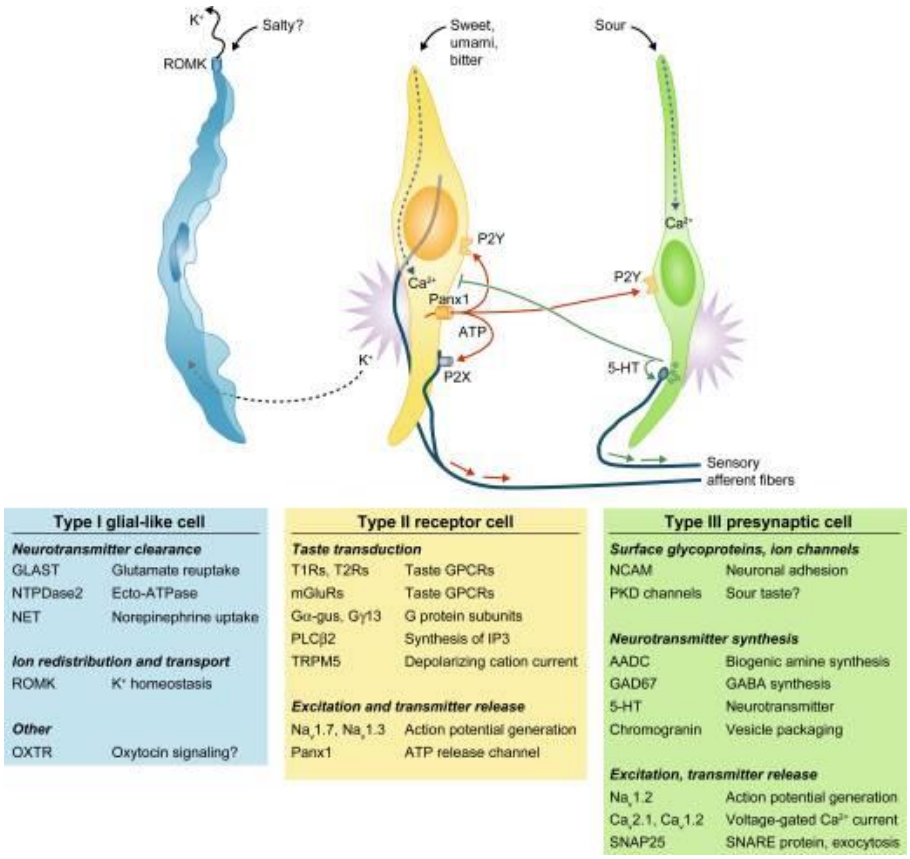

Fig.4.Taste cells: Ultrastructural features, patterns of gene expression, and functions of each of types I, II (receptor), and III (presynaptic) taste cells (Chaudhari and Roper 2010).

To summarize, type I cells appear to be glial-like supporting cells in the taste bud. Receptor, type II, cells are sensory cells for sweet, bitter, or umami tastes, all of which appear to be transduced by G protein coupled taste receptors. These stimuli trigger receptor cells to secrete ATP which in turn excites sensory afferent fibers and adjacent presynaptic taste cells. Presynaptic, type III, taste cells are directly stimulated by sour taste and indirectly by sweet, bitter, and umami taste. Thus, these cells seem to integrate multiple gustatory stimuli in

the taste bud. Presynaptic cells release serotonin, norepinephrine and GABA (Chaudhari and Roper 2010).

1.3.4 Cell-cell communication

When sweet, bitter, or umami tastants excite taste buds, receptor cells secrete ATP, that stimulates taste afferent nerve fibers. At the same time, ATP excites adjacent presynaptic cells and stimulates them to release 5-HT and/or NE (Chaudhari and Roper 2010). ATP secreted during taste stimulates themselves. Thus, ATP, acting as an autocrine transmitter, exerts positive feedback onto receptor cells, increasing its own secretion and presumably counteracting its degradation by ecto-ATPase (Huang et al. 2009) (Fig. 5). ATP is degraded within the taste bud to ADP and these purines boost further ATP release from receptor cells via P2Y1 and P2X2 purinoreceptors. ADP is further degraded to adenosine (Ado) which excites adenosine A2B receptors expressed selectively on sweet-responsive receptor cells (Roper 2013).

The 5-HT released by presynaptic cells also may have multiple targets. 5-HT exerts a negative feedback onto receptor cells. The opposing effects of positive (purinergic autocrine) and negative (serotonergic paracrine) feedback in the taste bud during taste activation combine to shape the signals transmitted from taste buds to the hindbrain. However, details of how these feedback pathways are balanced to shape the eventual sensory output awaits experimentation and many questions remain. One might speculate that 5-HT mediates “lateral inhibition,” suppressing the output of adjacent receptor (e.g., bitter) cells when a particular (e.g., sweet) receptor cell is stimulated (Chaudhari and Roper 2010). Alternatively, the negative feedback loop may participate in sensory by decreasing the afferent signal over time. Other sites of action for 5-HT (and NE) possibly include the nerve fibers that form synapses with presynaptic taste cells.

Presynaptic taste cells besides 5-HT and NE secrete GABA. As well as 5-HT, GABA is an inhibitory paracrine transmitter, acting on postsynaptic $GABA_{A,B}$ receptors on type II cells (Roper 2013). Lastly, receptor cells also release acetylcholine (ACh) which stimulates muscarinic (M3) receptors on type II cells (Roper 2013).

In summary, receptor cells detect and discriminate sweet, bitter, or umami tastants, generate Ca2+ signals, and release ATP transmitter onto afferent nerves. The ATP from different receptor cells converges onto and produces secondary excitation of presynaptic cells, thereby integrating signals representing all three taste qualities (Tomchik et al. 2007). It is not clear that the secondary responses of presynaptic cells to sweet, bitter, and umami stimuli are necessary for identifying or discriminating these taste qualities. Primary signals in presynaptic cells

are only generated by sour tastants, and this is the only quality that is lost when presynaptic cells are ablated (Huang et al. 2006).

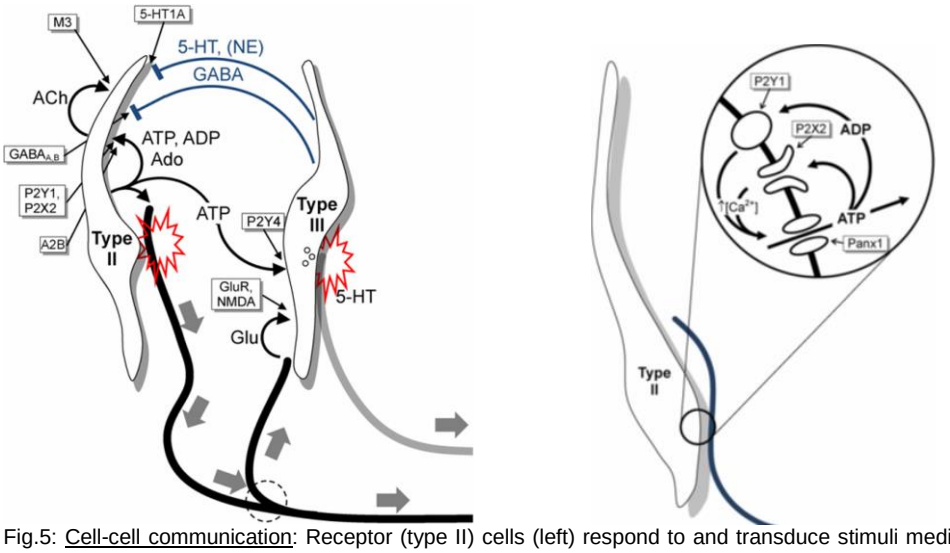

Fig.5: Cell-cell communication: Receptor (type II) cells (left) respond to and transduce stimuli mediated by taste GPCRs (sweet, bitter, or umami) and secrete ATP to excite primary sensory afferent fibers (thick black lines, large solid gray arrows). ATP also excites neighboring presynaptic (type III) cells (right). ATP is degraded within the taste bud to ADP and these purines act as autocrine transmitters to boost further ATP release from receptor cells via P2Y1 and P2X2 receptors. ADP is further degraded to adenosine (Ado) which excites A2B receptors expressed selectively on sweet-responsive Receptor cells. Lastly, Receptor cells also release acetylcholine (ACh) which stimulates muscarinic (M3) receptors on type II cells.
Presynaptic (type III) cells respond directly to acid (sour) taste stimuli and indirectly, via ATP, to sweet, umami, and bitter stimuli. Presynaptic taste cells secrete serotonin (5-HT), norepinenephrine (NE) and GABA. 5-HT and GABA are inhibitory paracrine transmitters, acting on postsynaptic 5-HT1A and receptors on type II cells, as shown. 5-HT is also believed to be the neurotransmitter at the synapses type III cells form with axon terminals (solid gray line). The full identification of these putative serotonergic axon terminals remains to be established (Roper 2013).

1.3.5 Taste Coding

Afferent nerve fibers transmit taste information from taste buds to the brain but how the activation of receptor translates into a neural code that specifies different taste qualities remains still debated. There are two major hypotheses (Fig.6) on how taste information is processed. The first, termed ‘labelled line’, refers to a coding model in which peripheral (or central) neurons that respond the most robustly to a given taste modality carry the totality of the information via segregated pathways. This coding scheme carries a particular taste modality (e.g. sucrose) from the periphery to the higher areas that signals. Intensity increases are indicated by an increase in neuronal activity. The second view asserts that a modality and its quantity (intensity) are encoded by ensembles of broadly tuned neurons. This ‘ensemble code’ is also known as ‘combinatorial’ or ‘across fibre pattern’ (Carleton and Accolla 2010).

In these two models, the specification of any one taste quality is embedded in a complex pattern of activity across various lines. Recent molecular and functional studies in mice have demonstrated that different taste receptor cells define the different taste modalities, and that activation of a single type of taste receptor cells is sufficient to encode taste quality, strongly supporting the labelled-line model.

A third, less-discussed option is a temporal code in which quality would be denoted by a timing pattern of action potentials such as occurs in auditory fibers.

Electrophysiological recordings from single afferent fibers or their parent sensory ganglion cells indicated that some neurons respond strongly to a single taste quality (usually sweet), but also have weak responses to other tastes. In contrast, other afferent neurons are excited by multiple tastes, i.e., are broadly responsive (Breza et al. 2010).

Thus, afferent taste neurons show response profiles similar to both narrowly tuned taste bud receptor cells and to broadly tuned presynaptic cells. The pattern of afferent neuron activity mirrors the heterogeneity of taste bud cellular responses (Breza et al. 2010) and suggests that neural activity encoding taste does not follow a simple dedicated labeled-line logic. Chemosensory researchers agree that labeled taste cells exist but labeled lines remain controversial.

In summary, sweet, bitter, and umami cells all secrete the same neurotransmitter, ATP, onto afferent fibers. Discrete synapses are lacking that might couple receptor cells with sensory afferent fibers to transmit single taste qualities.

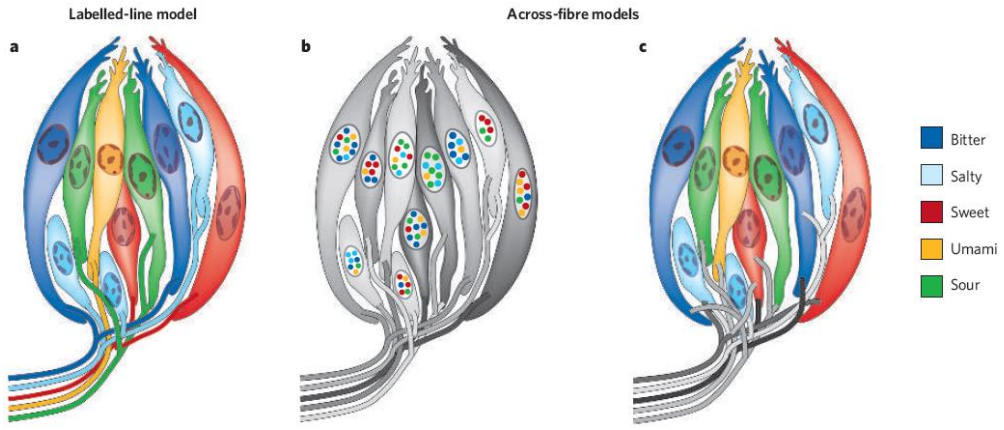

Fig.6. Encoding of taste qualities: There are two opposing models. a, In the labelled-line model, receptor cells are tuned to respond to single taste modalities and are innervated by individually tuned nerve fibres. b, c, In the 'across-fibre pattern' the individual taste cells are tuned to multiple taste qualities, and the same afferent fibre carries information for more than one taste modality (b), or taste cells are still tuned to single taste qualities but the same afferent fibre carries information for more than one taste modality (c) (Chandrashekar 2006).

Although some taste cells and sensory afferent neurons are tightly tuned, others are responsive to multiple taste qualities. Thus, it remains an open question exactly how information gathered by well-differentiated receptor cells in taste buds is “coded” for the eventual perception of distinct taste qualities.

1.3.6 Taste receptors

Sweet, umami, and bitter tastes are detected by 2 distinct families of G-protein–coupled receptors (GPCRs) localized on type II cells (Fig.7). The T1R taste receptor family is composed of 3 distinct members that heterodimerize to sense sweetness (T1R2 and T1R3) and amino acids (T1R1 and T1R3). The T2R taste receptor families include numerous divergent GPCRs that act as narrowly or broadly tuned bitter sensors to detect a myriad of bitter substances. By contrast, sour and salty tastes are sensed by ion channels (Sternini 2013).

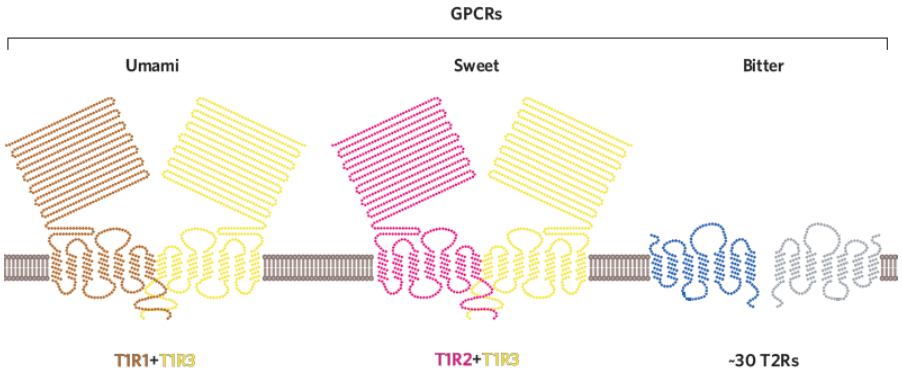

Fig.7. Taste receptors for umami, sweet, bitter and sour tastes: G-protein–coupled receptors (GPCRs) localized on type II cells. The T1R taste receptor family is composed of 3 distinct members that heterodimerize to sense sweetness (T1R2 and T1R3) and amino acids (T1R1 and T1R3); the T2R taste receptor families sense bitter (Chandrashekar 2006).

The T1Rs are dimeric class III GPCRs, with large N-terminal extracellular domains. This domain forms a venus flytrap structure as in other family members. T1Rs also possess a multitude of additional ligand-binding sites on the exterior faces of the flytrap, in the linker, and perhaps even in the plane of the membrane (Temussi 2009). In contrast, T2Rs resemble class I GPCRs with binding sites in the transmembrane helices, in keeping with the non-polar nature of many bitter ligands.

Type II cells expressing the heterodimer T1R2+T1R3 respond to sugars, synthetic sweeteners, and sweet-tasting proteins such as monellin and brazzein. Although the persistence of sensitivity to some

sugars in mice lacking T1R3 suggests that additional receptors for sweet may exist, candidate receptors have yet to be identified (Chaudhari and Roper 2010). The heterodimeric GPCR, T1R1+T1R3, responds to umami stimuli, particularly the combination of l-glutamate and GMP/IMP, compounds that accumulate in many foods after hydrolysis of proteins. Nevertheless, robust physiological responses and behavioral preference for umami tastants persist in mice in which T1R3 is knocked out, suggesting that additional taste receptors may contribute to umami detection (Chaudhari and Roper 2010).

Functional responses to various umami tastants occur in distinct subsets of cells within taste buds and neural responses show similarly heterogeneous patterns, observations that further suggest that umami taste is complex, and likely mediated through multiple types of taste receptors.

In summary, although the T1R1+T1R3 dimer clearly acts as an umami receptor, additional GPCRs may play complementary roles. Candidates for additional umami receptors include a taste-specific variant or other isoforms of G protein–coupled glutamate receptors expressed in taste buds (Chaudhari and Roper 2010).

Type II cells that express members of the T2R family of GPCRs sense bitter compounds. In different mammals, 20–35 separate genes encode members of the T2R family. These taste receptors exhibit heterogeneous molecular receptive ranges: some are narrowly tuned to 2–4 bitter-tasting compounds, whereas others are promiscuously activated by numerous ligands (Chaudhari and Roper 2010).

Bitter-sensing taste cells are known to functionally discriminate among bitter compounds. This pattern of T2R expression, along with polymorphisms across the gene family, is thought to allow humans and animals to detect the enormous range of potentially toxic bitter compounds found in nature. Detailed analyses on human taste buds point out that different bitter responsive taste cells express subsets of 4–11 of the T2Rs in partially overlapping fashion (Chaudhari and Roper 2010). This observation is important insofar as it provides a molecular basis for discriminating between different bitter compounds.

The salty taste is likely to be mediated by the epithelial sodium channel, ENaC (Fig.8), expressed by type I cells by directly permeating Na+ through apical ion channels and depolarizing taste cells (Chaudhari and Roper 2010).

This notion was confirmed by knocking out a critical ENaC subunit in taste buds, which impaired salt taste detection (Chandrashekar et al. 2010). Patch-clamp studies suggested that Na+ detecting cells are type I cells (Chaudhari and Roper 2010).

Pharmacological and other evidence suggests that salt transduction in human and animal models also occurs via additional membrane receptors or ion channels.

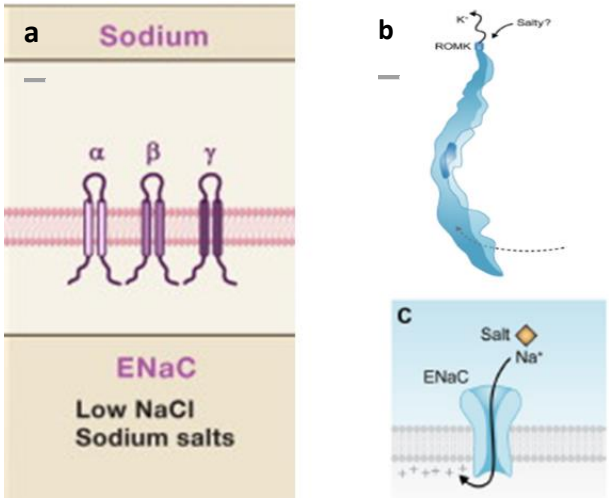

Fig.8. Salt receptor: a) ENaC , expressed by type I cells b) by directly permeating Na+ through apical ion channels and depolarizing taste cells c) (Chandrashekar 2006) .

Sour taste stimuli excite type III (Fig.9) but the membrane receptor or ion channel that transduces sour stimuli remains as yet unidentified. The polycystic kidney disease like channel (PKDL) has been proposed as the acid-sensing machinery detecting the sour taste (Sternini 2013). In particular, non-selective cation channels formed by PKD2L1 and PKD1L3 were proposed as candidate sour taste receptors. Yet, this channel is sensitive to extracellular pH rather than a drop in cytoplasmic pH, which is known to be the proximate stimulus for sour taste. More likely candidate sour receptors in type III cells are plasma membrane channels that are modulated by cytoplasmic acidification, such as certain K channels.

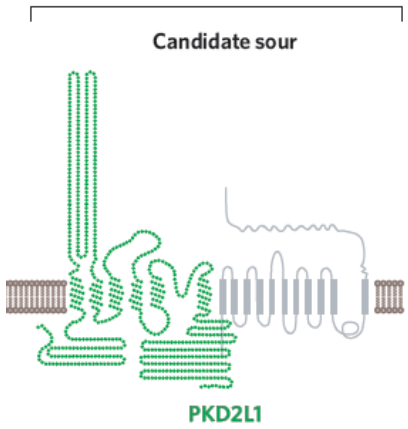

Fig.9. Sour receptor: The polycystic kidney disease like channel, PKDL, has been proposed as the acid-sensing machinery detecting the sour taste. The grey receptor next to PKD2L1 depicts a PKD1-family member as a candidate partner (Chandrashekar 2006).

In addition to the basic tastes, the taste system appears responsive to CO2 (Chandrashekar et al. 2009). Mammals have multiple sensory systems that respond to CO2, including nociception, olfaction, and chemoreception essential for respiratory regulation, yet the molecular mechanisms for CO2 reception remain poorly defined (Chandrashekar et al. 2009). CO2 is also detected by sour-sensing cells. However, the taste of carbonation is separated from sour detection because it is mediated by carbonic anhydrase 4, a glycosylphosphatidyl inositol-anchored enzyme tethered on these cells' surface (Fig.10).

This enzyme serves as the principal sensor of CO2 by catalyzing the conversion of CO2 into bicarbonates and protons, with the protons being the relevant signal. Thus, carbonation does not taste sour despite being detected by sour-sensing cells (Chandrashekar et al. 2009).

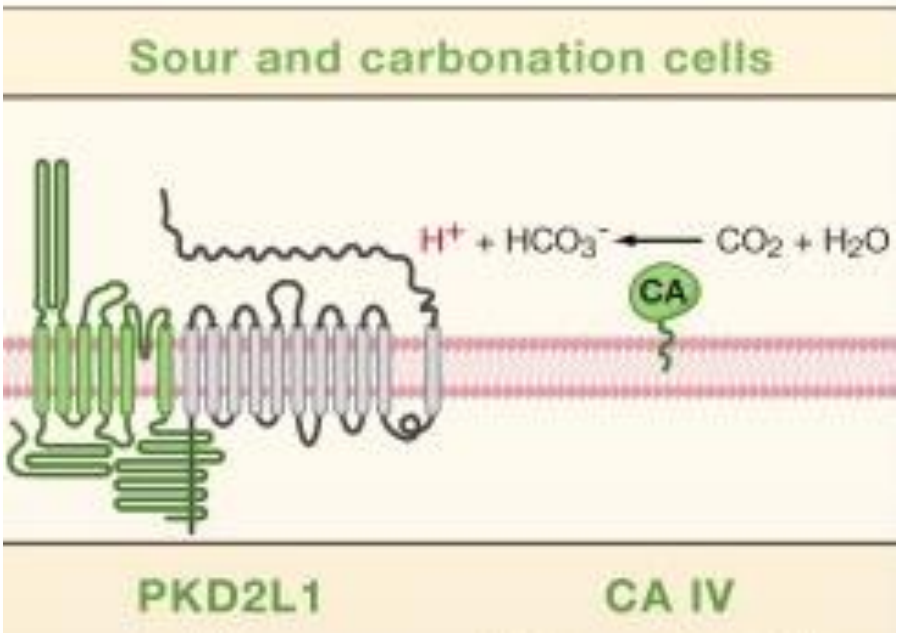

Fig.10: CO2 detection: (CA IV) carbonic anhydrase 4 serves as the principal sensor of CO2 by catalyzing the conversion of CO2 into bicarbonates and protons, with the protons being the relevant signal (Yarmolinsky 2009).

1.4 From taste buds to cortex

Upon tastant binding to receptors on microvilli of TRCs, transduction machinery is activated and neurotransmitters are released.

The afferent taste information is transmitted to neural fibers within the taste bud. The cell bodies of these taste neural fibers occur within the sensory ganglia of cranial nerves (CN) VII, IX, and X. The fibers project into the central nervous system at the level of the brainstem and synapse initially onto the nucleus of the solitary tract (NTS).

From there, afferent information projects cortically via the thalamus (ventroposteromedial and mediodorsal nuclei) to the primary opercular and insular taste cortex (IC), as well as to the orbitofrontal cortex (OFC), cingulate gyrus and to other multimodality integrative projection areas.

1.5 Taste cortex

Brain regions receiving direct sensory information from the thalamus are referred to as primary sensory areas. These primary areas are well established for somatosensation, vision or audition. However, for the sense of taste the site of the primary taste cortex (PTC) in humans is still being debated.

Our knowledge of the central processing of taste comes from animal experiments, clinical data, electrophysiological, and recently also functional neuroimaging experiments in humans, but it is still largely incomplete (Iannilli et al. 2014).

Studies in non-human primates suggested a divided primary representation in the anterior primary somatosensory cortex and in the anterior part of the insula and overlaying operculum (Iannilli et al. 2014). Whereas studies in humans based on cerebral lesions reported gustatory disturbances typically when the insula is damaged (Iannilli et al. 2014). Nevertheless, to provide a clear definition of the primary taste cortex meta-analyses of those studies failed to precisely localize or identify sub-regions within the insula and operculum (Small 2010, Veldhuizen et al. 2011).

Several reasons can account for this controversy: heterogeneity in function and structures of insular cortex, differences in neuroimaging techniques as well as difficulty to control the precise delivery of taste stimuli.

The primary taste cortex, however, represents not only taste but also non-taste information of oral stimuli, such as odorants, texture, temperature (Guest et al. 2007), and lingual somatosensory stimuli (Cerf-Ducastel et al. 2001, de Araujo and Rolls 2004, Kami 2008).

The most credited candidates to the function of human primary taste cortex (hPTC) are the frontal operculum and the anterior insula (FO/AI); the opercular cortex (OC) and the OFC are thought to code for secondary gustatory functions, whereas the amygdale (Amy) and the dorsolateral prefrontal cortex (PFC) are involved as hierarchically superior processing units (Di Salle et al. 2013, Kami et al. 2008, Marciani et al. 2006).

Furthermore, the OFC displays multimodal responses to both gustatory and olfactory stimuli, permitting their integration in the flavor of food (Phillips et al. 1997) and anterior cingulated cortex (ACC), which is also involved in the processing of gustatory (glucose and umami) and

olfactory stimuli, displays a broad responsiveness to motivationally relevant affective stimuli, contributing to the control of normal mood and involved in the pathology of depression (de Araujo et al. 2003).

The IC is an anatomically heterogeneous area with a multidimensional role in sensory systems. From the functional point of view the PTC reflects the identity and intensity of taste, and the secondary taste cortex reflects the emotional aspect of taste (Kami 2008).

The posterior part of insula is generally considered as related to the processing of sensory aspects of pain, whereas the anterior part is believed to play a role in the processing of emotional aspects of pain and pain memory (Iannilli 2008).

More recently, some studies in the human neuroimaging literature suggest that there are motivation/reward related differences in activation within the insular cortex in response to food-related stimuli that include both taste and olfactory components. Human neuroimaging and clinical studies on taste have suggested that sub-regions within the insula may sustain different functions in gustatory processing, such as taste somatosensory stimulation and hunger (Haase et al. 2009).

Sight, smell, taste and texture of food activate the OFC, which is also involved in the processing of expectancy or prediction of a subsequent taste sensation, and, particularly, in the evaluation of food pleasantness, allowing the convergence of sensory and affective processing of taste, and underpinning the appreciation of its hedonic and reward-related aspects (Rolls and McCabe 2007).

Moreover, the OFC displays multimodal responses to both gustatory and olfactory stimuli, permitting their integration in the flavor of food. ACC, which is also involved in the processing of gustatory (glucose and umami) and olfactory stimuli, displays a broad responsiveness to motivationally relevant affective stimuli, contributing to the control of normal mood and involved in the pathology of depression (de Araujo et al. 2003).

1.5.1 The insular neuroanatomy

The insula (Fig. 11) is that part of the cerebral cortex shaped like an inverted triangle folded within, and forming the base of, the lateral sulcus (sylvian fissure).

It is completely obscured in the lateral view of the exposed cerebral cortex by the overlying opercula of the temporal, parietal, and frontal lobes. Insula is a distinct lobe of the cerebral cortex (Butti and Hof 2010), designated by some as the “fifth lobe” (e.g., Augustine 1996). It is the first region of cerebral cortex to develop and differentiate, beginning at age 6 weeks of fetal life (Afif et al. 2007). In adults it comprises 2 % of the total cortical area.

The insula consists of five to six gyri arranged in a vertical fan-like manner with the circular sulcus forming an upper boundary.

It has long been recognized that the number and neuroanatomical arrangement of insula gyri varies naturally among neurologically intact individuals, even between the two sides of the same brain (Gasquoine 2014).

Early cytoarchitectonic studies on the human insula identified from 4 (areas 13–16: Brodmann) to 31 subregions. A frequently referenced subdivision of the insula based on cytoarchitectonic study defined concentric circular agranular (anterior/ventral), dysgranular (medial), and granular (posterior/dorsal) subregions emanating from the lowest point (Mesulum and Mufson 1982).

Variations in granularity pertain to the distribution of neurons at layer IV, typically considered as having an input or sensory function, of the cortical grey matter.

The human insula is much larger than that of the rhesus monkey and the boundaries of these subregions have not been precisely specified in terms of sulci and gyri (Afif et al. 2007).

Another oft used subdivision is into anterior (three or four “short” gyri) and posterior (two “long” gyri) subregions separated by the central insular sulcus (Afif and Mertens 2010).

The main branch of the middle cerebral artery lies within this sulcus. Subdivision of the human insula on the basis of cytoarchitecture remains contentious (Gasquoine 2014).

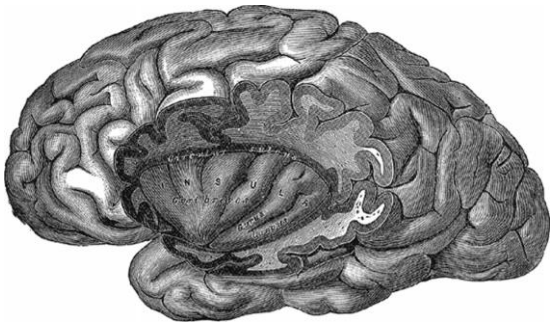

Fig. 11. Insular cortex: Insular cortex shown in a lateral view of the left cerebral hemisphere with the overlying opercula of the temporal, parietal, and frontal lobes removed (Gray’s Anatomy)

Similarly, there is little agreement on the functional specialization of subregions of the insula from meta-analyses of functional neuroimaging or electrical stimulation study (Gasquoine 2014).

The insula has bidirectional (Fig.12) connections with most of the brain, but especially with orbitofrontal, anterior cingulate, supplementary motor areas, parietal (primary and secondary somatosensory areas), and temporal cortices and with subcortical structures that include especially the Amy, globus pallidus of the basal ganglia, and thalamus (Augustine 1985).

There is gradation of connectivity throughout the region in that the AI has greater connectivity with the frontal lobe, whereas the posterior insula has greater connectivity with the parietal lobe.

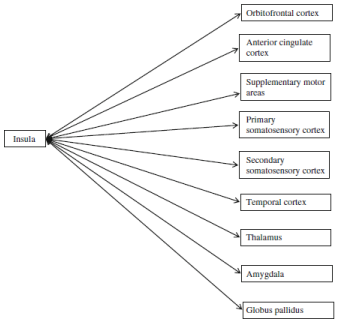

Fig. 12. Major bidirectional connections for the insula. (Gasquoine 2014)

1.5.2 Physiology of insula

The central architecture of taste processing has been, so far, only partially understood. FO/AI, the putative hPTC, (Ogawa 1994, Small et al. 2003) is devoted to the analysis of taste identity and intensity, but its functional organization still keeps several fundamental questions unanswered: first it has yet to be clarified whether hPTC is characterized by chemotopical organization; second, the rules of functional representation of gustatory qualities in hPTC, including their intensity, are still to be determined. Furthermore, its spatial architecture has not yet been evaluated (Schoenfeld 2004).

Different subjects perceive the same intensity of a given taste stimulus in a different manner. This suggests a substantial degree of intra-subjects variability in terms of neural representation (Schoenfeld 2004).

In the same cortical region neural activity also codifies for the selective attention to tastants and for some non-gustatory information, such as perception of odorants, texture, temperature, and lingual somatosensory stimuli (Veldhuizen et al., de Araujo and Rolls 2004, Cerf-Ducastel 2001).

In a broader perspective, the insula plays a key role in a wide range of brain processes, from viscerosensation and pain, to motivation and emotion, and possibly has also a role in the processing of empathy for emotional states (Jabbi et al. 2007).

Previous functional neuroimaging experiments revealed four functionally distinct regions on the human insula associated to the social-emotional, the sensorimotor, the olfactory-gustatory and the cognitive network of the brain (Kurth et al. 2010).

In particular olfactory-gustatory stimuli elicited activation in the central part of the insular cortex, whereas apart from somatosensory and motor processes, all tested functions overlapped on the anterior-dorsal insula.

Anyway, in spite of many functional studies across a wide range of functional conditions, human insula sensory organization and its relationship with a hypothetic integrative role remains to be understood.

Furthermore, the insula processes a much wider range of sensory stimuli. Most especially, it is the primary cortical reception area for interoceptive sensory information from the internal milieu associated with changes in autonomic nervous system activity. Thus the insula is considered as critical for emotional feelings in accord with the James-Lange theory of emotion. This role was historically associated with the limbic system.

Previous studies demonstrated that insular lesions are implicated in cognitive impairment across all neuropsychological domains, but especially in language. Although aphasic disturbances of various types frequently accompany dominant insula injury, the exact role of the insula in language processing remains unclear, as most cases involved lesions that extended into perisylvian language regions (Gasquoine 2014).

Lateralization effects in the insula reflect the well-established pattern of language processing in the dominant hemisphere, but also right sided processing of sympathetic effects and (possibly) left sided processing of parasympathetic effects.

Neuroimaging studies have linked abnormal grey matter volumes or hyper-and hypo-activity levels in the insula with schizophrenia, eating disorders, anxiety and mood disorders, conduct disorder, autism, addiction, and chronic pain. The significance of these abnormal activity patterns remains theoretical.

Other functional neuroimaging studies showed hyperactivations in the insula, typically in conjunction with anterior cingulate cortex, for all manner of cognitive tasks, including those involving perception, intentional action, and consciousness.

It is unlikely that the insula has a task-specific function in so many cognitive activities, especially as they have well-established links with other brain regions (Gasquoine 2014).

1.6 Functional Magnetic Resonance

A new, powerful tool to extend our knowledge of hPTC has been recently provided by fMRI, which has already proven essential in conveying extremely valuable information on the functional anatomy of other neural sensory pathways. fMRI has rapidly become, in recent decades, a key method neuroscience uses to operate a virtual

dissection of the living human brain on the basis of its regional activity (Ogawa et al. 1990, Bendettini et al. 1992).

The activity of the neurons constantly fluctuates in different activities, from simple tasks to complex cognitive tasks. The brain also has many specialized parts, so that activities involving vision, hearing, touch, language, memory, etc. have different patterns of activity. Even keeping at rest quietly the brain is still highly active, and the patterns of activity in this resting state are thought to reveal particular networks of areas that often act together.

Functional magnetic resonance imaging is a technique for measuring and mapping brain activity in noninvasive and safe way. It is a functional neuroimaging procedure using MRI technology that measures brain activity by detecting associated changes in blood flow. This technique relies on the fact that cerebral blood flow and neuronal activation are coupled. Indeed, when an area of the brain is in use, the blood flow to that region also increases.

The essential observation was that when neural activity increased in a particular area of the brain, the MR signal also increased by a small amount.

Functional magnetic resonance is being used in many studies to better understand how the healthy brain works, and in a growing number of studies it is being applied to understand how that normal function is disrupted in disease.

The picture of what happens is somewhat subtle, and depends on two effects. The first effect is that oxygen-rich blood and oxygen-poor blood have different magnetic properties related to the hemoglobin that binds oxygen in blood. This has a small effect on the MR signal, so that if the blood is more oxygenated the signal is slightly stronger. The second effect relates to an unexpected physiological phenomenon. For reasons that we still do not fully understand, neural activity triggers a much larger change in blood flow than in oxygen metabolism, and this leads to the blood being more oxygenated when neural activity increases. This somewhat paradoxical blood oxygenation level dependent (BOLD) effect is the basis for fMRI.

Therefore, fMRI does not depict neural activity directly but instead the perturbation of local haemodynamics induced by the neurovascular coupling, using the BOLD signal contrast.

This is an intrinsic limitation of the method, since it accounts for a rather indirect measure of neuronal functioning.

Nonetheless, fMRI has been effective and reliable in helping to develop fundamental milestones in the process of understanding the functional organization of human brain. This is mainly because of fMRI sensitivity in analyzing brain functional phenomena and the lack of biological invasiveness, resulting in unprecedented and unparalleled flexibility of use.

The decisive advantage of fMRI, compared to other functional neuroimaging methods, consists mainly of the unsurpassed spatial resolution that is in the range of fractions of millimetres.

Furthermore, compared to methods using nuclear tracers positron emission tomography, PET, or single photon emission computed tomography (SPECT), fMRI provides much higher temporal resolution (in the range of 100 ms or less) and an inherent coregistration to same-session structural studies with high anatomic detail.

As an additional advantage, fMRI studies, in contrast to tracer-based functional neuroimaging methods, do not necessarily require the analysis of a group of volunteers but can produce valuable results at the level of single individuals.

This advantage is not trivial at all in the study of the sensory system, much more advantageous than in other brain domains.

The analysis of single volunteers is absolutely crucial for studying small structures that show strong intra-individual variations (Di Salle et al. 2010), as is true for the insular cortex. In that case, averaging data across different subjects and normalizing them into a standard stereotactic system, such as that proposed by Talairach and Tournoux (1998), might well be associated with significant loss of information.

The ultimate goal of most functional brain mapping studies is to describe the regional and temporal nature of neuronal events.

A disadvantage of fMRI consists in its relying on indirect measures of neuronal activity by means of the haemodynamic effect associated with activation through a neurovascular ‘ coupling ’, composed of a cascade of complex and poorly understood mechanisms.

This limits the temporal resolution of fMRI to be orders of magnitude poorer than that of EEG or magnetoencephalography (MEG), and the resolution in space to face a natural blurring and misregistration of the spatial sources of the BOLD signal, which differ slightly from the neuronal source location (Di Salle et al. 2010), since haemodynamic events can be somewhat dislocated compared to the neural events. However, the complexity of the physiological scenario underlying fMRI phenomena permits creative implementation of experimental fMRI paradigms.

This has allowed us to consistently expand the potential of MRI in identifying the anatomic sources of the electrophysiological events together with their temporal behavior.

As an example, the use of the initial dip in the fMRI signal, instead of the large positive BOLD effect, has permitted the spatial resolution of fMRI to be pushed below the threshold of one millimeter towards the dimensional range of the iso-orientation cortical columns, at least in the visual cortex of the cat at high field strengths.

1.7 The effect of carbonation

Taste represents the main sensory modality influencing human feeding behaviors. Indeed, while we typically appreciate and evaluate a food's overall flavor as a gestalt comprising taste, smell, and somatosensation, taste has the last word in identifying a potential food (Hummel and Welge-Luessen 2006). The acceptance of a sweet taste signaling calories, and the rejection of a strongly bitter taste warning against toxins, are brain stem reflexes that appear prenatally in humans, are modified during life, but are never removed by experience (Steiner 1973, Steiner 1974).

Our knowledge of the central processing of taste comes from animal experiments, clinical data, electrophysiological, and recently also functional neuroimaging experiments in humans, but it is still largely incomplete (Smits et al. 2007).

As mentioned above, the most credited candidates to the function of hPTC are the FO/AI; whereas the opercular cortex (OC) and the OFC are thought to code for secondary gustatory functions, and Amy and the dorsolateral prefrontal cortex (PFC) are involved as hierarchically superior processing units (Kami et al. 2008, Marciani et al. 2006).

Conversely, more is known on the peripheral pathway of taste, including the molecular dynamics of many receptors (Chaudari and Roper 2010).

The five universally accepted basic tastes, sweet, salty, sour, bitter, and umami (a savory sensation elicited by monosodium glutamate) have specific receptors in oral, pharyngeal and laryngeal regions. Moreover the expression of taste receptors has been recently reported also in the gastrointestinal (GI) tract and particularly in the gut, although their function in digestive and ingestive processing remains unknown (Scalfani 2007).

In addition to the basic tastes, the taste system appears responsive to CO2 but the presence of specific CO2 peripheral receptors and central neural pathway is still debated (Chandrashekar 2009).

In the absence of a dedicated neural processing and cortical representation, CO2 might still induce a powerful modulation of different taste inputs, implying that sweetness, bitterness, sourness, saltiness, and umami, or their combination in specific beverages, may be perceived as profoundly different in the presence of carbonation. Everyday experience provides ample evidence in favor of this hypothesis. For instance, Kaushal (2004) found that CO2 was able to improve color, body, taste, flavor, and the overall acceptability of fruit juices (apple and pear juices).

Among the different interferences carbonation may produce, the modulation of sweet perception appears of particular practical interest, given the widespread use of CO2 in sweet beverages.

Interestingly, CO2 may differently impact the taste processing of various sweet substances, producing significant consequences in the appreciation of beverages containing either sucrose or sugar substitutes. As an example, Meyer and Riha (2002) suggested that regular and diet beverages, were indistinguishable due to the preponderant role of CO2 in the sensory profiles of the two beverages.

The existence of specific neural activity and peripheral molecular machinery dedicated to the perception of carbonation has been recently demonstrated in the fruitfly Drosophila melanogaster and in mice (Chandrashekar et al. 2009).

The mechanism of CO2 detection in mice depends strictly on the function of PKD2L1 positive cells, sensitive to sourness, and on their specific expression of carbonic anhydrase 4 which catalyzes the conversion of CO2 into bicarbonate ions and free protons, making CO2 perception intersect the mechanisms of sour taste (Chandrashekar et al. 2009). The clear perceptual differentiation between CO2 and sour taste may further depend on the simultaneous stimulation of other sensory pathways, including a robust stimulation of the somatosensory system; thus, the final percept of carbonation may be a combination of multiple sensory inputs (Smits 2007, Iannilli et al. 2008). So the contribution of carbonation to taste may not even be properly gustatory in nature, given that the CO2 stimulation operates on mechanical and chemical trigeminal receptors that provide tactile, proprioceptive, chemosensory and nociceptive information from face, mouth, and nose (Iannilli et al. 2008). For instance, the purpose of nociceptive afferents exposed in the oral and nasal mucosa and easily accessible to chemical irritants as CO2, is to prevent the inhalation of potentially life-threatening substances (Iannilli et al. 2008).

Alternatively, carbonic anhydrase may have a dual function as both enzyme and sensor (a “senzyme”), as demonstrated for other enzymes, where a conformational change upon binding with CO2 might be detected by specific proteins coupled to a signaling pathway (Frommer 2010).

In any case, if harm avoidance may justify the presence of CO2 sensing, this probably represents only one side of the coin in sensory organization. While for animals in the wild the sense of taste plays a critical role in determining whether a food is nutritious or potentially toxic-eliciting acceptance or avoidance behaviors, in humans it is primarily used to enhance the hedonistic enjoyment of food (Scott 2005).

Proportionately to the limited choice of behavioral outputs, the sense of taste is categorized into just a limited number of different modalities. In general, sweet, umami, and low-salt tastes elicit food acceptance behavior, whereas bitter, sour, and high-salt tastes elicit avoidance (Scott 2005). It is likely that CO2 sensing follows the same finality of

behavioral guidance, evolved as a mechanism to recognize CO2-producing sources to avoid or, conversely, seek fermenting foods.

In Drosophila, CO2 perception has behaviorally divergent effects, depending on the sense perceptually involved, with avoidance caused by olfactory detection and acceptance by gustatory detection (Fischler 2007). The latter may be grounded in the feeding convenience of detecting CO2 production by growing microorganisms, allowing fruitflies to identify and consume nutrients that these microorganisms provide (Fischler 2007). On the contrary, the olfactory detection of CO2 in the air may signal unfavorable conditions such as hypoxia, presence of macroorganisms, overly rotten fruit, or stressful environments (Fischler 2007). Nonetheless, the behavioral role of the taste for carbonation in humans still remains unexplained.

Since taste is primarily used in our species for hedonistic purposes (Scott 2005), CO2 perception may represent an evolutionary remnant trait, or may have the role of creating a richer and more gratifying perceptual input through a somatosensory trigeminal stimulation and a multisensory convergence of perceptual inputs.

1.8 Chemotopic representation of taste

Many efforts have been done to understand the function of sensory systems and characterize the mechanism underlying perception from the chemical transduction to the neural coding. In the visual, auditory, and somatosensory systems spatial information in the peripheral sense organs is maintained in the sensory cortex. In these neocortices, cells responsive to similar stimulus features are clustered, and response properties vary smoothly across the cortex (Seifritz et al. 2006, De Martino et al. 2013, Abdollahi et al. 2014).

Unlike other sensory systems, the topography in the olfactory system does not depend on the spatial properties of the stimuli. Relieved of the requirement to map the position of an olfactory stimulus in space, the olfactory system employs spatial segregation of sensory input to encode the quality of an odorant (Stettler and Axel 2009, Auffarth 2013).

Like olfaction, taste requires a process of chemoreception, but, differently, taste seems to be a more functionally oriented sense, with each taste domain tuned to identify specific nutrients or poisons and associated with particular physiological functions, such as detecting energy content (sweet, umami), maintaining electrolyte balance (salt), guarding pH level (sour), or avoiding toxins (bitter) (Lundstrom et al. 2011).

The peripheral taste system likely maintains a specific relationship between taste bud cells selectively responsive to one taste quality and the ganglion cells signaling that particular quality. This explains the

response specificity of some individual taste nerve, particularly because sweet, umami, and bitter receptors are expressed in distinct populations of taste cells.

Although anatomical evidence for such an exclusive relationship is lacking at the level of single receptor and ganglion cells, the relationship between single buds and their innervating ganglion cells is neuroanatomically “traceable”.

In taste, attempts to identify a spatial representation of taste receptors or taste qualities have revealed only an indistinct functional topography in the brain. Nevertheless, taste ganglion cells must distribute peripheral fibers to particular receptor cell types and disseminate impulses centrally in a structurally organized manner.

Two major hypotheses on how taste information is processed currently exist. The first, called “labelled line” refers to a coding model in which peripheral (or central) neurons that respond the most robustly to a given taste modality, carry the totality of the information on segregated pathways. In this coding scheme, receptor cells are tuned to respond to single taste modalities — sweet, bitter, sour, salty or umami — and are innervated by individually tuned nerve fibres. In this case, each taste quality is specified by the activity of non-overlapping cells and fibres (Chandrashaker et al. 2006).

The second hypothesis affirms that either individual TRCs are tuned to multiple taste qualities, and consequently, the same afferent fibre carries information for more than one taste modality, or that TRCs are still tuned to single taste qualities but the same afferent fibre carries information for more than one taste modality. This “ensemble code” is also known as “combinatorial” or “across fibre pattern” (Carleton et al. 2010).

Evidence suggests that the peripheral taste system ─at least for the five perceptually distinct taste modalities─ uses a labelled line coding scheme (Chandrashaker et al. 2006). The issue of whether this scheme is conserved and utilized within the higher nervous system levels of the pathway is still debated.

Since taste consists of only five primary qualities, a remaining question is whether other different taste qualities such as carbonation, are differently represented in the brain.

Some authors analyzed the topography of hemodynamic activity elicited by five basic taste stimuli in six single subjects, and a group analysis revealed regions that were activated more by one specific taste than by any of the other tastes (Schoenfeld et al. 2004). However, these studies do not give new insight on the underlying neuronal pathways of taste quality coding or recognition, and other studies state that different taste qualities activate similar cortical regions (Rudenga et al. 2010).

Non-human studies on chemotopic organization of taste system are controversial, as Scott and Plata-salaman (1999) reported no clear

topographic organization of taste sensitivity in the primary taste cortex of macaques.

However, more recently, Chen X et al. (2011) demonstrated striking topographic segregation in the functional architecture of the gustatory cortex of mice. With two-photon calcium imaging they monitor different tastant-evoked (bitter, sweet, NaCl and umami) neural activity across the taste cortex in mice, showing a clear topographic separation of sweet and bitter taste into non-overlapping gustatory fields in insular cortex. This hypothesis is in accordance with organization of visual, somatic and auditory cortex (Humphries et al. 2010) where neurons that respond to similar features of the sensory stimulation are topographically organized into spatial maps of the cortex, but not with smell.

Recent studies on the representation of smell in the primary olfactory cortex showed a distributed pattern of neuronal activity. Even though each odor is encoded by a unique ensemble of neurons, there is not a spatial clustering in piriform cortex of mouse (Stettler and Axel 2009).

Techniques commonly used in demonstrating somatotopic, auditory and visual maps, were electrical stimulation of the cortex through microelectrode, single-cell recording, Transcranial Magnetic Stimulation (TMS), and more recently fMRI. Many of the existing topographic maps have been further studied or refined using fMRI. For instance, Hubel and Wiesel (1998) originally studied the retinotopic maps in the primary visual cortex using single-cell recording. Recently, however, imaging of the retinotopic map in the cortex and in sub-cortical areas, such as the lateral geniculate nucleus, have been improved using the fMRI technique (Schneider et al. 2004).

To study insular cortex the traditional techniques are less adequate due to the depth of this region and the difficulties in recording cortical activity from superficial electrodes. Moreover activations land in similar but not overlapping anatomical regions (Fedorenko et al. 2010) across different subjects, as for example the visual motor area has been noted to vary over individuals by more than 2 cm after Talaraich normalization (Sabuncu et al. 2009).

To overcome the uncertainties due to the folding of the cortex in the primary taste region, we used a cortex-based alignment (CBA) procedure to pool taste-related fMRI responses from different subjects (Frost and Goebel 2012)

2. AIM

2.1 The effect of carbonation

In this study, we investigated the central neural processing of taste. In particular, since carbonation is considered an additional taste *per se,* we investigated whether it has its own cortical representation.

To evaluate the modulation operated by carbonation on other taste modalities we studied carbonation in terms of: a) its effect on the brain processing of sweet stimuli, and b) its differential effect on sucrose and artificial sweeteners.

To clarify the specific neural correlates of carbonation alone and the potential role of sour receptors co-activation in the carbonation-related responses, we analyzed the effect of carbonation alone in unflavored water, without any associated sweet perception and the spatial distribution of neural activity related to sourness and carbonation within AI.

This information is essential in the formulation of diet food and beverages, which are designed to be perceived as much similar as possible to regular ones, but with a reduced caloric intake, very useful in treatment of obesity, particularly in children.

The cortical representation of taste-related neural responses has been studied by a Philips 3T scanner in an echo planar BOLD experiment, while gustatory stimuli were delivered by computer-controlled automatic injectors.

2.2 Chemotopic representation of taste

Since taste consists of only five (or six including CO2) primary qualities, a remaining question is whether the different qualities are differently represented in the brain and whether in hPTC there is a chemotopic organization of the basic tastes. Furthermore, it is not clear whether cortical areas respond the most robustly to a given taste modality or not respond at all to it, as well as it seems to happen at peripheral level. Indeed, based on the “labelled line” coding model, receptor cells are tuned to respond to single taste modalities and are innervated by individually tuned nerve fibers. Furthermore, peripheral neurons that respond the most robustly to a given taste modality, carry the totality of the information on segregated pathways.

In these series of experiments we performed the mapping of hPTC responses not only to the five basic tastes but also to carbonation by means of fMRI in combination with a high resolution cortical registration method to improve the spatial correspondence across individual brains (Goebel et al. 2006).

3. MATERIALS AND METHODS

3.1 The effect of carbonation

This experimental section involved three functional neuroimaging experiments: 1. the first analyzing the effect of carbonation in sweet solutions; 2. the second analyzing the specific neural activity elicited by carbonation alone in non-sweetened water and, 3. the third studying the spatial location of the strongest neural effects of sour taste and CO2 within the insular cortex.

The first experiment involved nine volunteers (mean age 23 years, 5 men and 4 women), not reporting any olfactory, gustatory, neurological or psychiatric disorder, and free from the use of any medication. Informed consent was obtained by all participants and the study was approved by the local ethic committee.

The brain functional examination was performed through the acquisition of time-series of BOLD Magnetic Resonance images using a 3 Tesla MR scanner (Philips, Eindhoven, The Netherlands) during the delivery of gustatory stimuli.

Four computer controlled automatic injectors delivered the stimuli directly triggered by the MR radiofrequency pulses, while the subjects laid still in the scanner. A total of four different gustatory stimuli were used, each a variation of a commercial beverage (Sprite™; The Coca-Cola Company, Atlanta, GA) differing only for the presence of carbonation or for the sweetening agent: 1) carbonated, sweetened with sucrose, 2) noncarbonated, sweetened with sucrose, 3) carbonated, sweetened with aspartame & acesulfame (As-Ac), and 4) noncarbonated, sweetened with As-Ac.

All tastants were kept at controlled low temperature (4°C).

Each MR compatible injector (Spectris Solaris, Medrad™) delivered two solutions both in the quantity of 10 ml each (speed of injection: 5ml/sec).

To avoid cross-contamination of stimuli, each stimulus was delivered by the principal line of a specific injector, whereas the secondary line delivered water. The alternation of stimuli and water prevented physical and perceptual overlapping between the different tastes.

The subjects held the solution or the water in their mouth for 10 seconds and then swallowed it, following acoustic cues given 1 second prior to the injection and swallowing phases. Stimulation and washing periods were composed of three phases (Injection=2sec, Tasting=10 sec, Swallowing= 3sec), were separated by a resting period of 15 seconds, and were repeated 5 times per each condition for a total volume of 50 ml of each solution (200 ml) and 200 ml of water (Fig.13).

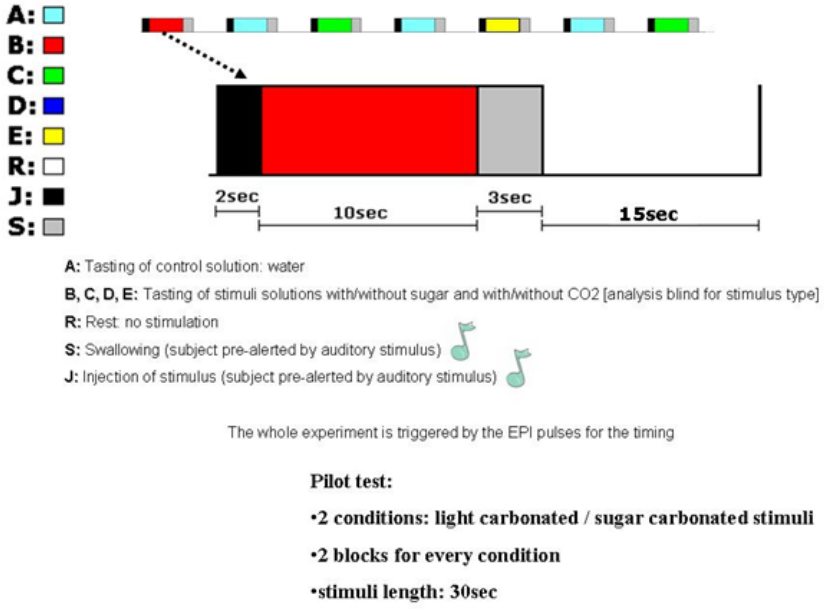

Fig.13. Effect of carbonation, paradigm: Stimulation and washing periods were composed of three phases (Injection=2sec, Tasting=10 sec, Swallowing= 3sec), were separated by a resting period of 15 seconds, and were repeated 5 times per each condition for a total volume of 50 ml of each solution (200 ml) and 200 ml of water.

In the second experiment, using the same experimental procedures, we tested the specific neural activity elicited by carbonation alone in non-sweetened water on 4 subjects. A single functional contrast was analyzed, comparing carbonated and non-carbonated water.

In the third experiment, using the same experimental procedures, we determined the regions of the strongest neural effects of sour taste and CO2 in 8 subjects compared with a baseline of water, within the insular cortex.

3.1.1 Behavioral data

To correlate neuroimaging findings with behavioral data, the same set up was used to assess the ability of carbonation to modulate sweetness perception. To this purpose, 14 subjects were randomly administered 5 ml of the above indicated Sprite™ solutions and, after 10 seconds from the administration of each solution, they were asked to score the level of perceived sweetness on a Visual Analogue Scale (VAS) ranging from 0 to 100 mm. In brief, it consists of a continuous scale made of a 100-mm horizontal line anchored by 2 verbal descriptors—one for each symptom extreme (0= Not sweet, 10 cm= maximum perceived sweet taste). Similarly, we tested the effect of 1585 parts-per-million of CO2

added to a 10% glucose solution on sweetness perception in 7 subjects.

3.1.2 *fMRI acquisition and pre-processing*

The functional time-series, consisting in the repetition of whole brain volumes, were acquired with a Philips Achieva scanner at 3T (IRCCS SDN Naples, Italy) by means of T2*-weighted gradient echo planar imaging sequences (TE 35 ms; matrix 96x96; FOV 210x210 mm; in-plane voxel size, 2.1875x2.1875 mm; flip angle 90°; slice thickness 4mm). Functional volumes consisted of twenty-two bi-commissural slices, acquired with a volume repetition time (TR) of 2000 ms with an inter-slice time of 90ms. A total of 610 volumes were acquired for each subject, and the first two volumes were discarded to ensure steady-state longitudinal magnetization. Subsequently, a high resolution structural volume was acquired via a T1-weighted 3D TFE SENSE sequence (sagittal; matrix 256 x 256; FOV 256 x 256 mm; 181 slices; slice thickness 1 mm; no gap; in-plane voxel size 1mm x 1mm; flip angle 8°; repetition time TR 7.658 ms; TE 3.483ms) to provide the anatomical reference for the functional scan. Functional data were pre-processed using Brain Voyager™ QX, version 1.9 (Brain Innovation, Maastricht, The Netherlands), correcting the slice timing dispersion and the motion in the time series, and removing linear and nonlinear “drifts” in the time courses (temporal high pass filter of two cycles). Finally, functional data were aligned with T1-volumes and warped into the standard anatomical space of Talairach and Tournoux (1988). The resulting time-series were filtered in space with a spatial smoothing Gaussian kernel of 5mm FWHM.

3.1.3 Data analysis

The statistical processing of fMRI data was carried out through Brain Voyager™, by analyzing the random effects of a General Linear Model (n=9, P[cluster corrected]<0.05), after correction of serial correlation [AR-1], Z-transformation of predictors, and correction for multiple comparisons through randomization. Six functional contrasts were analyzed, 1) carbonated versus noncarbonated solutions, 2) sucrose versus As-Ac sweetened solutions, 3) carbonated versus noncarbonated sucrose sweetened solutions, 4) carbonated versus noncarbonated As-Ac sweetened solutions, 5) sucrose versus As-Ac sweetened carbonated solutions, and 6) sucrose versus As-Ac sweetened non-carbonated solutions. The functional contrasts were projected on the average anatomy of the Talairach-transformed T1-weighted 3D TFE SENSE of all the subjects, after reaching a threshold of P<0.05. In the second experiment a single functional contrast was

analyzed, comparing carbonated and non-carbonated water. In the third experiment two functional contrasts were analyzed, 1) carbonated (containing 1585 ppm of CO2) and 2) sour tasting solutions (containing 50mM of citric acid) versus non-carbonated neutral water. Behavioral data were analyzed by paired t-test and reported as mean ± SD.

3.2 Chemotopic representation of taste

Understanding the functional organization of the insular cortex is an essential step elucidating the neural mechanisms underlying the perception of taste, including feeding and dietary behaviors.

An additional aim of the study was to map PTC responses to the five basic tastes and carbonation by means of fMRI in combination with a high resolution cortical registration method in humans, to improve the spatial correspondence across individual brains (Goebel et al. 2006).

To overcome the uncertainties due to the folding of the cortex in the primary taste region, we used a CBA procedure to pool taste-related fMRI responses from different subjects (Frost and Goebel 2012).

Eight adult healthy volunteers (3 males and 5 females, mean age ± standard deviation 24,45 ± 2,1) not reporting any olfactory, gustatory, neurological or psychiatric disorder, and free from the use of any medication took part in the study. Informed consent was obtained by all participants and the study was approved by the local ethic committee.

Solutions of 10mM of quinine hydrochloride (bitter), 30mM of Acesulfamate K (sweet), 120mM sodium chloride (salt), 30mM of mono potassium glutamate +0,5mM inosine 5' mono phosphate (umami), 50mM citric acid (sour) and carbonated water were used both for behavioral and fMRI study.

All subjects underwent an fMRI experiment consisting in the administration of six tastants (basic tastes plus CO2) in a pseudo-randomized order while lying in the magnet. All tastants were kept at controlled low temperature (4°C). The six tastants plus rinsing water were administered via four medical injectors (Spectris Solaris, Medrad^{TM}) equipped with two syringes each electronically controlled through a digital I/O device connected to a laptop.

Each tastant plus rinsing water was delivered through a dedicated line to avoid cross-contamination of stimuli, the six lines were pulled together and fixed to the center of the lips of the subjects thus avoiding shifting of the tubes or the need to keep it during the experiment. Synchronization with fMRI acquisitions and stimuli delivery were controlled with Presentation (www.neurobs.com).

Each taste event consisted in the delivery of 5ml of taste solution over 2 sec (2,5 ml/sec injection speed). The delivery of solution was announced by an auditory cue, followed by a gustatory period of 10 sec during which the solution was distributed all over the mouth avoiding

lateralization of the stimulation. A second auditory cue announced the swallowing period (3 sec) and was followed by a rest period of 15. Subsequently was administered rinsing water with the same modality (Fig.14).

The alternation of stimuli and water prevented physical and perceptual overlapping between the different tastes. Each tastant was delivered four times in a pseudo-randomized order according to Fig.15.

Fig.14. Chemotopic representation of taste, paradigm: Delivery of 5ml of taste solution over 2 sec (2,5 ml/sec injection speed). The delivery of solution was announced by an auditory cue, followed by a gustatory period of 10 sec during which the solution was distributed all over the mouth avoiding lateralization of the stimulation. A second auditory cue announced the swallowing period (3 sec) and was followed by a rest period of 15 sec.

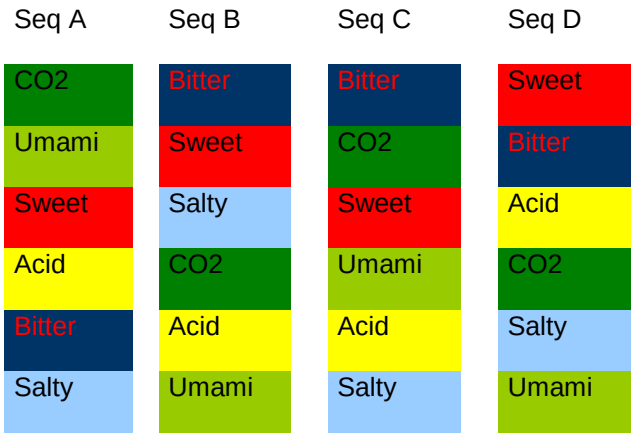

Fig. 15. Taste sequences: Each tastant was delivered four times in a pseudo randomized order according.

3.2.1 Behavioral data

To correlate neuroimaging findings with behavioral data, the same set up was used to assess the ability of subjects to identify the different tastants at different concentrations. All subjects underwent the VAS questionnaire, which includes questions on identification and intensity of each solution (0= Not perceived, 100 mm= maximum perceived).

3.2.2 fMRI acquisition

Total fMRI scan duration was 24 min with the acquisition of 720 dynamic scans and total beverage volume of 240ml. Images were acquired on a 3T Achieva scanner (Philips Medical System, Eindhoven,

Holland) with an EPI single-hot acquisition (TE=35ms, TR=2000ms, 64x64 matrix, in-plane voxel 3,59 x 3,59 mm, 22 slices 4 mm thick and 1 mm gap). Patients were firmly fixed with foam pads to minimize head movements during swallowing. At the end of the fMRI acquisition, a T1-weighted 3D TFE SENSE volume was acquired (sagittal; matrix 256 x 256; FOV 220 x 220 mm; 181 slices; slice thickness 1.2 mm; no gap; in-plane voxel size 0,86mm x 0.86mm; flip angle 10°; repetition time TR 8 ms; TE 2.2 ms, 2 averages) to provide the anatomical reference for the functional scan and to allow cortical realignment of subjects brains.

3.2.3 Data analysis

Data were preprocessed using SPM8 (Wellcome Department of Imaging Neuroscience, University College. London, www.fil.ion.ucl.ac.uk/spm) running under Matlab R2011b (Mathworks Inc.). After correcting for slice timing, data were realigned to the first volume and motion corrected. A spatial smoothing Gaussian kernel of 8 mm FWHM was applied to the fMRI time series.

All dynamic scans were kept in their original spaces and analysis of first level fMRI data were performed. A General Linear Model (GLM) were created with 6 regressors for each tastant, a regressor for solution injection, a regressor for swallowing and a regressor for water rinsing. In the model movement regressors were also added and an high pass filter of 128 sec was applied prior to statistical analysis.

The model include the canonical Hemodynamic Response with time derivatives to account for shift in the taste activation responses. For each patients 6 contrast maps were obtained, looking at the statistical effect produced of each tastant (Umami, Sweet, Bitter, Acid, Salty and CO2) versus rest.

The contrast maps obtained for each patient and for each tastant in the original space of the fMRI acquisitions were imported together with each anatomical volume in Brain Voyager™ QX, (Brain Innovation, Maastricht, The Netherlands) for cortical alignment. We applied a high-resolution cortical alignment method to improve the spatial correspondence across brains and look at the group response in the insula.

3.2.4 Cortical alignment and prevalence mapping

For each subject, the cortical surface was reconstructed as a three-dimensional mesh from the segmented Talairach-transformed anatomical images. To represent topological taste activations on the insular cortex, individual GLM beta maps for each contrast were first projected onto the individual cortical mesh and then averaged across subjects subsequent to the CBA procedure (Goebel et al. 2006).

For each separate hemisphere, CBA was used to map the individual cortical surface vertices to an average cortical surface, to be used as internal common target surface for representing maps.

For each single vertex of the common target surface, we averaged the (anatomically aligned) beta weight values resulting from the individual GLM analyses in the voxel space after projecting from the individual cortical mesh. The use of a CBA approach for group-level analysis was chosen to maximally preserve the anatomical specificity of each individual beta map (Goebel et al. 2006). We applied CBA as implemented in Brain Voyager QX 2.8.2, using all default parameter settings and choosing the "moving target" approach, according to which all individual brains were iteratively aligned to a dynamically updated average brain only based on the cortical folding patterns. The cortical folding patterns were quantitatively obtained by the curvature values calculated of the cortex shape (mesh) and therefore represented the alternation of gyri and sulci of the brain. The matching procedure essentially aligned corresponding gyri and sulci across individual's brains with the result of reducing the anatomical intersubject variability (Goebel et al. 2006, Frost and Goebel 2012, Frost et al. 2014, Herdener et al. 2013).

To quantify topological taste prevalence and the spatial relations among tastes within the insular cortex, for each vertex on the target mesh, we calculated the number of standard deviation of the beta map from the mean beta of the insular mask, corresponding to the projected beta value of that vertex (z-score). Furthermore we repeated this calculation across all vertices of the insula. Then, we assigned a different color code to the vertex depending on the highest z-score value among all taste stimuli. In this way, we intended to emphasize the relative prevalence of the stimulus across the entire insula, regardless of possible overall differences in the amount of activity elicited in the insular cortex. For each clusters of prevalence we looked also at the negative values of each taste to associate the non-prevalence information.

A common mask for the entire insula was obtained from the anatomical high resolution acquisition of one subject using BrianParser v5.0 and then projected on the target brain to define the space of prevalence mapping and (non-)prevalence quantification.

4. RESULTS

4.1 The effect of carbonation

4.1.1 Behavioral data

CO2 is able to significantly reduce sweet-induced taste perception, as assessed by VAS measurement in 14 healthy volunteers. Indeed, in the presence of carbonation, sweet-induced perception of a 10% glucose solution was significantly reduced (36±16 vs. 53 ±14 mm, p=0.02). Similarly, the perception of sweetness of Sprite was also significantly abated by CO2 (48 ±19 vs. 63±17 and 48±18 vs. 55±15 mm for As-Ac and sucrose, p<0.01 and p<0.04, respectively) (Fig. 16 A-B).

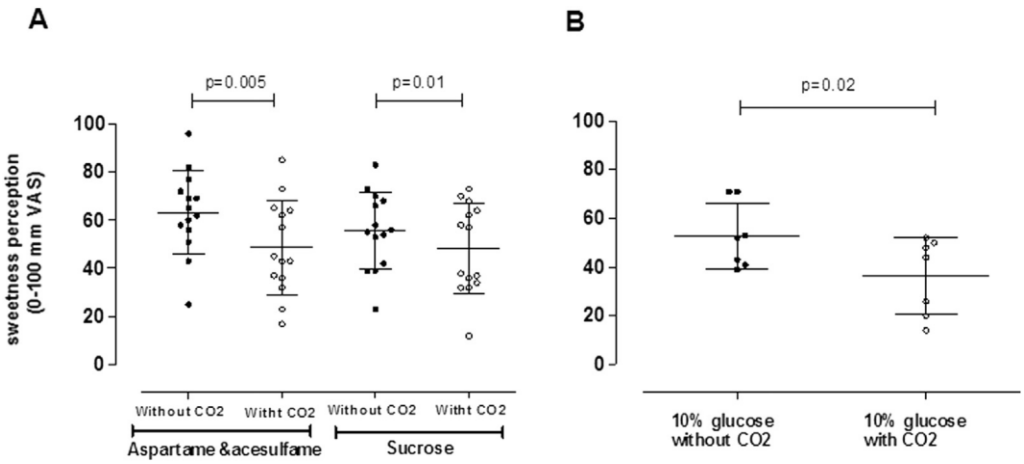

Fig. 16. Behavioral data: (A) Perception of sweetness in 14 healthy volunteers during administration of carbonated or noncarbonated Sprite beverages sweetened with As-Ac or sucrose. (B) Perception of sweetness in healthy volunteers during administration of carbonated or noncarbonated 10% glucose solution. Data are represented as individual values and mean ± SD.

4.1.2 fMRI data

The presence of carbonation (carbonated versus non-carbonated beverages), independently of the sweetening agent (sucrose, As-Ac) produced (Fig. 17) i) a bilateral reduction of neural activity in the insular cortex (IC) and in the lateral OFC, ii) in the right hemisphere a reduced activity of the superior frontal gyrus (SFG), the perigenual frontal cortex (PGFC) and the temporo-parietal (TP) junction and iii) in the left hemisphere a reduced activity in the posterior parahyppocampal gyrus (PPHG), the middle frontal girus (MFG), and the superior cerebellar cortex (SCrC).

The main results can be summarized as follows:

The reduction of perceptual salience of sweetness as assessed by behavioral data (Fig.16 A-B).

A focally decreased activity in the left side of the posterior pons may encompass the cranial (gustatory) part of the nucleus of the NTS.

Only a small focus of increased neural activity in the presence of carbonation was evident in the inferior occipito-temporal cortex (OTC) of the left side.

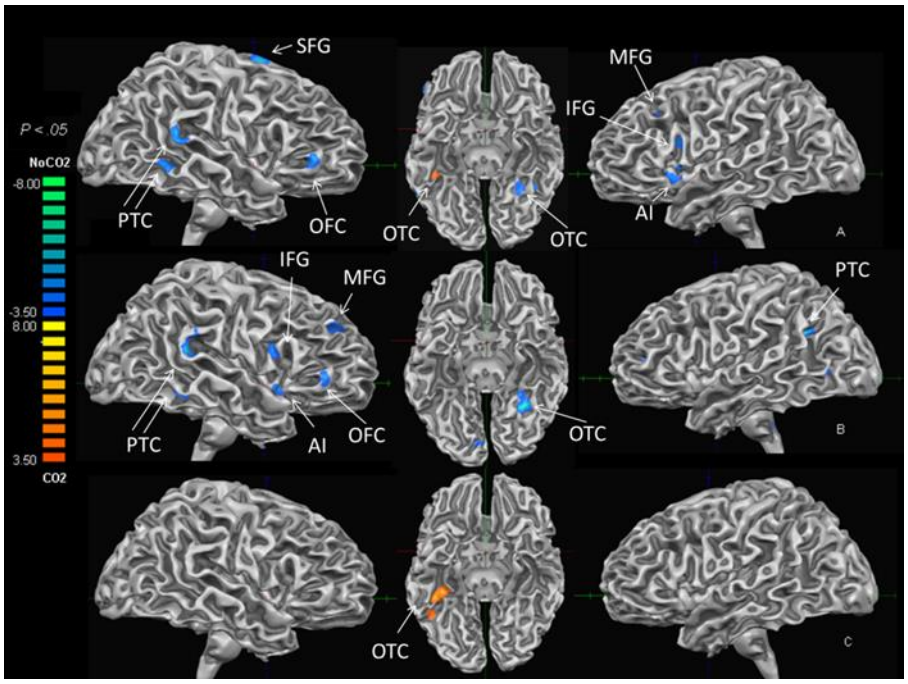

Fig. 17. Effect of Carbonation on neural activity: The presence of carbonation independently of the sweetening agent (A) reduced (blue-green color) activity in AI, OFC, SFG, PT, OTC, MFG, and increased activity in OTC. With sucrose (B), CO2 reduced activity in PT, AI, OFC, IFG, MFG, OTC. With As-Ac (C) CO2 increased activity in OTC.

In the contrast weighting *the effect of the sweetening agent*, the neural activity produced by sucrose was compared with As-Ac, independently of carbonation (carbonated and non-carbonated beverages).

Sucrose sweetened solutions showed increased neural activity bilaterally in Amy (Fig. 18), whereas As-Ac sweetened solutions presented an increased activity in the right IC and the subgenual frontomesial cortex (SGFMC).

Separating the effects of carbonation in the sucrose sweetened and As-Ac sweetened solutions, a much higher effect of carbonation was present in combination with sucrose sweetening.

Indeed, the *presence of carbonation* (carbonated versus non-carbonated beverages) in the sucrose sweetened solutions again produced (Fig.17) a relative decrease in taste-related brain activity, evident in the right hemisphere in the IC, lateral OFC, ventrolateral prefrontal cortex (VLPFC), bilaterally in the cingulate cortex (CgC), the

TP and temporo-occipital (TO) junction, and the cerebellar vermis (CrV) and in the left side in the inferior occipito-temporal cortex (OTC) and the hemispheric cerebellar cortex (CrC).

On the contrary, the *presence of carbonation* (carbonated versus non-carbonated beverages) in the As-Ac sweetened solutions produced (Fig.17) only a spatially focused change in brain activity in the right basal occipito-temporal cortex (OTC), with neural activity being prevalent in carbonated solutions.

In the *presence of carbonation*, brain activity was higher with the As-Ac sweetened solution than with the sucrose sweetened solution, in the right IC, the right TO junction, the right occipito basal cortex (OBC) and the left hemispheric CrC (Fig.18).

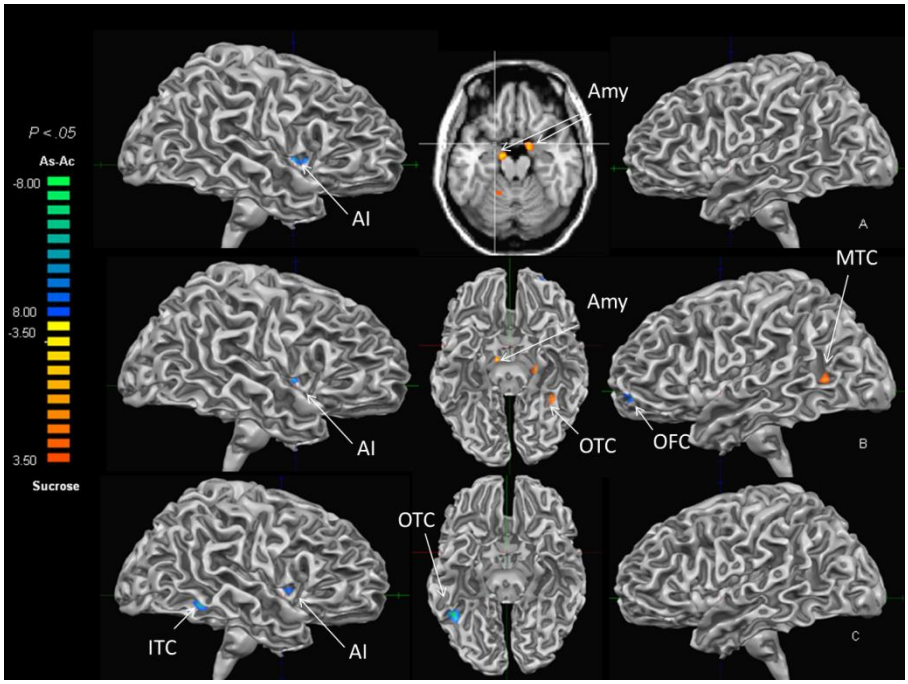

Fig. 18. Effect of the sweetening agent: Independently of carbonation (A), sucrose increased (yellow-red) activity compared to As-Ac in Amy, As-Ac increased activity in AI. Differential brain activity for sucrose vs As-Ac was more evident without (B) than with CO2, and diffusely in favor of sucrose (CgC, CrC, left OTC, MTC and OFC). CO2 (C) reduced differential brain activity, higher for As-Ac in AI, OTC, ITC, OFC and CrC.

In the absence of carbonation, the differential brain activity for the sucrose vs As-Ac sweetened solutions was much more evident and diffusely in favor of the sucrose sweetened solutions, with the CgC, the TO junction of the left side, the mesial temporal (MTC) and the occipito-basal cortex (OBC) of the left side, and the CrC, all more active with the sucrose sweetened solutions, and only the right IC and the left fronto-basal cortex (FBC) more active with the As-Ac sweetened solutions (Fig.18). The specific neural signature induced by carbonation is shown by the changes found in subjects exposed to CO2 alone in unflavored

water. Under these conditions, without any associated sweet perception, CO2 alone markedly increased the activity of AI and OFC (Fig.19).

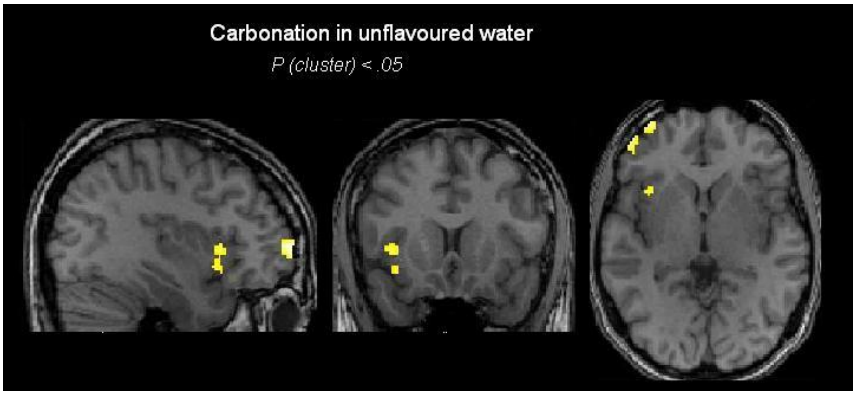

Fig 19. Effect of Carbonation on neural activity in unflavored solutions: The presence of CO2 in unflavored water (carbonated versus non-carbonated water) increased focally neural activity in the insula (AI) and orbitofrontal cortex (OFC).

To clarify the potential role of sour receptors co-activation in the carbonation-related responses, we analyzed the spatial distribution of neural activity related to sourness and carbonation within AI.

We found the response to both tastes presenting two insular clusters, with a clear spatial separation between their neural representations (Fig. 20) pointing against the hypothesis that the same cortical activity is elicited from sour- and carbonation-sensing pathways.

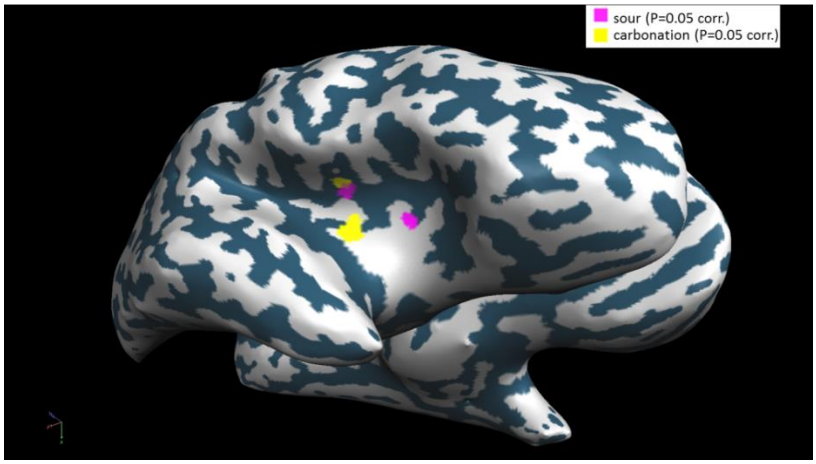

Fig. 20. Sour-carbonation co-activation: the peaks of brain activity related to carbonation and to sour taste compared with a baseline of water are represented on the partially inflated surface of brain hemispheres. Both tastes evoked neural activity with two distinct maxima in the insular cortex (P = 0.05 corr). Two peaks are located in the insular sulcus and appear partially overlapping, two peaks are located in the insular gyri and are well separated from each other.

4.2 Chemotopic representation of taste

4.2.1 Behavioral data

Behavioral data for each solution are reported in Tab. 1 together with the rate of taste identification.

	CO2	Umami	Sweet	Sour	Bitter	Salty
VAS	46 ± 30	40 ± 29	74 ± 19	54 ± 20	87 ± 14	65 ± 18
Identification	90%	90%	95%	80%	75%	100%

Tab.1 . Behavioral data: VAS ±SD and rate of taste identification.

4.2.2 fMRI data

Cortical activation maps showed higher main effects of the response to stimuli in the right insular cortex compare to the left, for all tastes, as reported in Table 2, where the Talairach coordinates and the T-statistic values are listed for peak activations.

	Right insula				**Left insula**			
	x	y	Z	T	x	y	z	T
Umami	28	4	14	5,28	-58	-32	18	4,2
Sour	32	0	12	6,26	-42	-20	-8	3,92
Bitter	34	-4	-4	4,86	-54	-32	18	2,84
CO2	38	-6	0	5,4	-38	10	2	3,88
Salty	36	-8	0	5,96	-56	-32	18	3,29
Sweet	40	-24	4	5,06	-48	4	6	3,1

Tab. 2. Talairach Coordinates: responses in the right insula were higher than in the left insula.

Cortical surface representation of insular activation of the standardized five basic tastes and CO2 is reported in Fig.21 for left and right hemispheres.

The prevalence map of the right insula showed the presence of three principal clusters of activation: i) a more posterior cluster of sweet-bitter and CO2, ii) a central cluster of CO2 and salty and iii) a more anterior cluster of umami-sweet and sour that is present in a well-corresponding location in the left insula.

In these maps, each voxel of the insular cortex is mapped with the taste that has the biggest response with a difference from the second most representative taste of at least three standard deviations (Fig 21). The maps demonstrate that each taste including CO2 has its own

cluster of prevalence representation, separated from the other tastes both in the right and left insular cortex.

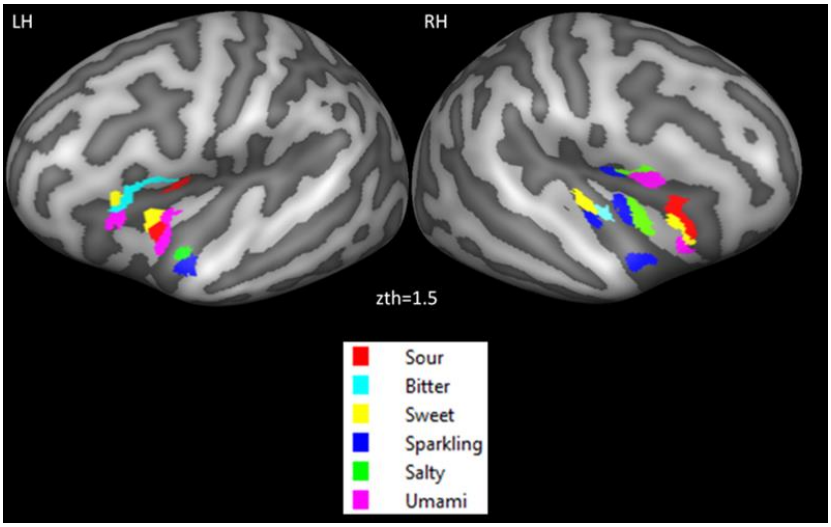

Fig. 21. Prevalence map: Each taste including CO2 has its own cluster of prevalence representation, separated from the other tastes both in the right and left insular cortex.

In Fig. 22 the non-prevalence information, calculated for the clusters of taste prevalence in the right insular cortex, is also shown for the cluster sweet-bitter-CO2 and umami-sweet-sour that are the only two for which there is a clear non-prevalence map. For the cluster sweet-bitter there is a non-prevalence map of umami and sour (Fig. 22), whereas for the cluster umami-sweet-sour there is a non-prevalence map for bitter, salty and CO2. In the left insula the coupling of tastes bitter-sweet, salt-CO2, umami-sweet-sour are also identifiable (albeit in different locations) in the right insula.

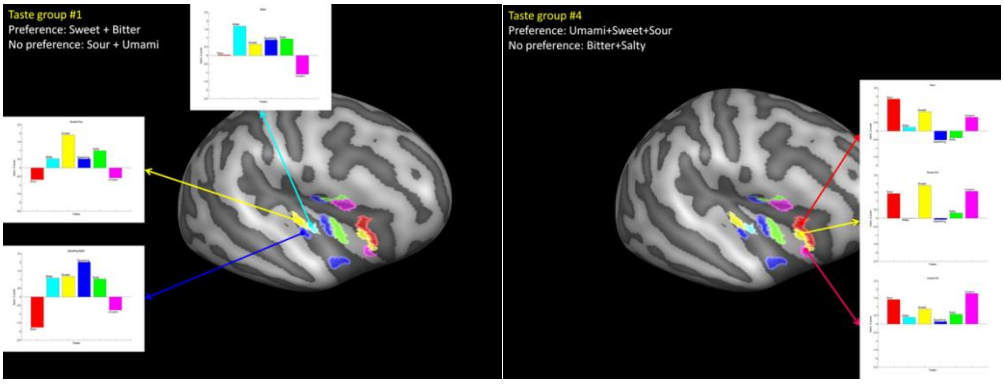

Fig.22. Non-prevalence map: The cluster sweet-bitter-CO2 and umami-sweet-sour are the only two for which there is a clear non-prevalence map. For the cluster sweet-bitter there is a non-prevalence map of umami and sour, whereas for the cluster umami-sweet-sour there is a non-prevalence map for bitter, salty and CO2. In the left insula the coupling of tastes bitter-sweet, salt-CO2, umami-sweet-sour are also identifiable (albeit in different locations) in the right insula.

5. DISCUSSION

Taste is the main sensory modality influencing food preferences and dietary behavior, and affecting body weight, aging, and health.

In contrast to the growing knowledge of the peripheral perceptual mechanisms, the central architecture of taste processing has been, so far, only partially understood.

For example, FO/AI, the putative hPTC, (Ogawa 1994, Small et al. 2003) is devoted to the analysis of taste identity and intensity, but its spatial architecture has not been evaluated yet (Schoenfeld et al. 2004).

Moreover, its functional organization is still unknown and there are many important questions not addressed yet. First, it is not known whether hPTC is characterized by chemotopical organization; second, the rules and the map of functional representation of gustatory qualities in hPTC, including their intensity, are still to be determined.

The same cortical region also codifies for the selective attention to “tastants” and for some non-gustatory information, such as perception of odorants, texture, temperature, and lingual somatosensory stimuli (Veldhuizen et al. 2007, de Araujo and Rolls 2004, Cerf-Ducastel et al. 2001).

Sight, smell, taste and texture of food activate the OFC, which is also involved in the processing of expectancy or prediction of a subsequent taste sensation. Specifically, this region is involved in the evaluation of food pleasantness, allowing the convergence of sensory and affective processing of taste, and underpinning the appreciation of its hedonic and reward-related aspects (Rolls and McCabe 2007).

In a broader perspective, the insula plays a key role in a wide range of brain processes, from viscerosensation and pain, to motivation and emotion, and possibly has also a role in the processing of empathy for emotional states (Jabbi et al. 2007).

In this study, we investigated the cortical representation of taste-related neural responses, the neural mechanisms underlying the perception of taste and the chemotopic organization of taste modalities in the hPTC. Furthermore, we studied the effect of CO2 on the brain processing of sweet stimuli, and its differential effect on sucrose and artificial sweeteners.

5.1 The effect of carbonation

Notwithstanding a growing body of literature on the peripheral perceptual mechanisms for sucrose and sugar substitutes (Frank et al. 2008, Smeets et al. 2011), the brain information processing relative to these two classes of substances, and, the differential modulation operated by other taste modalities are still to be fully unraveled.

For instance, in addition to the basic tastes (sweet, salty, sour, bitter, and umami), the taste system appears responsive to CO2, which powerfully modulates gustatory processing of basic tastes and of their combination (Chandrashekar et al. 2009).

Given the widespread use of CO2 in sweet beverages, the modulation of sweet perception is particularly interesting. Thus, CO2 may differently impact the neural processing of different sweet substances, affecting the liking of beverages containing sucrose or sugar substitutes (Kappes et al. 2007). Furthermore, mammals have multiple sensory modalities for CO2, including nociception, olfaction, and chemoreception, essential for respiratory regulation, yet their specific molecular mechanisms remain poorly defined (Simons et al. 1999).

Perception of CO2 is accompanied by trigeminal somatosensory stimulation, that creates a rich multisensory convergence of perceptual inputs, and may be underpinned in humans by evolutionary remnant traits indicating a nutrient-rich feeding environment.

5.1.1 Global effect of carbonation

The final percept of carbonation, both at peripheral and central level, seems to be a combination of multiple sensory inputs, including somatosensory and chemical sensations (Chandrashekar et al. 2009). Indeed, the chemical stimulation operated by CO2 can activate receptors for other senses (usually involved in pain, touch, and thermal perception) producing a sensation of irritation, mediated by the trigeminal nerve (TN) known as chemesthesis.

Chemesthesis is responsible for at least part of the perception of CO2 in beverages, of the hotness of a chili pepper, or coolness of menthol, and also plays a role in improving swallowing in individuals with dysphagia, probably through the enhancement of gustatory input to the NTS (Hu et al. 2007).

In addition to the enhancement of sourness perception, little is known about the modulation operated by CO2 on other tastes (Yau and McDaniel 1992). Of particular interest is the effect of carbonation on sweetness perception consisting in the reduction of sweetness perception depending on CO2 concentration (Yau and McDaniel 1992).

Contrasting with a growing knowledge on the peripheral perceptual mechanisms of sweetness, its central neural processing, and the modulation operated on sweetness by other taste modalities like CO2, are still to be unraveled (Smeets et al. 2011, Frank et al. 2008).

To date, there is no consistent evidence of the impact of carbonation on other tastes (Green 1996).

As a general rule, when taste compounds are mixed together in solution, they often interact with one another so that each tastant is

perceived differently than it would be alone at the same concentration. This could be due to enhancement and suppression phenomena based on peripheral, central and cognitive interactions.

In the present study, we investigated the central neural pathway in response to taste stimulation by sucrose or by a combination of Ac-As, a common sweetener used in diet formulations of beverages. In addition, we analyzed the modulation of sweet perception operated by carbonation, monitoring the changes in blood oxygenation with BOLD fMRI.

Many artificial sweeteners have an easily detectable aftertaste, commonly reduced by combining two or more high-intensity sweeteners. In particular, the combination of Ac-As has been reported to be more pleasant compared to aspartame alone (Kappes et al. 2007).

According to some authors, carbonation plays such a large role in the sensory profiles of beverages containing sugar and artificial sweeteners as to inhibit their perception and make the two classes of sweet substances virtually indistinguishable (Meyer and Riha 2002). This inhibitory effect may be considered favorable in the formulation of diet beverages, which are designed to be perceived as much similar as possible to regular ones but with a reduced caloric intake (Kappes et al. 2007).

Our data indicate that the presence of carbonation in sweet solutions, independently of the sweetening agent (sucrose or As-Ac), reduced neural activity in AI, OFC (Fig.17) and posterior pons, and the perceptual salience of sweetness as assessed by behavioral data (Fig. 16).

This neural effect was present in a widespread cortical and subcortical pattern (Fig.17). The effects of carbonation were largely independent of the sweetening agent present in the beverage.

This central inhibitory effect seems to mirror the peripheral “lateral inhibition” operated by type III cells, responsible for the perception of CO_2, on type II cells, responsible for the perception of sweet, via 5-HT, NA or GABA (Figg.4-5).

The negative modulation of behavioral taste sensitivity and neural processing of sweetness operated by carbonation deserves a discussion in the light of the increasing brain activity that carbonation is able to produce.

A somatosensory stimulation accompanies the presence of carbonation in beverages. The neural processing of lingual somatosensory perceptions extensively overlaps gustatory processing, particularly in the IC and the TO, justifying the inclusion of lingual somatosensory information as a major feature of flavor perception (Cerf-Ducastel et al. 2001).

CO_2 perception is accompanied by trigeminal somatosensory stimulation creating a rich multisensory convergence of perceptual inputs, and may be underpinned in humans by evolutionary remnant traits indicating a nutrient-rich feeding environment (Scott 2005).

For instance, TN is able to carry sensorial inputs from CO_2 with the complex mechanism of chemestesis, where a mixture of sensory information is used to ensure adequate behavioral responses to chemical irritants (like CO_2).

The neural correlates of chemestesis have been partly explored in a recent fMRI study (Iannilli et al. 2008) focusing on the first trigeminal branch (ophthalmic nerve), the authors reported an increase brain activity after intranasal CO_2 stimulation. This effect was particularly evident in the ACC, the primary and secondary somatosensory cortex (SI, SII), the IC, thalamus (Th), and PFC (Iannilli et al. 2008).

Translating this experimental framework to the mouth, as in our experiment, the sensory environment changes completely. In the presence of a double and simultaneous sensory input (chemestesic and gustatory) insisting on the same body topography, it is reasonable to expect a sensory prioritization, enhancing the most environmentally relevant and ecologically “necessary” of the two inputs in the light of a required consequent behavior.

If the sensory convergence includes the taste perception of sweetness which has a prevalent hedonic and caloric value, and the chemestesic perception of CO_2 whose purpose is to defend against chemical irritants, it is reasonable for the latter to prevail.

Along the same lines, the sensory convergence of chemestesis carrying information on local CO_2 concentration, and tastants that differ from sweetness with a reduced hedonic and caloric value, may have completely dissimilar behavioral effects.

Sourness, for instance, appears to be enhanced by carbonation (Yau and McDaniel 1992).

In our experimental setting, to clarify the specific neural correlates of carbonation alone and the potential role of sour receptors co-activation in the carbonation-related responses, we analyzed the effect of carbonation alone in unflavored water, without any associated sweet perception and the spatial distribution of neural activity related to sourness and carbonation within AI.

We found that CO_2 alone in unflavored water, without any associated sweet perception, markedly increased the activity of AI and OFC (Fig.19).

Furthermore our data demonstrated that the response to both tastes presented two insular clusters, with a clear spatial separation between their neural representations (Fig.20) suggesting that the same cortical activity is elicited from sour- and carbonation-sensing pathways.

5.1.2 Global effect of the sweetening agent

Different types of sweet stimuli (glucose and saccharin) cannot be distinguish on a range of subjective measures (sweetness, pleasantness and viscosity), despite their distinct neural representation (Chambers et al. 2009). In particular, glucose activates a number of brain regions that appear unresponsive to saccharin, including the ACC and the right caudate. These regions, in particular the dopaminergic pathways within the striatum, are believed to mediate the emotional and behavioral response to rewarding food stimuli (Rolls and McCabe 2007).

In animal models, sucrose activates taste afferents differently than artificial sweeteners, so that the brain receives the information about the caloric or non-caloric nature of a sweet stimuli; a correspondingly differentiated functional response has been recently demonstrated in humans as well (Frank et al. 2008).

In our experimental setting, a combination of two sweeteners (As-Ac) has been chosen, instead of saccharin, to reduce the perceptual impact of their single aftertastes. At the neural level, and independently of the carbonation (carbonated and non-carbonated beverages taken together), the effect of the sweetening agent (sucrose versus As-Ac) has shown a complex pattern. We detect the prevalence of neural activity in more “primary like” cortices─the right IC and the SGFMC for As-Ac stimulation, and a prevalent activity evoked by sucrose bilaterally in Amy─implicated in the emotional processing of stimuli, especially associated with reward and with hedonic related components (Fig.18).

Amy is also known to respond to stimulus significance, hunger and both aversive and pleasant taste stimuli, proportionally to emotional intensity (Smeets et al. 2011).

5.1.3 Differential effect of carbonation

In our study the effect of carbonation for each sweetening agent was much more evident in combination with sucrose than with As-Ac, and produced a relative decrease in taste-related activity in multiple brain regions.

Studies about taste interactions showed a consistent pattern of mixture suppression in which sucrose sweetness tended to be both the least suppressed quality and the strongest suppressor of other tastes (Green et al. 2010). The regulation of food intake is, among others, driven by a combination of sensory information, somatosensory signals of gastric fullness and chemical signals indicative of nutrient depletion.

Gastric distension, present incrementally in our experiment and in non-experimental conditions, may converge with taste-related CO2

effects on sweetness perception. To rule out gastric distension-related effects, our experimental design randomly intermixes taste stimuli presenting each stimulus 5 times and preventing any stimulus measurements to cluster in time. In this way, the linearly incremental factor of gastric distension is not able to weigh differentially our statistical analysis favoring any one of taste stimuli.

5.1.4 Differential effect of the sweetening agent

In the presence of carbonation, the difference in brain activity between As-Ac vs sucrose sweetened solutions was reduced. This piece of information is of utmost importance for the design of hypocaloric food and converges with the behavioral evidence that the interaction between carbonation and sweetening agents strongly attenuates the ability of the human brain to differentiate conventional sugar from artificial sweetening agents.

The presence of carbonation is able to strongly interact with the central processing of sweetness. Our data support the view that carbonation is able to interfere with sweetness perception, reducing the global sensitivity to sweetness. Proportionally it reduces more the sensitivity to sucrose than to artificial sweeteners and the perceptual difference between sucrose and As-Ac.

With regard to the regulation of food intake, the autonomic circuitry of the brainstem plays a critical role in the integration of homeostatic functions including regulation of food ingestion and GI functions. Specifically NTS neurons display heterogeneous properties and contribute to the integration of synaptic inputs from vagal afferent axons as well as inputs from higher regions in the central nervous system (Browning and Travagli 2011).

We speculate that taste information together with CO2 stimuli, which are also transmitted via cranial nerves to the NTS, may interact at this level, influencing food intake and dietary choices, integrating in this context information from and to the GI tract and other viscera.

5.2 Chemotopic representation of taste

In mammals, bitter and sweet and/or umami are the two main taste modalities evoking aversion and attraction, respectively. Humans also express pleasure for sweet taste but displeasure for bitter taste. On the other hand, mammals learn to reject a tastant if this taste is associated with subsequent visceral malaise. Therefore, it is likely that the mammalian gustatory system is an excellent system to address the question of how emotion interacts with cognition and memory (Sugita and Shiba 2005).

The hPTC is devoted to the analysis not only of taste identification but also of taste intensity. However, the different subjective perception of the same intensity of a given taste stimulus suggests a substantial variability in terms of neural representation among individuals (Schoenfeld et al. 2004).

Furthermore, it remains to be clarified whether hPTC is characterized by a chemotopical organization, as demonstrated in other sensory systems.

Many papers have addressed the taste representation in hPTC, but only Schoenfeld et al. (2004) designed the experiment to specifically search for a chemotopic organization of the five basic tastes. For instance, the authors reported separate, as well as overlapping, insular activations of the different tastes with the presence of an intra-subject variability that might have masked a group activation pattern.

To overcome the anatomical subjective variability in this study, we used a cortical alignment procedure that matches each sulcus of each subject in a common space using high resolution T1-w MR acquisitions.

We analyzed right and left insular cortices and reported both similarities and differences between the two hemispheres. Although evidence of bilateral insular processing of tastes has been reported in (Hummel, 2008, Kurth et al. 2010, Iannilli et al. 2012, Stevenson et al. 2013), there are differences in the role of the two hemispheres.

Notably, in a study on patients with either left or right insular lesions Stevenson et al. (2013) demonstrated that both sides of the tongue were processed by left and right insular cortices, but taste discrimination was better after right side stimulation, whereas taste quality judgments were better after left side stimulation. Furthermore, they reported that left insular lesions produced a selective deficit in processing salt-related information.

In addition, Kobayashi M et al. (2004) showed that the left insula was predominantly activated by gustatory imagery tasks rather than the gustatory task itself.

Our study was designed to stimulate the majority of taste buds because subjects held in their mouth 5 ml of solutions for 10 sec without any asymmetrical stimulation. Moreover, the concentration of the tastants was chosen to be easily detectable and distinguishable but not too strong.

Although the activation maps showed some similarities, after bilateral stimulation of the tongue we found a predominant activation of the right insular cortex for all tastants in terms of absolute statistical values, in accordance with the results of Schoenfeld et al. (2004).

In addition to the five basic tastes, we analyzed whether CO2 has its own representation in the PTC separated from sour with which it shares the same peripheral receptor mechanism. In the map of prevalence of the right insular cortex we found that all the five basic tastes plus CO2

have their own cluster representation distributing from the posteromedial to the anterior insular cortex (Fig.21).

Furthermore, there is growing evidence that many vertebrates and invertebrates use their gustatory system to detect the presence of other compounds that may include Ca^{2+}, water, fats, and CO2. Therefore, there could be cortical representations of other additional taste qualities (Liman et al. 2014).

Also, the analysis of the maps showed a more posterior cluster in which bitter and sweet were the most represented tastes and umami and sour the less represented tastes in that area (Fig.21). We found a central cluster anteriorly and a more anteriorly cluster in which CO2 and salt, and umami-sweet and sour were the most represented tastes respectively, and bitter and CO2 the less represented (Fig.21). More dorsally we found a cluster induced by CO2, salt and umami and more caudally a cluster activated by CO2.

In the map of prevalence (Fig.21) of the left insula we again recognize similar coupling among tastants, finding the same coupling of bitter and sweet, salt and CO2 and sweet-umami-sour, although taste clusters were more anterior than the cluster in the map of prevalence of the right insular cortex. Nevertheless, the difference in statistical power and the lack of a clear non-prevalence representations of tastants might point out a different role of the left insular cortex, in which the chemotopic representation of tastants might reflect additional processing other than identifications of tastants.

As suggested by Stevenson et al. (2013) left insular cortex might play a role in hedonic judgment of tastants. This is in agreement with Kobayashi et al. (2004) that reported a higher activation of the left insular cortex during imagery taste processing.

Overall, the chemotopic organization of the insular cortex seems to reflect the peripheral transduction machinery orchestrated by distinct populations of selectively tuned cells, which express specific receptors for different taste gustatory stimuli, clustered to form taste buds (Fig.6).

5.2.1 Bitter-Sweet-Umami

In our experiment (Fig.6) we found two different clusters of bitter-sweet-umami selective coupling; a cluster in which bitter and sweet were represented next to each other without umami and a second cluster in which umami and sweet were represented without bitter (Fig.22).

Among taste receptors, sweet, umami, and bitter receptors are the best characterized. They are detected by 2 distinct families of G-protein–coupled receptors (GPCRs) and are important for food acceptance (Fig.7).

Sweet and bitter are considered behavioral opposite tastes with some chemical similarities. Bitter and sweet tastants, both natural and synthetic, belong to a very large number of chemical families and in many cases slight structural modifications may change a sweet molecule into a bitter one. Moreover, at specific concentration, some sweet compounds such as acesulfame-k and saccharin, have a distinct bitter aftertaste and viceversa (Kuhn et al. 2004, Temussi 2009). As it turns out, at high concentration these two artificial sweeteners not only activate the sweet taste receptor (Nelson et al. 2001, Li et al. 2002), but they also activate specific bitter receptors (Kuhn et al. 2004, Pronin et al. 2007). This observation may explain the characteristic “aftertaste” associated with these tastants (Yarmolinsky et al. 2009).

Although the relationship between sweet and bitter tastes is influenced by concentration, the main cause of changing tastes is the chemical isomerism (Temussi 2009). The most common pairs of bitter-sweet compounds derive from positional isomers of aromatic compounds and from congeners, conformational analogues and optical isomers (Temussi 2009).

Moreover, sweet-bitter taste interactions are almost always suppressive as shown in hamster, in which sucrose-best neurons showed significant suppression to quinine-sucrose mixtures compared to sucrose alone (Formaker et al.1997).

On the basis of this evidence it was hypothesized that there are mutual inhibitory mechanisms mediating responsive to appetitive and aversive taste stimuli (Tokita and Boughter 2012) and that this mutual suppression of bitter and sweet tastes is due to neural inhibition rather than chemical interactions (Lawless 1979). The presence of the cluster sweet-bitter, found in insular cortex, might be in favor of this hypothesis in the sense that the prevalence inhibits the adjacent area and viceversa, similar to the lateral inhibition process in other sensory cortex (Najac et al. 2015).

Moreover, Tokita et al. (2012) showed a stronger suppressive effect of quinine hydrochloride (bitter) on sweet than on umami compounds. Thus the absence of inhibitory effect of quinine on umami is compatible with the representation in our chemotopic map of two far away areas of bitter and umami clusters and with the mutually exclusive prevalence and non-prevalence of the two tastants (Fig.22).

Mammals have essentially only one sweet receptor, the T1R2-T1R3 heterodimer (Fig.6), so the wide range of substances recognized by sweet receptors cannot be explained in terms of an equal or similar number of sweet receptors.

On the other hand, our findings showed that sweet is double represented in both right and left insula, suggesting a more distributed processing at cortical level. The presence of a cluster of sweet taste in the anterior part of the insular cortex associated with a negative

prevalence of bitter, might also suggest the existence of emotional implications related to the sweet taste and is shown by Small et al. (2003) that reported valence-specific responses in anterior insula/operculum to sweet compared to bitter solutions.

The cortical representation of the sweet-umami cluster (Fig.21) might reflect a characteristic of acesulfame-k (sweet) and monosodium glutamate (umami), since it has been shown that they are the only apparent cases of synergism. i.e. a mixture of the two components elicits responses stronger than any linear model would predict based on their tastes when unmixed (Breslin 1996).

5.2.2 Sour-Salt-Carbonation

As previously discussed, sour and salt are sensed by ion channels and molecular mechanisms for sour and CO2 perception are related to each other. For instance, PKD2L1-expressing cells are required for the taste response to CO2. This response depends on a membrane-anchored carbonic anhydrase isoform 4, Car4 (Chandrashekar et al. 2009), which converts CO2+H2O into H+ + HCO3 (Fig.10). Although the mechanism by which Car4 contributes to the activation of sour cells is still unclear (Liman et al. 2014), our results confirmed our previous findings (Di Salle et al. 2013). Indeed, our map showed two distinct activation areas for CO2 and sour in the insular cortex. In particular, sour was located more frontally and CO2 in the middle insular cortex in a cluster coupled to salt.

Salt seems to have a double behavioral meaning, since it can be attractive or aversive depending on concentration. For instance, lower concentrations (<100 mM) evoke attractive behavior. This phenomenon reflects the fact that low levels of salt are necessary to maintain muscle contraction, action potentials, and many other physiological functions, whereas excessive salt intake is deleterious and in humans can lead to hypertension.

A similar behavioral dichotomy has also been demonstrated for CO2. Thus, it is likely that CO2 sensing would follow the same finality of behavioral guidance evolved as a mechanism to recognize CO2-producing sources, to avoid fermenting foods or, conversely, to search for them.

In Drosophila, CO2 perception has behaviorally divergent effects, depending on the sense perceptually involved, with avoidance caused by olfactory detection and acceptance by gustatory detection (Fischler et al. 2007). This latter may be grounded in the feeding convenience of detecting the production of CO2 by growing microorganisms, allowing fruitflies to identify and consume nutrients that these microorganisms provide. On the contrary, the olfactory detection of CO2 in the air may

signal unfavorable conditions such as hypoxia, presence of macroorganisms, overly rotten fruit or stressful environments.

Furthermore, subunit of sodium channel ENaC are detected in a wide range of cell types, including PKD2L1-expressing and TRPM5-expressing cells (Liman et al. 2014).

At cortical level sour cluster is located in the anterior part of the insular cortex close to sweet in a region, where CO2 is the less represented tastant (Fig.22).

Regarding the peripheral sour-sweet coupling it is well known that type II cells deputed to the perception of sweet, bitter and umami, and type III cells deputed to the perception of sour, communicate to each other (Figg.4-5).

In addition, each cell releases different neurotransmitters (Huang et al. 2007). To date, type II cells are known to release ATP, type III cells on the other hand, secrete serotonin (5-HT) and norepinephrine (NE).

When sweet (or bitter, or umami) tastants excite taste buds, ATP secreted from type II cells stimulates gustatory afferent nerve fibers. At the same time, ATP also excites adjacent presynaptic cells and stimulates them to release 5-HT and/or NE (Fig.4-5). Thus, sweet (or bitter, umami) stimulation of taste buds directly excites type II cells and indirectly activates type III cells. Probably, this interaction occurs also at cortical level and is stronger for the sweet and umami than for bitter as suggested by sweet-sour coupling.

Another interesting interaction between sweet and sour tastes is the taste-modifying activity converting sour stimuli to sweetness mediated by miraculin, a homodimeric protein isolated from the red berries of Richadella dulcifica (Koizumi 2011). Miraculin refers to the ability of miracle berry to change sour taste into sweet. At neutral pH, the active component of the berry, the protein miraculin, binds the T1R2/T1R3 receptor with high affinity, but it does not activate the receptor. A switch to acid pH (4,8-6,5) change the conformation and causes the bound ligand to become a strong agonist, eliciting a sweet sensation.

In conclusion, the prevalence and non-prevalence maps show that insular subregions respond most robustly to a single taste modality (sweet, bitter, umami, sour, salt or CO2) and do not respond at all to others modalities. This functional organization is similar to that seen at the peripheral level, where, as suggested by the “labelled line” coding model, receptor cells are tuned to respond prevalently to single taste modalities and are innervated by individually tuned nerve fibers, carrying the totality of the information on separated pathways.

6. CONCLUSIONS

In conclusion, these findings provide insightful information on the central architecture of taste processing with the application of fMRI technique, elucidating, from a behavioral point of view, some peripheral molecular mechanisms.

Our data suggest that CO2 modulates sweetness perception, reducing the perception of natural and artificial sweetener with a stronger reduction of sucrose processing. Furthermore, the gustatory system seems responsive to CO2, both at peripheral and central levels. Indeed, CO2 shows its own cortical representation, separated from sour, with which CO2 shares a similar peripheral mechanism.

Thus, CO2 appears to be the sixth taste.

The ability of brain to differentiate between the different types of sweeteners is intriguing and provocative. Indeed, tricking the brain about the type of sweet could be advantageous to weight loss because it facilitates the consumption of low-calorie drinks because their taste is perceived as pleasant as the sugary equivalent. However, the altered energy homeostasis and balance induced by the reduced sweetness perception might stimulate sugar consumption.

This interpretation might better explain the prevalence of eating disorders, metabolic diseases, and obesity among diet soda drinkers.

Future studies that combine analysis of carbonation effect on other taste modalities detection in taste buds and responses elicited by the carbonated sweetened beverages in the gastrointestinal lumen, are required to elucidate the puzzling link between reduced calorie intake with diet drinks and increased incidence of obesity and metabolic diseases.

Furthermore, this study clarified some aspects of functional organization of hPTC, that that display a well defined chemotopical organization, very similar to that seen in other sensory systems. In particular, we found taste coupling in the chemotopy of the human insular cortex.

Overall, the chemotopic organization of the insular cortex seems to reflect the peripheral transduction machinery orchestrated by distinct populations of selectively tuned cells, which express specific receptors for different gustatory stimuli, clustered to form taste buds.

7. ACKNOWLEDGEMENTS

I am very grateful to Prof. Enrico Avvedimento for his support and precious advice.

I would like to express my special thanks to Prof. Maurizio Iengo for encouraging my research and for allowing me to grow as a research scientist. Your advice on both research as well as on my career have been priceless.

8. REFERENCES

Abdollahi RO, Kolster H, Glasser MF, Robinson EC, Coalson TS, Dierker D, Jenkinson M, Van Essen DC, Orban GA. Correspondences between retinotopic areas and myelin maps in human visual cortex. NeuroImage 2014;99:509-524.

Afif A, Mertens P. Description of sulcal organization of the insular cortex. Surgical and Radiologic Anatomy 2010; 32: 491–98.

Auffarth B. Understanding smell-the olfactory stimulus problem. Neuroscience and biobehavioral reviews 2013;37:1667-1679.

Augustine J R. Circuitry and functional aspects of the insular lobe in primates including humans. Brain Research Reviews 1996;22: 229–44.

Bandettini PA, Wong EC, Hinks RS, Tikofsky RS, Hyde JS. Time-course EPI of human brain function during task activation. Magn Reson Med. 1992;25:390 – 7.

Bartel DL, Sullivan SL, Lavoie EG, Sévigny J, Finger TE. Nucleoside triphosphate diphosphohydrolase-2 is the ecto-ATPase of type I cells in taste buds. J Comp Neurol 2006;497:1–12.

Bray S, Amrein H. A putative Drosophila pheromone receptor expressed in male-specific taste neurons is required for efficient courtship. Neuron 2003;39:1019–29.

Breslin PA. Interactions among salty, sour and bitter compounds. trends in foods science &technology 1996;7:390-399.

Breza JM, Nikonov AA, Contreras RJ. Response latency to lingual taste stimulation distinguishes neuron types within the geniculate ganglion. J Neurophysiol 2010;103:1771–84.

Browning KN, Travagli RA. Plasticity of vagal brainstem circuits in the control of gastrointestinal function. Auton Neurosci. 2011;161:6-13.

Butti C, Hof, PR. The insular cortex: a comparative perspective. Brain Structure and Function 2010;214: 477–93.

Carleton A, Accolla R, Simon SA. Coding in the mammalian gustatory system. Trends in Neurosciences 2010; 33:326–34.

Cerf-Ducastel B, Van de Moortele PF, MacLeod P, Le Bihan D, Faurion A. Interaction of gustatory and lingual somatosensory perceptions at the cortical level in the human: a Functional Magnetic Resonance Imaging study. Chem Senses 2001; 26: 371-383.

Chambers ES, Bridge MW, Jones DA. Carbohydrate sensing in the human mouth: effects on exercise performance and brain activity J Physiol. 2009; 587:1779–94.

Chandrashekar J, Hoon MA, Ryba NJ, Zuker CS. The receptors and cells for mammalian taste. Nature. 2006;444:288-94.

Chandrashekar J, Yarmolinsky D, von Buchholtz L, Oka Y, Sly W, Ryba NJ, Zuker CS The taste of carbonation. Science 2009; 326:443-45.

Chandrashekar J, Kuhn C, Oka Y, Yarmolinsky DA, Hummler E, Ryba NJ, Zuker CS. The cells and peripheral representation of sodium taste in mice. Nature 2010; 464:297–301.
Chen X, Gabitto M, Peng Y, Ryba NJ, Zuker CS. A gustotopic map of taste qualities in the mammalian brain. Science 2011;333:1262-1266.
Chaudhari N, Roper SD. The cell biology of taste. Journal of Cell Biology. 2010;190:285–96.
de Araujo IE, Rolls ET, Representation in the human brain of food texture and oral fat. J Neurosci 2004;24:3086-93.
De Martino F, Moerel M, van de Moortele PF, Ugurbil K, Goebel R, Yacoub E, Formisano E. Spatial organization of frequency preference and selectivity in the human inferior colliculus. Nature communications. 2013;4:1386.
Di Salle F, Cantone E, Auletta G, Marciano E. Functional dissection of auditory cortex with magnetic resonance imaging. Audiological Medicine 2010; 8: 88–99
Di Salle F, Cantone E, Savarese MF, Aragri A, Prinster A, Nicolai E, Sarnelli G, Iengo M, Buyckx M, Cuomo R. Effect of carbonation on brain processing of sweet stimuli in humans. Gastroenterology 2013;145:537-9.
Drayna D. Human taste genetics. Annu Rev Genomics Hum Genet 2005; 6:217–35.
Dvoryanchikov G, Sinclair MS, Perea-Martinez I, Wang T, Chaudhari N. Inward rectifier channel, ROMK, is localized to the apical tips of glial-like cells in mouse taste buds. J Comp Neurol 2009;517:1–14.
Fedorenko E, Hsieh PJ, Nieto-Castanon A, Whitfield-Gabrieli S, Kanwisher N. New method for fMRI investigations of language: defining ROIs functionally in individual subjects. Journal of neurophysiology 2010,104:1177-1194.
Finger TE, Danilova V, Barrows J, Bartel DL, Vigers AJ, Stone L, Hellekant G, Kinnamon SC. ATP signaling is crucial for communication from taste buds to gustatory nerves. Science. 2005; 310:1495–99.
Fischler W, Kong P, Marella S, Scott K. The detection of carbonation by the Drosophila gustatory system. Nature. 2007;448:1054-57.
Formaker BK, MacKinnon BI, Hettinger TP, Frank ME. Opponent effects of quinine and sucrose on single fiber taste responses of the chorda tympani nerve. Brain research. 1997;772:239-242.
Frank GKW, Oberndorfer TA, Simmons AN, Paulus MP, Fudge JL, Yang TT, Kaye WH. Sucrose activates human taste pathways differently from artificial sweetener. NeuroImage. 2008;39:1559-69.
Frommer WB. Biochemistry. CO2mmon sense. Science 2010; 327:275-76.

Frost MA, Goebel R. Measuring structural-functional correspondence: spatial variability of specialised brain regions after macro-anatomical alignment. NeuroImage 2012;59:1369-1381.
Frost MA, Esposito F, Goebel R. Improved correspondence of resting-state networks after macroanatomical alignment. Human brain mapping 2014;35:673-682.
Gasquoine PG. Contributions of the insula to cognition and emotion. Neuropsychol Rev 2014;24:77-87.
Goebel R, Esposito F, Formisano E. Analysis of functional image analysis contest (FIAC) data with BrainVoyager QX: From single-subject to cortically aligned group general linear model analysis and self-organizing group independent component analysis. Human brain mapping 2006;27:392-401.
Grammer K, Fink B, Neave N. Human pheromones and sexual attraction. Eur J Obstet Gynecol Reprod Biol 2005;118:135–42.
Green BG. Chemesthesis: pungency as a component of flavor. Trends Food Sci Technol. 1996;7:415–20.
Green BG, Lim J, Osterhoff F, Blacher K, Nachtigal D. Taste mixture interactions: Suppression, additivity, and the predominance of sweetness. Physiol Behav. 2010;101:731–37
Haase L, Cerf-Ducastel B, Murphy C. Cortical activation in response to pure taste stimuli during the physiological states of hunger and satiety. NeuroImage 2009;44:1008-21.
Herdener M, Esposito F, Scheffler K, Schneider P, Logothetis NK, Uludag K, Kayser C. Spatial representations of temporal and spectral sound cues in human auditory cortex. Cortex; a journal devoted to the study of the nervous system and behavior 2013;49:2822-33.
Hu J, Zhong C, Ding C, Chi Q, Walz A, Mombaerts P, Matsunami H, Luo M. Detection of Near-Atmospheric Concentrations of CO2 by an Olfactory Subsystem in the Mouse. Science. 2007; 317, 953.
Huang AL, Chen X, Hoon MA, Chandrashekar J, Guo W, Trankner D, et al. The cells and logic for mammalian sour taste detection. Nature 2006; 442:934–8.
Huang YJ, Maruyama Y, Dvoryanchikov G, Pereira E, Chaudhari N, Roper SD. The role of pannexin 1 hemichannels in ATP release and cell-cell communication in mouse taste buds. Proc Natl Acad Sci U S A. 2007;104:6436-41.
Huang YA, Dando R,. Roper SD. Autocrine and paracrine roles for ATP and serotonin in mouse taste buds. J. Neurosci 2009; 29:13909–18.
Hubel DH, Wiesel TN. Early exploration of the visual cortex. Neuron 1998;20:401-12.
Hummel T, Welge-Luessen A. Taste and smell, an update. Basel: Kurger; 2006.
Hummel T. Retronasal perception of odors. Chemistry & biodiversity 2008;5:853-861.

Humphries C, Liebenthal E, Binder JR. Tonotopic organization of human auditory cortex. NeuroImage 2010;50:1202-1211.
Iannilli E, Del Gratta C, Gerber JC, Romani GL, Hummel T. Trigeminal activation using chemical, electrical, and mechanical stimuli. Pain. 2008; 139:376-88.
Iannilli E, Singh PB, Schuster B, Gerber J, Hummel T. Taste laterality studied by means of umami and salt stimuli: an fMRI study. NeuroImage 2012;60:426-435.
Iannilli E, Noennig N, Hummel T, Schoenfeld AM. Spatio-temporal correlates of taste processing in the human primary gustatory cortex. Neuroscience. 2014;273:92-9.
Jabbi M, Swart M, Keysers C. Empathy for positive and negative emotions in the gustatory cortex. NeuroImage. 2007;34: 1744–53
Kami YN, Goto TK, Tokumori K, Yoshiura T, Kobayashi K, Nakamura Y, Honda H, Ninomiya Y, Yoshiura K. The development of a novel automated taste stimulus delivery system for fMRI studies on the human cortical segregation of taste. J Neurosci Methods 2008; 172: 48–53.
Kappes SM, Schmidt SJ, Lee SY. Relationship between physical properties and sensory attributes of carbonate beverages. J Food Sci. 2007; 72:1-11.
Kaushal NK, Lal Kaushal BB, Sharma PC. Optimization of total soluble solids and carbon dioxide gas pressure for the preparation of carbonated beverages from apple and pear juices. J Food Sci Technol. 2004;41:142–9.
Koizumi A, Tsuchiya A, Nakajima K, Ito K, Terada T, Shimizu-Ibuka A, Briand L, Asakura T, Misaka T, Abe K. Human sweet taste receptor mediates acid-induced sweetness of miraculin. Proc Natl Acad Sci U S A. 2011;108:16819-24.
Kuhn C, Bufe B, Winnig M, Hofmann T, Frank O, Behrens M, Lewtschenko T, Slack JP, Ward CD, Meyerhof W. Bitter taste receptors for saccharin and acesulfame K. The Journal of neuroscience: the official journal of the Society for Neuroscience. 2004;24:10260-65.
Kobayashi M, Takeda M, Hattori N, Fukunaga M, Sasabe T, Inoue N, Nagai Y, Sawada T, Sadato N, Watanabe Y. Functional imaging of gustatory perception and imagery: "top-down" processing of gustatory signals. NeuroImage 2004;23:1271-82.
Kurth F, Zilles K, Fox PT, Laird AR, Eickhoff SB. A link between the systems: functional differentiation and integration within the human insula revealed by meta-analysis. Brain structure & function 2010;214:519-34.

Lawton DM, Furness DN, Lindemann B, Hackney CM. Localization of the glutamate-aspartate transporter, GLAST, in rat taste buds. Eur. J. Neurosc. 2000; 12:3163–3171.
Li X, Staszewski L, Xu H, Durick K, Zoller M, Adler E. Human receptors for sweet and umami taste. Proceedings of the National Academy of Sciences of the United States of America. 2002;99:4692-96.
Liman ER, Zhang YV, Montell C. Peripheral coding of taste. Neuron. 2014;81:984-1000.
Lindemann B. Receptor seeks ligand: on the way to cloning the molecular receptors for sweet and bitter taste. Nat Med 1999; 5:381–82.
Lawless HT. Evidence for neural inhibition in bittersweet taste mixtures. Journal of comparative and physiological psychology 1979;93:538-547.
Lundström JN, Boesveldt S, Albrecht J. Central Processing of the Chemical Senses: an Overview ACS Chem Neurosci 2011;2:5-16.
Marciani L, Pfeiffer J C, Hort J, Head K, Bush D, Taylor AJ, Spiller RC, Francis S, Gowland PA. Improved methods for fMRI studies of combined taste and aroma stimuli. J Neurosci Methods. 2006; 158:186–194.
Meyer S, Riha WE. Optimizing sweetener blends for low-calorie beverages. Food Technol 2002;56:42–5.
Mesulum MM, Mufson EJ. Insula of the old world monkey. I. Architectonics in the insula-orbito-temporal component of the paralimbic brain. Journal of Comparative Neurology 1982; 212: 1–22.
Michlig S, Damak S, Le Coutre J. Claudin-based permeability barriers in taste buds. J Comp Neurol 2007;502:1003–11.
Miller IJ Jr. Anatomy of the peripheral taste system. In: Doty RL editor. Handbook of olfaction and gustation. NY: Marcel Dekker; 1995. p. 521-47.
Murray RG. Cellular relations in mouse circumvallate taste buds. Microsc. Res Tech 1993;26:209–24.
Najac M, Sanz Diez A, Kumar A, Benito N, Charpak S, De Saint Jan D. Intraglomerular lateral inhibition promotes spike timing variability in principal neurons of the olfactory bulb. J Neurosci. 2015; 11;35:4319-31.
Nelson G, Hoon MA, Chandrashekar J, Zhang Y, Ryba NJ, Zuker CS. Mammalian sweet taste receptors. Cell 2001;106:381-390.
Ogawa S, Lee TM, Kay AR, Tank DW. Brain magnetic resonance imaging with contrast dependent on blood oxygenation. Proc Natl Acad Sci U S A. 1990;87:9868-72.
Ogawa H. Gustatory cortex of primates: anatomy and physiology. Neurosci. 1994;20:1–13.

Okubo T, Clark C, Hogan BL. Cell lineage mapping of taste bud cells and keratinocytes in the mouse tongue and soft palate. Stem Cells 2009; 27:442–50.
Phillips ML, Young AW, Senior C, Brammer M, Andrew C, Calder AJ, Bullmore ET, Perrett DI, Rowland D, Williams SC, Gray JA, David AS A specific neural substrate for perceiving facial expressions of disgust. Nature. 1997; 389: 495–498.
Pronin AN, Xu H, Tang H, Zhang L, Li Q, Li X. Specific alleles of bitter receptor genes influence human sensitivity to the bitterness of aloin and saccharin. Current biology: CB 2007;17:1403-08.
Rolls ET, McCabe C. Enhanced affective brain representations of chocolate in cravers vs. non-cravers. European Journal of Neuroscience 2007; 26: 1067–76
Roper SD. Taste buds as peripheral chemosensory processors. Semin Cell Dev Biol 2013;24:71-9.
Rudenga K, Green B, Nachtigal D, Small DM. Evidence for an integrated oral sensory module in the human anterior ventral insula. Chemical senses 2010;35:693-703.
Sabuncu MR, Yeo BT, Van Leemput K, Vercauteren T, Golland P. Asymmetric image-template registration. Medical image computing and computer-assisted intervention: MICCAI International Conference on Medical Image Computing and Computer-Assisted Intervention 2009:12:565-573.
Scalfani A. Sweet taste signaling in the gut PNAS. 2007; 104:14887-8.
Seifritz E, Di Salle F, Esposito F, Herdener M, Neuhoff JG, Scheffler K. Enhancing BOLD response in the auditory system by neurophysiologically tuned fMRI sequence. NeuroImage. 2006; 29:1013-1022.
Schneider KA, Richter MC, Kastner S. Retinotopic organization and functional subdivisions of the human lateral geniculate nucleus: a high-resolution functional magnetic resonance imaging study. The Journal of neuroscience : the official journal of the Society for Neuroscience 2004;24:8975-8985.
Schoenfeld MA, Neuer G, Tempelmann C, Schussler K, Noesselt T, Hopf JM, Heinze HJ. Functional magnetic resonance tomography correlates of taste perception in the human primary taste cortex. Neuroscience 2004;127:347-353.
Scott K. Taste recognition: food for thought. Neuron 2005; 48:455-64.
Scott TR, Plata-Salaman CR. Taste in the monkey cortex. Physiology & behavior 1999,67:489-511.
Shigemura N, Shirosaki S, Sanematsu K, Yoshida R, Ninomiya Y. Genetic and molecular basis of individual differences in human umami taste perception. PLoS One 2009;4:6717.
Simons CT, Dessirier JM, Carstens MI, O'Mahony M, Carstens E.Neurobiological and Psychophysical Mechanisms Underlying the

Oral Sensation Produced by Carbonated Water. J. Neurosci. 1999; 19: 8134.
Small DM, Prescott J. Odor/taste integration and the perception of flavor. Exp Brain Res 2005; 166:345–57.
Small DM, Gregory MD, Mak YE, Gitelman D, Mesulam MM, Parrish T. Dissociation of neural representation of intensity and affective valuation in human gustation. Neuron 2003;39:701-711.
Small DM Taste representation in the human insula. Brain Struct Funct. 2010; 214:551–61.
Smeets P, Weijzen P, de Graaf C, Viergever MA.Consumption of caloric and non-caloric versions of a soft drink differentially affects brain activation during tasting. NeuroImage. 2011;54:1367–74.
Smits M, Peeters R, van Hecke P, Sunaert S. A 3 T event-related functional magnetic resonance imaging (fMRI) study of primary and secondary gustatory cortex localization using natural tastants. Neuroradiology. 2007; 49:61–71.
Steiner JE. The gustofacial response: observation on normal and anencephalic newborn infants. Symp Oral Sens Percept 1973;4:254–278
Steiner JE. Discussion paper: innate, discriminative human facial expressions to taste and smell stimulation. Ann NY Acad Sci 1974;237:229–33.
Sternini C. In search of a role for carbonation: is this a good or bad taste? Gastroenterology 2013;145:500-3.
Stettler DD, Axel R. Representations of odor in the piriform cortex. Neuron 2009; 63:854-64.
Stevenson RJ. An initial evaluation of the functions of human olfaction. Chem Senses 2010;35:3–20.
Stevenson RJ, Miller LA, McGrillen K. The lateralization of gustatory function and the flow of information from tongue to cortex. Neuropsychologia 2013;51:1408-16.
Sugita M, Shiba Y. Genetic tracing shows segregation of taste neuronal circuitries for bitter and sweet. Science. 2005;309:781-5.
Tokita K, Boughter JD. Sweet-bitter and umami-bitter taste interactions in single parabrachial neurons in C57BL/6J mice. Journal of neurophysiology. 2012;108:2179-90.
Talairach J, Tournoux P. Co-planar stereotaxic atlas of the human brain. New York: Thieme Medical Publishers; 1988.
Temussi PA. Sweet, bitter and umami receptors: a complex relationship. Trends Biochem Sci 2009;34:296-302.
Tomchik SM, Berg S, Kim JW, Chaudhari N, Roper SD. Breadth of tuning and taste coding in mammalian taste buds. Journal of Neuroscience 2007; 27:10840–8.
Vandenbeuch A, Clapp TR, Kinnamon SC. Amiloride-sensitive channels in type I fungiform taste cells in mouse. BMC Neurosci 2008; 9:1.

Veldhuizen MG, Bender G, Constable R T, Small DM. Trying to detect taste in a tasteless solution: modulation of early gustatory cortex by attention to taste. Chem. Senses. 2007;32:569–81.
Veldhuizen MG, Albrecht J, Zelano C, Boesveldt S, Breslin P, Lundström JN. Identification of human gustatory cortex by activation likelihood estimation. Hum Brain Mapp 2011; 32:2256–66.
Yamamoto K, Ishimaru Y. Oral and extra-oral taste perception. Semin Cell Dev Biol. 2013;24:240-46.
Yarmolinsky DA, Zuker CS, Ryba NJ. Common sense about taste: from mammals to insects. Cell, 2009;139:234-44.
Yau NJN, McDaniel MR. Carbonation interactions with sweetness and sourness. J Food Sci. 1992;57:1412–16.
Welge-Luessen A, Hummel T. Management of Smell and Taste Disorders. New York: Thieme Medical Publishers; 2013.
Wyatt TD. Introduction to Chemical Signaling in Vertebrates and. In: Mucignat-Caretta C, editor. Neurobiology of Chemical Communication. Boca Raton (FL): CRC Press; 2014. p.1-29.

9. LIST OF PUBLICATIONS

1) Di Salle F, **Cantone E**, Savarese MF, Aragri A, Prinster A, Nicolai E, et al. ***Effect of carbonation on the brain processing of sweet stimuli in humans***. Gastroenterology. 2013;145:537-539.

2) **Cantone E**, Prinster A, Cuofano R, Lullo AMD, Cuomo R, et al. ***CO2 Modulates the Central Neural Processing of Sucrose Perception.*** J Neurol Disord 2015;3:200.

3) Manara R, Salvalaggio A, Favaro A, Palumbo V, Citton V, Elefante A, Brunetti A, Di Salle F, Bonanni G, Sinisi AA; *for the Kallmann Syndrome Neuroradiological Study Group*. **Cantone E**. member of the Kallmann Syndrome Neuroradiological Study Group. ***Brain changes in Kallmann syndrome***. Am J Neuroradiol. 2014 Apr 30.

4) Manara R, Salvalaggio R, Citton V, V, D'Errico A, Elefante A, Briani C, **Cantone E**, et al. ***Brain anatomical substrates of mirror movements in Kallmann syndrome***. Neuroimage 2015, Jan 1;104:52-8.

Gastroenterology

www.gastrojournal.org Volume 145 Number 3 September 2013

Fizzy Drinks & Sugar Cravings

The Effects of Carbonation on Brain Processing of Sweets

OFFICIAL JOURNAL OF THE AGA INSTITUTE

BRIEF REPORTS

Effect of Carbonation on Brain Processing of Sweet Stimuli in Humans

FRANCESCO DI SALLE,[1,2] ELENA CANTONE,[3,4] MARIA FLAVIA SAVARESE,[5] ADRIANA ARAGRI,[1] ANNA PRINSTER,[6] EMANUELE NICOLAI,[7] GIOVANNI SARNELLI,[5] MAURIZIO IENGO,[3] MAXIME BUYCKX,[8] and ROSARIO CUOMO[5]

[1]Department of Medicine, Salerno University, Salerno, Italy; [2]Department of Cognitive Neuroscience, Faculty of Psychology and Neuroscience, Maastricht University, Maastricht, The Netherlands; [3]ENT Department, [4]Department of Molecular and Cellular Biology and Pathology, and [5]Gastroenterology Unit, Department of Clinical Medicine and Surgery, "Federico II" University, Naples, Italy; [6]Biostructure and Bioimaging Institute, National Research Council, Naples, Italy; [7]IRCCS-SDN Foundation, Naples, Italy; and [8]Nutrition and Health, The Coca-Cola Company, Atlanta, Georgia

See Covering the Cover synopsis on page 493; see editorial on page 500.

Little is known about how CO_2 affects neural processing of taste. We used functional magnetic resonance imaging to investigate the effects of carbonation on brain processing of sweet stimuli, which has relevance to studies of food selection and satiety. The presence of carbonation produced an overall decrease in the neural processing of sweetness-related signals, especially from sucrose. CO_2 reduced the neural processing of sucrose more than that of artificial sweeteners. These findings might be relevant to dietary interventions that include noncaloric beverages, whereas the combination of CO_2 and sucrose might increase consumption of sucrose.

Keywords: Gustatory System; fMRI; Beverage Consumption; Brain.

Taste is the main sensory modality influencing food preferences and dietary behavior and affecting body weight, risk of chronic disease, and health. While we typically appreciate a food's overall flavor as a gestalt comprising taste, smell, and somatosensory information, taste has the last word in identifying a potential food. The acceptance of a sweet taste signaling calories, and the rejection of a strongly bitter taste warning against toxins, are brain stem reflexes that appear prenatally in humans and are modified during life but are never removed by experience.[1] Knowledge of the central neural processing of taste is still largely incomplete. It involves the anterior insula (AI) and frontal operculum (human primary taste cortex), opercular cortex and orbitofrontal cortex (OFC), amygdala (Amy), and prefrontal cortex.[2] In addition to basic tastes (sweet, salty, sour, bitter, and umami), the gustatory system appears to be responsive to CO_2, which powerfully modulates gustatory processing of basic tastes and of their combination in beverages.[3] Given the widespread use of CO_2 in sweet beverages, the modulation of sweet perception is particularly interesting. CO_2 may affect the neural processing of various sweet substances differently, affecting the liking of beverages containing sucrose or sugar substitutes.[4] Perception of CO_2 is accompanied by trigeminal somatosensory stimulation, creating a rich multisensory convergence of perceptual inputs, and may be underpinned in humans by evolutionary remnant traits indicating a nutrient-rich feeding environment.[5] Contrasting with growing knowledge of the peripheral perceptual mechanisms of sweetness,[6,7] its central neural processing and the modulation operated on sweetness by other taste modalities are still to be unraveled.

In this study, we investigated the interference between CO_2 and perception of sweetness and the differential effects of CO_2 on sucrose and artificial sweeteners (aspartame-acesulfame [As-Ac], a common combination used in diet beverages) by monitoring the changes in regional brain activity using functional magnetic resonance imaging.

The presence of carbonation in sweet solutions, independently of the sweetening agent (sucrose and As-Ac), reduced neural activity in the AI, OFC (Figure 1), and posterior pons. Furthermore, the perceptual salience of sweetness was assessed by behavioral data (Supplementary Materials and Methods and Supplementary Figure 1).

The effect of carbonation on sucrose was much higher (bihemispheric pattern of decreased activity including gustatory cortices) than on perception of As-Ac (Figure 1). The existence of neural activity and peripheral perceptual machinery for perception of CO_2 was recently shown in *Drosophila* and mice.[3] Perception of CO_2 intersects in mice the mechanisms of sour taste, differentiated perceptually by the stimulation of mechanical and chemical trigeminal receptors that provide tactile and nociceptive information from the oral and nasal mucosa (chemesthesis).[3]

Activation by CO_2 induces harm-avoidance behavior (olfactory detection in *Drosophila*),[8] preventing the inhalation of life-threatening substances, or acceptance (gustatory detection in *Drosophila*), drawing toward growing microorganisms and nutrients.[9]

Abbreviations used in this paper: AI, anterior insula; Amy, amygdala; As-Ac, aspartame and acesulfame; OFC, orbitofrontal cortex.

0016-5085/$36.00
http://dx.doi.org/10.1053/j.gastro.2013.05.041

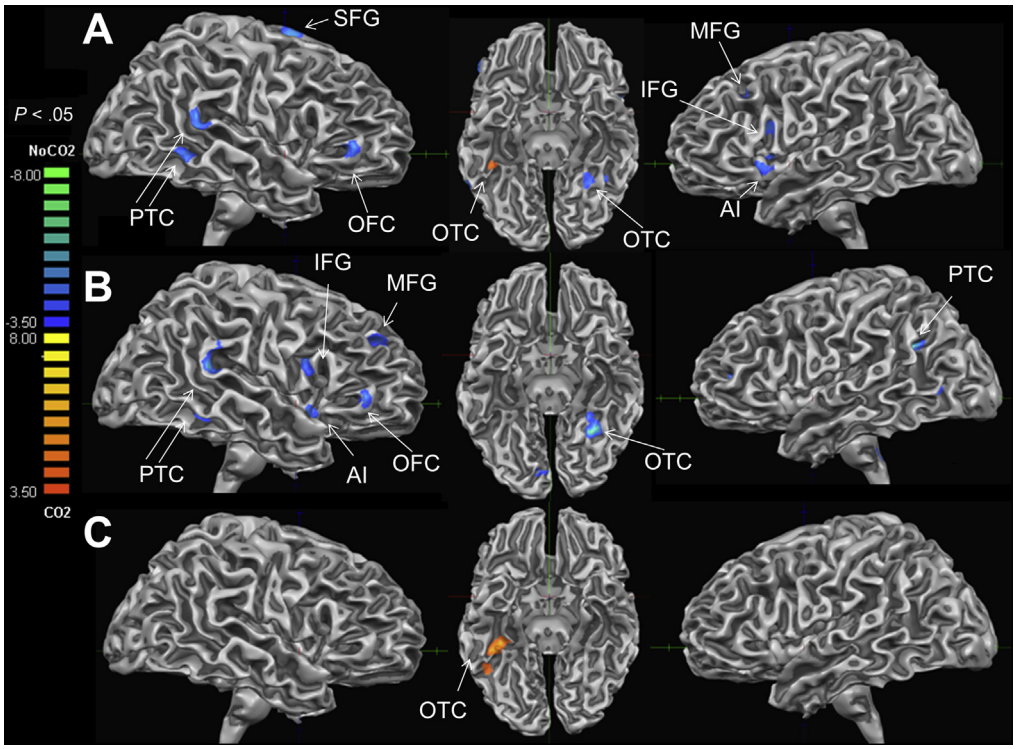

Figure 1. Effect of carbonation on neural activity. (*A*) The presence of carbonation independently of the sweetening agent reduced (*blue-green*) activity in the AI, OFC, SFG, PTC, OTC, and MFG and increased activity in OTC. (*B*) With sucrose, CO_2 reduced activity in the PTC, AI, OFC, IFG, MFG, and OTC. (*C*) With As-Ac, CO_2 increased activity in the OTC. IFG, inferior frontal gyrus; MFG, middle-frontal gyrus; OTC, occipito-temporal cortex; PTC, posterior-temporal cortex; SFG, superior frontal gyrus.

To clarify the specific neural correlates of carbonation alone and the potential role of sour receptors in coactivation in the carbonation-related responses, we analyzed the spatial distribution of neural activity related to sourness and carbonation within the AI. We found that the response to both tastes presented 2 insular clusters, with a clear spatial separation between their neural representations (Supplementary Figure 2), and pointing

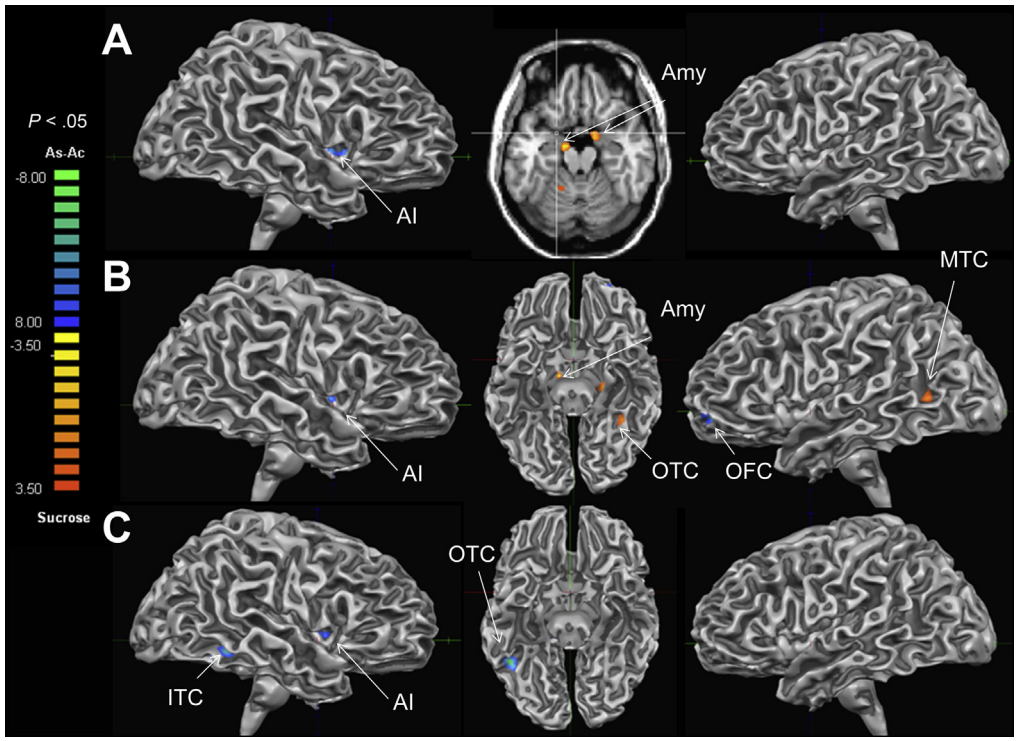

Figure 2. Effect of the sweetening agent. (*A*) Independently of carbonation, sucrose increased (*yellow-red*) activity in Amy and As-Ac increased activity in AI. (*B*) Differential brain activity for sucrose versus As-Ac was more evident without than with CO_2 and diffusely in favor of sucrose (left OTC, MTC, and OFC). (*C*) CO_2 reduced differential brain activity, which was higher for As-Ac in AI, OTC, ITC, and OFC. ITC, inferior temporal cortex; MTC, mesial-temporal cortex; OTC, occipitotemporal cortex.

against the hypothesis that the same cortical activity is elicited from sour- and carbonation-sensing pathways.

At the perceptual level, in keeping with our finding of reduced central neural activity, carbonation reduces the perception of sweetness[10] and the differences between the sensory profiles of sucrose and As-Ac.[4] Although this effect may increase intake of sucrose, it is also favorable to the formulation of diet beverages, designed to reduce caloric intake, being perceived as similar to that of regular beverages.[4] It is also coherent with a process of prioritization among perceptual inputs (chemesthesic and gustatory information) deriving from the same body topography and converging to the same cortical regions (AI, OFC).[11,12] Chemesthesic information, recently explored in the first trigeminal branch,[8] triggers behavioral responses to chemical irritants and is reasonably attributed with a sensory prioritization over sweet perception, enhancing the most environmentally relevant and ecologically "necessary" of the 2 converging sensory inputs. Predictably, CO_2 sensory prioritization affects sucrose more strongly than As-Ac processing, given the stronger hedonic and caloric value of sucrose, conflicting more openly with the CO_2 warning value as a chemical irritant.[10] Independently of carbonation, As-Ac increased neural activity in "primary-like" cortices (AI) and sucrose in Amy (Figure 2).[13] The differential brain activity between sucrose and As-Ac was much more evident and diffusely in favor of sucrose in the absence of carbonation and strongly reduced with CO_2 (Figure 2).

Our findings do not discriminate whether the effects of CO_2 are conveyed through taste or a multisensory chemesthesic pathway, where textural/tactile oral perceptual differences between carbonated and noncarbonated beverages play a pivotal role. The recent finding of a colocalization of taste and texture information in the primary taste cortex[14] indicates that this information is probably beyond the resolution of functional magnetic resonance imaging.

Gastric distention, present incrementally in our experiment and in nonexperimental conditions, may converge with taste-related effects of CO_2 on perception of sweetness. To rule out gastric distention–related effects, our experimental design randomly intermixed taste stimuli, presenting each stimulus 5 times and preventing any stimulus measurements to cluster in time. In this way, the linearly incremental factor of gastric distention is not able to weigh differentially our statistical analysis by favoring any one of the taste stimuli.

Our data suggest that CO_2 modulates the perception of sweetness, reducing the global neural processing of sweetness, the processing of sucrose more than of As-Ac, and the processing difference between sweetening agents. This piece of information is of utmost importance for designing carbonated beverages and is relevant to the regulation of caloric intake. This effect is driven by the integration of information on gastric fullness and on nutrient depletion, conveyed to a brain network where the autonomic brainstem circuitry and tractus solitarius neurons play a critical role in homeostatic functions.[15] From a speculative point of view, taste and CO_2-related information would influence food intake and dietary choices through integration in the tractus solitarius with inputs from the gastrointestinal tract. The reduced discrimination between sucrose and As-Ac induced by CO_2 would promote the consumption of low-calorie beverages and would converge with CO_2-induced gastric distention in limiting caloric intake.

Supplementary Material

Note: To access the supplementary material accompanying this article, visit the online version of *Gastroenterology* at www.gastrojournal.org, and at http://dx.doi.org/10.1053/j.gastro.2013.05.041.

References

1. Steiner JE. Symp Oral Sens Percept 1973;4:254–78.
2. Marciani L, et al. J Neurosci Methods 2006;158:186–194.
3. Chandrashekar J, et al. Science 2009;326:443–445.
4. Kappes SM, et al. J Food Sci 2007;72:1–11.
5. Scott K. Neuron 2005;48:455–464.
6. Smeets PA, et al. NeuroImage 2011;54:1367–1374.
7. Frank GK, et al. NeuroImage 2008;39:1559–1569.
8. Iannilli E, et al. Pain 2008;139:376–388.
9. Fischler W, et al. Nature 2007;448:1054–1057.
10. Yau NJN. J Food Sci 1992;57:1412–1416.
11. Cerf-Ducastel B, et al. Chem Senses 2001;26:371–383.
12. Veldhuizen MG, et al. Chem Senses 2007;32:569–581.
13. Rolls ET. Proc Nutr Soc 2007;66:96–112.
14. Rolls ET. Int J Obes 2011;35:550–561.
15. Browning KN. Auton Neurosci 2011;161:6–13.

Received June 11, 2012. Accepted May 20, 2013.

Reprint requests

Address requests for reprints to: Rosario Cuomo, MD, Gastroenterology Unit, Department of Clinical Medicine and Surgery, "Federico II" University, Via Sergio Pansini, 5 - 80131 Naples, Italy. e-mail: rcuomo@unina.it; fax: +39 (081) 7463892.

Conflicts of interest

The authors disclose the following: Rosario Cuomo was sponsored by The Coca-Cola Company. The remaining authors disclose no conflicts.

Funding

Supported in part by The Coca-Cola Company (Atlanta, GA).

Supplementary Materials and Methods

Methods

The study involved 2 functional neuroimaging experiments; the first analyzed the effect of carbonation in sweet solutions, and the second studied the spatial location of the strongest neural effects of sour taste and CO_2 within the insular cortex. The first experiment involved 9 volunteers (mean age, 23 years; 5 men and 4 women) not reporting any olfactory, gustatory, neurological, or psychiatric disorders and not using any medication. Informed consent was provided by all participants, and the study was approved by the local ethics committee. The brain functional examination was performed through the acquisition of time-series blood oxygenation level–dependent magnetic resonance (MR) images using a 3 Tesla MR scanner (Philips, Eindhoven, The Netherlands) during the delivery of gustatory stimuli. Four computer-controlled automatic injectors delivered the stimuli directly triggered by the MR radiofrequency pulses while the subject laid still in the scanner. A total of 4 different gustatory stimuli were used, each a variation of a commercial beverage (Sprite; The Coca-Cola Company, Atlanta, GA) differing only for the presence of carbonation or for the sweetening agent: (1) carbonated, sweetened with sucrose; (2) noncarbonated, sweetened with sucrose; (3) carbonated, sweetened with As-Ac; and (4) noncarbonated, sweetened with As-Ac. All of the tastants were kept at a controlled low temperature (4°C). Each MR-compatible injector (Spectris Solaris, Medrad, PA) delivered 2 solutions, both in the quantity of 10 mL each (speed of injection, 5 mL/s). To avoid cross-contamination of stimuli, each stimulus was delivered by the principal line of a specific injector and the secondary line delivered water. The alternation of stimuli and water prevented physical and perceptual overlapping between the different tastes. The subjects held the solution or the water in their mouth for 10 seconds and then swallowed it, following acoustic cues given 1 second before the injection and swallowing phases. Stimulation and washing periods were composed of 3 phases (injection, 2 seconds; tasting, 10 seconds; swallowing, 3 seconds), were separated by a resting period of 15 seconds, and were repeated 5 times for each condition for a total volume of 50 mL of each solution (200 mL) and 200 mL of water.

In the second experiment, using the same experimental procedures, we determined the regions of the strongest neural effects of sour taste and CO_2 compared with a baseline of water within the insular cortex in 8 subjects.

To correlate neuroimaging with behavioral data, the same setup was used to assess the ability of carbonation to modulate perception of sweetness. To this purpose, 14 subjects were randomly administered 5 mL of the previously described Sprite solutions and, 10 seconds after the administration of each solution, were asked to score the level of perceived sweetness on a visual analogue scale ranging from 0 to 100 mm (no sweet taste or maximum perceived sweet taste). Similarly, in 7 subjects, the effect of 1585 ppm of CO_2 added to a 10% glucose solution on the perception of sweetness was also tested.

Functional Magnetic Resonance Imaging Acquisition and Preprocessing

The functional time series, consisting of the repetition of whole brain volumes, was acquired with a Philips Achieva scanner at 3 Tesla (IRCCS SDN Naples, Italy) by means of T2*-weighted gradient echo planar imaging sequences (echo time [TE], 35 milliseconds; matrix, 96 × 96; field of view, 210 × 210 mm; in-plane voxel size, 2.1875 × 2.1875 mm; flip angle, 90°; slice thickness, 4 mm). Functional volumes consisted of 22 bicommissural slices, acquired with a volume repetition time (TR) of 2000 milliseconds with an interslice time of 90 milliseconds. A total of 610 volumes were acquired for each subject, and the first 2 volumes were discarded to ensure steady-state longitudinal magnetization. Subsequently, a high-resolution structural volume was acquired via a T1-weighted 3D TFE SENSE sequence (sagittal; matrix, 256 × 256; field of view, 256 × 256 mm; 181 slices; slice thickness, 1 mm; no gap; in-plane voxel size, 1 mm × 1 mm; flip angle, 8°; repetition time: TR 7.658 milliseconds; TE 3.483 milliseconds) to provide the anatomic reference for the functional scan. Functional data were preprocessed using BrainVoyager QX version 1.9 (Brain Innovation, Maastricht, The Netherlands), correcting the slice timing dispersion and the motion in the time series and removing linear and nonlinear "drifts" in the time courses (temporal high-pass filter of 2 cycles). Finally, functional data were aligned with T1 volumes and warped into the standard anatomic space of Talairach and Tournoux.[1] The resulting time series was filtered in space with a spatial smoothing Gaussian kernel of 5 mm full width at half maximum.

Data Analysis

The statistical processing of functional magnetic resonance imaging data was performed through BrainVoyager by analyzing the random effects of a general linear model ($n = 9$, P [cluster corrected] $< .05$) after correction of serial correlation (AR-1), Z-transformation of predictors, and correction for multiple comparisons through randomization. Six functional contrasts were analyzed: (1) carbonated versus noncarbonated solutions, (2) sucrose versus As-Ac–sweetened solutions, (3) carbonated versus noncarbonated sucrose-sweetened solutions, (4) carbonated versus noncarbonated As-Ac–sweetened solutions, (5) sucrose versus As-Ac–sweetened carbonated solutions, and (6) sucrose versus As-Ac–sweetened noncarbonated solutions. The functional contrasts were projected on the average anatomy of the Talairach-transformed T1-weighted 3D TFE SENSE of all the subjects after reaching a threshold of $P < .05$. In the second experiment, 2 functional contrasts were analyzed: (1) carbonated (containing 1585 ppm of CO_2) and (2) sour-tasting solutions (containing 50 mmol/L of citric

acid) versus noncarbonated neutral water. Behavioral data were analyzed by paired *t* test and reported as mean ± SD.

Results

Behavioral Tests

Figure 1 shows that CO_2 is able to significantly reduce sweet-induced taste perception, as assessed by visual analogue scale measurement in healthy volunteers. The perception of Sprite-associated sweetness was also significantly reduced by CO_2 (48 ± 19 vs 63 ± 17 and 48 ± 18 vs 55 ± 15 mm for As-Ac and sucrose; $P < .01$ and $P < .04$, respectively; Figure 1*A*). Similarly, in the presence of carbonation, sweet-induced perception of a 10% glucose solution was significantly reduced (36 ± 16 vs 53 ± 14 mm; $P = .02$; Figure 1*B*).

Supplementary Reference

1. Talairach J, et al. New York, NY: Thieme Medical Publishers, 1988.

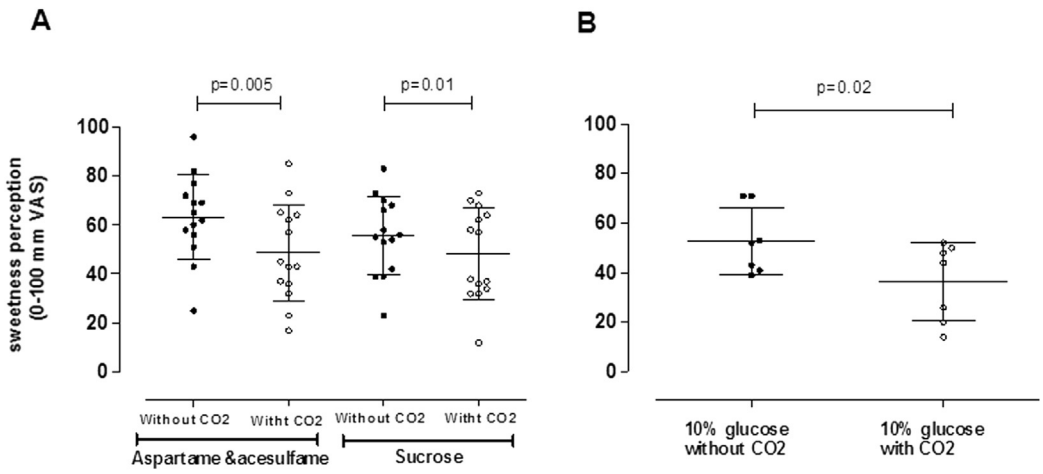

Supplementary Figure 1. (*A*) Perception of sweetness in 14 healthy volunteers during administration of carbonated or noncarbonated Sprite beverages sweetened with As-Ac or sucrose. (*B*) Perception of sweetness in 7 healthy volunteers during administration of carbonated or noncarbonated 10% glucose solution. Data are represented as individual values and mean ± SD.

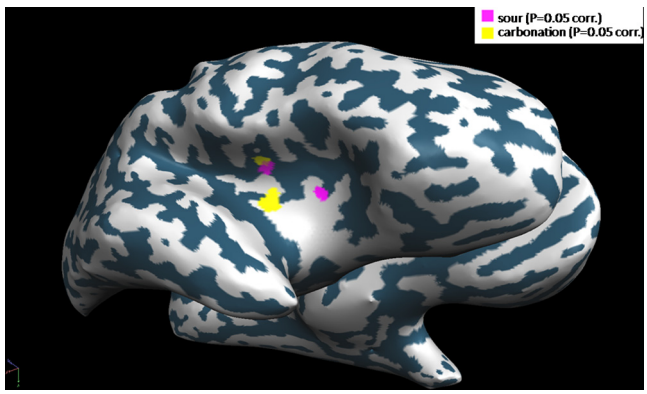

Supplementary Figure 2. The peaks of brain activity related to carbonation and to sour taste compared with a baseline of water are represented on the partially inflated surface of brain hemispheres. Both tastes evoked neural activity with 2 distinct maxima in the insular cortex ($P = .05$ correlation). Two peaks are located in the insular sulcus and appear partially overlapping, and 2 peaks are located in the insular gyri and are well separated from each other.

Neurological Disorders

Cantone, et al., J Neurol Disord 2015, 3:1
http://dx.doi.org/10.4172/2329-6895.1000200

Short Communication Open Access

CO_2 Modulates the Central Neural Processing of Sucrose Perception

Elena Cantone[1,2*], Anna Prinster[3], Rossella Cuofano[1], Antonella Miriam Di Lullo[1], Rosario Cuomo[4], Francesco Di Salle[5] and Maurizio Iengo[1]

[1]*Department of Neuroscience, Reproductive and Odontostomatologic Science, Section of ENT, "Federico II" University, Naples, Italy*

[2]*Department of Molecular Medicine and Medical Biotechnology, "Federico II" University, Naples, Italy*

[3]*Biostructure and Bioimaging Institute, National Research Council, Naples, Italy*

[4]*Gastroenterology Unit, Department of Clinical and Experimental Medicine, "Federico II", Naples, Italy*

[5]*Department of Medicine, Salerno University, Italy*

[*]**Corresponding author:** Elena Cantone, Department of Neuroscience, Reproductive and Odontostomatologic Science, Section of ENT and Department of Molecular Medicine and Medical Biotechnology, "Federico II" University, Naples, Italy, Tel: 339817463598; E-mail : elenacantone@libero.it

Rec date: Nov 07, 2014, **Acc date:** Dec 26, 2014, **Pub date:** Dec 28, 2014

Keywords: Taste; Carbonation; Sweet

Introduction

The five universally accepted tastes, sweet, salty, sour, bitter, and umami (a savory sensation elicited by monosodium glutamate) have specific receptors in oral, pharyngeal and laryngeal regions [1].

The most credited candidates to the function of human primary taste cortex are the frontal operculum and the anterior insula; while the opercular cortex and the orbitofrontal cortex are thought to code for secondary gustatory functions, while the amygdale and the dorsolateral prefrontal cortex are involved as hierarchically superior processing units [2]. Conversely, more is known on the peripheral pathway of taste, including the molecular dynamics of many receptors [3].

In addition to the basic tastes, the gustatory system appears responsive to CO_2 but the presence of specific CO_2 peripheral receptors and central neural pathway is still debated [4]. In the absence of a dedicated neural processing and cortical representation, CO_2 might still induce a powerful modulation of different gustatory inputs, implying that sweetness, bitterness, sourness, saltiness, and umami, or their combination in specific beverages, may be perceived as profoundly different in the presence of carbonation.

Everyday experience provides ample evidence in favor of this hypothesis. Among the different interferences carbonation may produce, the modulation of sweet perception appears of particular practical interest, given the widespread use of CO_2 in sweet beverages [5]. In particular, the contribution of carbonation to taste may not even be properly gustatory in nature, given that the CO_2 stimulation operates on mechanical and chemical trigeminal receptors that provide tactile, proprioceptive, chemosensory and nociceptive information from face, mouth, and nose [6].

A new, powerful tool to extend our knowledge of hPTC has been recently provided by fMRI, which has already proven essential in conveying extremely valuable information on the functional anatomy of other neural sensory pathways. In this study, we investigated the effect of carbonation on the brain processing of sweet stimuli. The cortical representation of taste-related neural responses has been studied by a Philips 3 T scanner in an echo planar blood oxygenation-level–dependent (BOLD) experiment, while gustatory stimuli were delivered by computer-controlled automatic injectors.

Methods

The study involved nine volunteers (mean age 23 years, 5 men and 4 women), not reporting any olfactory, gustatory, neurological or psychiatric disorder, and free from the use of any medication. Informed consent was given by all the participants and the study was approved by the local ethics committee. The brain functional examination was performed through the acquisition of time-series of Magnetic Resonance (MR) images using a 3 Tesla MR scanner (Philips, Eindhoven, The Netherlands) during the delivery of gustatory stimuli.

Two computer controlled automatic injectors delivered the stimuli directly triggered by the MR radiofrequency pulses, while the subjects laid still in the scanner.

A total of two different gustatory stimuli were used, each a variation of a commercial beverage differing only for the presence of carbonation agent: 1) carbonated, sweetened with sucrose, 2) non-carbonated, sweetened with sucrose. All the tastants were kept at controlled low temperature (4°C). Each MRI-compatible injector (Spectris Solaris, MedradTM) delivered two solutions both in the quantity of 10 ml each (speed of injection: 5ml/sec). To avoid cross-contamination of stimuli, each stimulus was delivered by the principal line of a specific injector, while the secondary line delivered water. The alternation of stimuli and water prevented physical and perceptual overlapping between the different tastes. The subjects held the solution or the water in their mouth for 10 seconds and then swallowed it, following acoustic cues given 1 second prior to the injection and swallowing phases.

Stimulation and washing periods were composed of three phases (Injection=2 sec, Tasting=10 sec, Swallowing= 3 sec), and were separated by a resting period of 15 seconds.

MRI acquisition and pre-processing

The functional time-series, consisting in the repetition of whole brain volumes, were acquired with a Philips Achieva scanner at 3T (IRCCS SDN Naples, Italy) by means of T2*-weighted gradient echo planar imaging sequences (TE 35 ms; matrix 96 × 96; FOV 210 ×210 mm; in-plane voxel size, 2.1875 × 2.1875 mm; flip angle 90°; slice thickness 4 mm).

Functional volumes consisted of twenty-two bi-commissural slices, acquired with a volume repetition time (TR) of 2000 ms with an inter-slice time of 90 ms. A total of 610 volumes were acquired for each subject, and the first two volumes were discarded to ensure steady-state

longitudinal magnetization. Subsequently, a high-resolution structural volume was acquired via a T1-weighted 3D TFE SENSE sequence (sagittal; matrix 256 × 256; FOV 256 × 256 mm; 181 slices; slice thickness 1 mm; no gap; in-plane voxel size 1 mm × 1 mm; flip angle 8°; repetition time TR 7.658 ms; TE 3.483 ms) to provide the anatomical reference for the functional scan.

Functional data were pre-processed using BrainVoyager™ QX, version 1.9 (Brain Innovation, Maastricht, The Netherlands), correcting the slice timing dispersion and the motion in the time series, and removing linear and non-linear "drifts" in the time courses (temporal high pass filter of two cycles). Finally, functional data were aligned with T1-volumes and warped into the standard anatomical space of Talairach and Tournoux. The resulting time-series were filtered in space with a spatial smoothing Gaussian kernel of 5 mm FWHM.

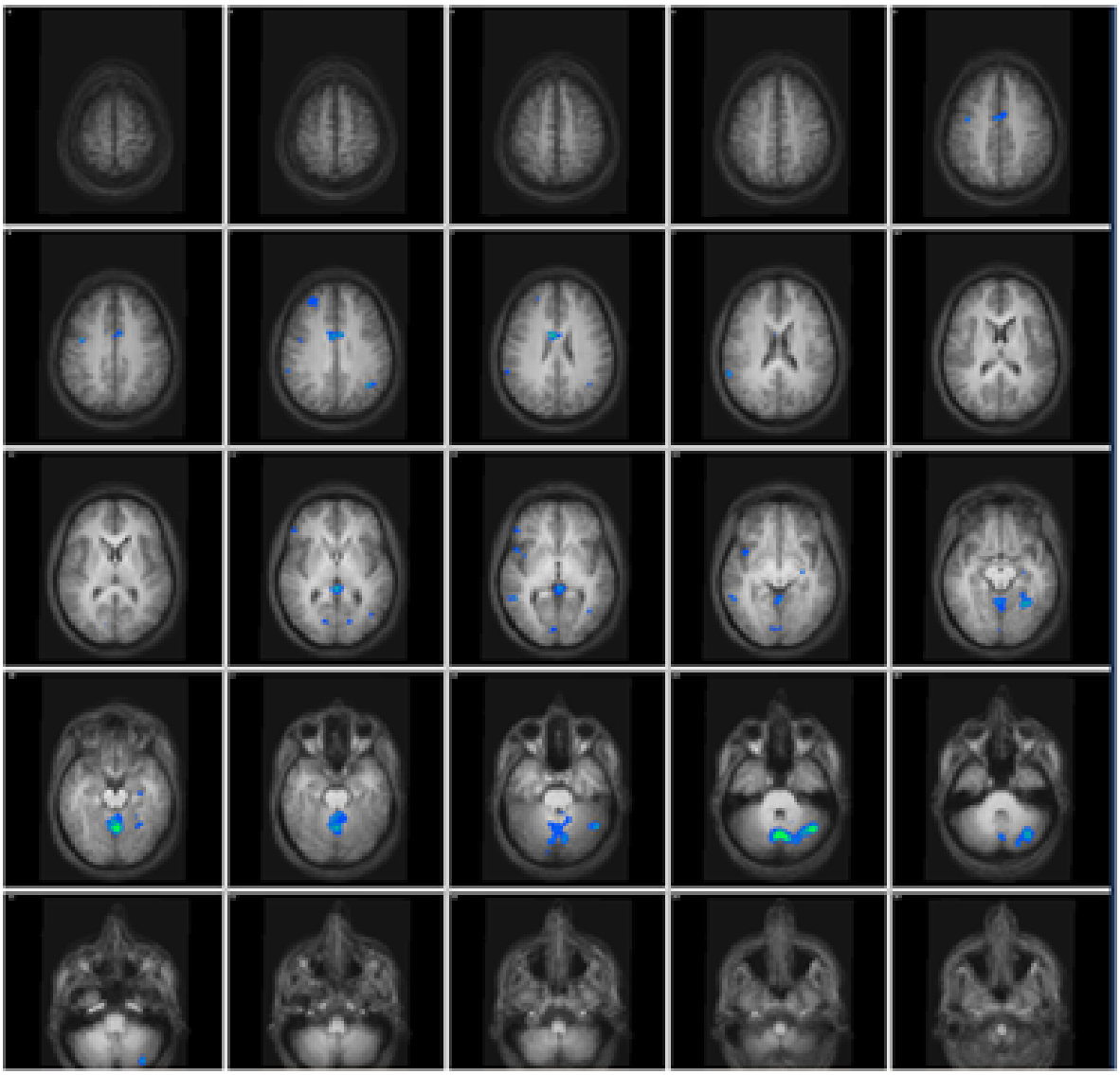

Figure 1: The presence of (carbonation versus non-carbonated beverages) in the sucrose sweetened solutions produces relative decrease (blue) in taste-related brain activity, evident in the right hemisphere in the insular cortex, latera orbitofrontal cortex, ventrolateral prefrontal cortes, bilaterally in the cingulate cortes, the tempero-parietel and tempero-occipital junction, and the cerebellar vermis and in the left side in the inferior occipito-temporal cortex and the hemispheric cerebellar cortex.

Data analysis

The statistical processing of fMRI data was carried out through BrainVoyager™, by analyzing the random effects of a General Linear Model (n=9, P[cluster corrected]<0.05), after correction of serial correlation [AR-1], Z-transformation of predictors, and correction for multiple comparisons through randomization.

Carbonated versus non-carbonated sucrose sweetened solutions were analyzed. The functional contrast was projected on the average anatomy of the Talairach-transformed T1-weighted 3D TFE SENSE of all the subjects, after reaching a threshol of $P<0.05$.

Results

The presence of carbonation (carbonated versus non-carbonated beverages) in a sucrose sweetened solutions produced (Figure 1) a relative decrease in taste-related brain activity, evident in the right hemisphere in the insular cortex, lateral orbitofrontal cortex, ventrolateral prefrontal cortex, bilaterally in the cingulate cortex, the temporo-parietal and temporo-occipital junction, and the cerebellar vermis and in the left side in the inferior occipito-temporal cortex and the hemispheric cerebellar cortex.

Discussion

In the present study, we investigated the central neural pathway in response to gustatory stimulation by sucrose and the modulation of sweet perception operated by carbonation, monitoring the changes in blood oxygenation with BOLD fMRI.

According to some authors, carbonation plays such a large role in the sensory profiles of beverages containing sugar as to inhibit their perception.

In our experiment, the presence of carbonation decreased the neural processing of sweetness, in keeping with the behavioral decrease in sensitivity. This neural effect was present in a widespread cortical and subcortical pattern (Figure 1).

The negative modulation of behavioral taste sensitivity and of the neural processing of sweetness operated by carbonation, deserves a discussion in the light of the increasing brain activity that carbonation is able to produce.

Studies about taste interactions showed a consistent pattern of mixture suppression in which sucrose sweetness tended to be both the least suppressed quality and the strongest suppressor of other tastes. The regulation of food intake is, among others, driven by a combination of sensory information, somatosensory signals of gastric fullness and chemical signals indicative of nutrient depletion.

The presence of carbonation is able to induce evident effects on the brain, by interacting strongly with the central processing of sweetness. These data support the view that carbonation is able to markedly interact with sweetness perception, reducing the global sensitivity to sucrose.

In conclusion these findings provide insightful information on the interaction between carbonation and sweet taste processing, and may help design new beverages where pleasantness and diet requirements would reach the best possible compromise.

References

1. Steiner JE (1974) Discussion paper: innate, discriminative human facial expressions to taste and smell stimulation. Ann N Y Acad Sci 237: 229-233.
2. Kami YN, Goto TK, Tokumori K, Yoshiura T, Kobayashi K, et al. (2008) The development of a novel automated taste stimulus delivery system for fMRI studies on the human cortical segregation of taste. J Neurosci Methods 172: 48-53.
3. Weiss LA, Dahanukar A, Kwon JY, Banerjee D, Carlson JR (2011) The molecular and cellular basis of bitter taste in Drosophila. Neuron 69: 258-272.
4. Chandrashekar J, Yarmolinsky D, von Buchholtz L, Oka Y, Sly W, et al. (2009) The taste of carbonation. Science 326: 443-445.
5. Kaushal NK, Lal Kaushal BB, Sharma PC (2004) Optimization of total soluble solids and carbon dioxide gas pressure for the preparation of carbonated beverages from apple and pear juices. J Food Sci Technol 41:142-9.
6. Iannilli E, Del Gratta C, Gerber JC, Romani GL, Hummel T (2008) Trigeminal activation using chemical, electrical, and mechanical stimuli. Pain 139: 376-388.

Brain Changes in Kallmann Syndrome

R. Manara, A. Salvalaggio, A. Favaro, V. Palumbo, V. Citton, A. Elefante, A. Brunetti, F. Di Salle, G. Bonanni, and A.A. Sinisi, for the Kallmann Syndrome Neuroradiological Study Group

ABSTRACT

BACKGROUND AND PURPOSE: Kallmann syndrome is a rare inherited disorder due to defective intrauterine migration of olfactory axons and gonadotropin-releasing hormone neurons, leading to rhinencephalon hypoplasia and hypogonadotropic hypogonadism. Concomitant brain developmental abnormalities have been described. Our aim was to investigate Kallmann syndrome–related brain changes with conventional and novel quantitative MR imaging analyses.

MATERIALS AND METHODS: Forty-five male patients with Kallmann syndrome (mean age, 30.7 years; range, 9–55 years) and 23 age-matched male controls underwent brain MR imaging. The MR imaging study protocol included 3D-T1, FLAIR, and diffusion tensor imaging (32 noncollinear gradient-encoding directions; b-value = 800 s/mm^2). Voxel-based morphometry, sulcation, curvature, and cortical thickness analyses and tract-based spatial statistics were performed by using Statistical Parametric Mapping 8, FreeSurfer, and the fMRI of the Brain Software Library.

RESULTS: Corpus callosum partial agenesis, multiple sclerosis–like white matter abnormalities, and acoustic schwannoma were found in 1 patient each. The total amount of gray and white matter volume and tract-based spatial statistics measures (fractional anisotropy and mean, radial, and axial diffusivity) did not differ between patients with Kallmann syndrome and controls. By specific analyses, patients with Kallmann syndrome presented with symmetric clusters of gray matter volume increase and decrease and white matter volume decrease close to the olfactory sulci; reduced sulcal depth of the olfactory sulci and deeper medial orbital-frontal sulci; lesser curvature of the olfactory sulcus and sharper curvature close to the medial orbital-frontal sulcus; and increased cortical thickness within the olfactory sulcus.

CONCLUSIONS: This large MR imaging study on male patients with Kallmann syndrome featured significant morphologic and structural brain changes, likely driven by olfactory bulb hypo-/aplasia, selectively involving the basal forebrain cortex.

ABBREVIATIONS: KS = Kallmann syndrome; FA = fractional anisotropy; MNI = Montreal Neurological Institute; TBSS = tract-based spatial statistics; VBM = voxel-based morphometry

Kallmann syndrome (KS) is a rare inherited disorder (affecting about 1 in 10,000 males),[1] clinically characterized by the association of hypogonadotropic hypogonadism and hypo-/anosmia.[2] Both KS clinical hallmarks derive from a disturbed intrauterine migration process involving olfactory axons and gonadotropin-releasing hormone neurons from the olfactory placode to the hypothalamus.[3,4] The failure of the migration process results in hypo-/aplasia of the rhinencephalon (olfactory bulbs and tracts)[3-6] and in altered gonadotropic axis function with low levels of sex hormones. Besides rhinencephalon abnormalities, distinctive KS neuroradiologic changes have been detected in the brain and bone structures of the anterior cranial fossa by conventional MR imaging[7-14] and CT studies.[15] The most known morphologic brain feature is the reduction in depth and length of the

Received December 20, 2013; accepted after revision February 3, 2014.

From the Department of Neuroradiology (R.M., F.D.S.), University of Salerno, Salerno, Italy; Istituto di Ricovero e Cura a Carattere Scientifico S. Camillo (R.M., V.C.), Venezia, Italy; Departments of Neurology (A.S.), and Psychiatry (A.F.), Department of Neurosciences; Unità di Endocrinologia (G.B.), Department of Medicine, University of Padova, Padova, Italy; Department of Clinical and Experimental Medicine and Surgery (V.P., A.A.S.), Endocrinology and Medical Andrology Section, Second University of Napoli, Napoli, Italy; and Department of Neuroradiology (A.E., A.B.), Department of Scienze Biomediche Avanzate, and ENT section (R.M., A.S.), Department of Neurosciences, "Federico II" University, Napoli, Italy.

Renzo Manara and Alessandro Salvalaggio equally contributed to the study and should be considered first authors.

Guglielmo Bonanni and Antoio Agostino Sinisis should be considered senior coauthors.

Paper previously presented in part at: Annual Meeting of the European Society of Neuroradiology, September 28 to October 1, 2013; Frankfurt, Germany.

Please address correspondence to Renzo Manara, MD, Neuroradiology, University of Salerno, Via S Allende 1, Baronissi 89081 (SA), Italy; e-mail: rmanara@unisa.it

indicates article with supplemental on-line appendix and table.

http://dx.doi.org/10.3174/ajnr.A3946

olfactory sulcus, which typically turns medially, opening anteriorly into the interhemispheric fissure.[7-13] This sulcal abnormality is thought to be driven by the absence/hypoplasia of the olfactory bulbs and represents an intriguing model of genetically driven developmental brain abnormalities. Furthermore, a few case reports postulated the strict relationship between KS and midline brain abnormalities, such as corpus callosum agenesis and holoprosencephaly,[6,16] though pathologic and neuroimaging data are relatively scarce and often contradictory.[7]

In 2008, a pioneering study by voxel-based morphometry (VBM) MR imaging analysis revealed distinct regional gray and white matter volume changes in male patients with KS outside the frontal orbital regions.[17] No study so far has replicated a larger sample of these findings, which would imply a much more profound effect of KS-related genes (*KAL1*, *FGFR1*, *PROK2*, *PROKR2*, *FGF8*, *NELF*, etc.)[18] and/or sex hormone deficiency on brain morphogenesis and development. Moreover, no study has investigated regional white matter changes revealed by VBM by diffusion tensor imaging, a powerful quantitative technique able to investigate the structural nature of white matter involvement. Finally, novel MR imaging–based analyses have been developed that allow assessing precise curvature, sulcation, and cortical thickness quantitative evaluations,[19-21] thus providing further insights into cortex developmental abnormalities. Such analyses have not been applied to KS, though they might represent useful tools for investigating the structural underpinnings of neurologic and psychiatric disorders anecdotally reported in patients with KS.[22,23]

By conventional MR imaging and novel quantitative sulcation, curvature, cortical thickness, and tract-based spatial statistics (TBSS) analyses, we aimed to feature, more precisely and in a large sample of male patients, the morphologic and structural brain involvement in KS.

MATERIALS AND METHODS

Subjects

Forty-five male patients (mean age, 30.7 years; range, 9–55 years) affected with KS underwent brain MR imaging. All patients met the diagnostic criteria for KS based on clinical observations and smell analysis (main clinical and demographic features are shown in On-line Table 1). One patient had a history of severe head trauma. Twenty-three healthy male subjects (mean age, 32.6 years; range: 12–55 years) or patients referred to neuroimaging for headache with no history of prematurity, head trauma, neurologic or psychiatric disease, or neurosurgery represented our control group.

Seven patients with KS and 2 controls were left-handed, according to the Edinburgh Handedness Inventory.[24] No patients or subjects required sedation during MR imaging acquisition. The study was approved by the local ethics committee, and written informed consent was obtained from patients or their parents.

Patients with KS younger than 12 years of age or presenting with midline brain abnormalities or significant parenchymal lesions were excluded from VBM, sulcation, curvature, and TBSS analyses to avoid the interference of maturation, malformative, or incidental factors on the quantitative parenchymal and morphologic evaluation.

MR Imaging Acquisition

All MR imaging scans were obtained in 2 centers (University Hospital of Padova and Medicanova Diagnostic Center, Battipaglia, Italy) equipped with the same 1.5T MR imaging scanner (Achieva; Philips Healthcare, Best, the Netherlands) with a standard quadrature head coil. The MR imaging study protocol included the following: 3D T1-weighted imaging (TR/TE, 20/3.8 ms; flip angle, 20°; section thickness, 1 mm; acquired pixel size, 1 × 1 mm; reconstructed pixel size, 0.66 × 0.66 mm; acquisition matrix, 212 × 210; reconstructed matrix, 320 × 320; acquisition time, approximately 7 minutes); and FLAIR (TR/TE/TI, 10,000/140/2800 ms; echo-train length, 53; flip angle, 90°; section thickness, 5 mm; intersection gap, 0.5 mm; acquisition pixel, 0.90 × 1.15 mm; reconstructed pixel, 0.9 × 0.9 mm; acquisition time, 3 minutes 20 seconds).

Diffusion tensor images were acquired with single-shot echo-planar diffusion-weighted imaging (TR/TE, 11,114/80 ms; acquisition matrix, 112 × 110; echo-train length, 59; reconstructed matrix, 128 × 128; acquisition pixel, 2 × 2 mm; reconstructed pixel, 1.75 × 1.75 × 2 mm; sensitivity encoding p reduction, 2; section thickness, 2 mm without gap; NEX, 2; acquisition time, 12 minutes 24 seconds). The axial sections covered the whole brain including the cerebellum. The diffusion-sensitizing gradients were applied along 32 noncollinear gradient-encoding directions with maximum b=800 s/mm^2. One additional image without diffusion gradients (b=0 s/mm^2) was also acquired.

Image Processing

Data Processing of Volumetric Images and DTI (TBSS). The imaging processing methods are presented in detail in the On-line Appendix.

Specifically, we used the optimized VBM protocol (Diffeomorphic Anatomical Registration Through Exponentiated Lie Algebra) available in the statistical parametric mapping software (SPM8; Wellcome Department of Imaging Neuroscience, London, UK, www.fil.ion.ucl.ac.uk/spm).[25] For statistical analyses, we used parametric t tests as implemented by SPM8, by using age as a covariate of no interest. Results for gray matter were considered significant for $P < .05$, family-wise error–corrected.

All 3D T1-weighted data were also processed by FreeSurfer (http://surfer.nmr.mgh.harvard.edu/) to derive quantitative estimates of cortical thickness, sulcation, and curvature. The sulcation conveys information on how far a particular surface vertex point is from a hypothetic "midsurface," which exists between the gyri and sulci. The curvature conveys information on the curvature (not distance) at a specific vertex point. The sharper the curve, the higher the value (positive or negative) is. The color conveys the sign and is just an arbitrary choice. Cortical thickness, sulcation, and curvature were estimated for the whole brain. Group analysis was performed by using generalized linear models, including age as a nuisance variable. Results were considered significant for $P < .05$, false discovery rate–corrected.

All DTI data were preprocessed by the FMRIB Diffusion Toolbox within FSL (http://www.fmrib.ox.ac.uk/fsl/fdt/index.html).[26] For group comparisons concerning fractional anisotropy (FA) and diffusivity values, data were fed into the voxelwise statistics analysis, which was based on nonparametric permutation testing (5000 permutations) by using the threshold-free cluster enhance-

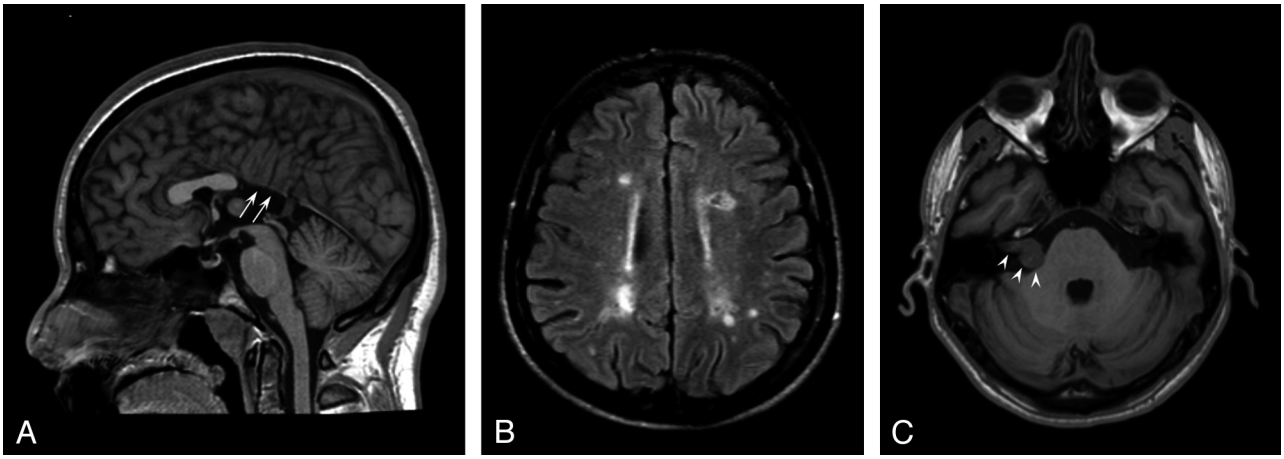

FIG 1. Conventional brain MR imaging findings in 45 patients with Kallmann syndrome. *A*, Midsagittal T1-weighted image of a patient with agenesia of the posterior portion of the corpus callosum (*white arrows*). *B*, Axial FLAIR image of the patient disclosing several multiple sclerosis–like white matter signal abnormalities in the centrum semiovale bilaterally. *C*, Non-enhanced axial T1-weighted image at the level of the internal acoustic meatus showing a right intra/extrameatal dumbell-shaped mass consistent with an acoustic schwannoma.

ment[27] method to account for multiple comparison correction across space. Age and sites of MR imaging acquisition were entered into the analysis as covariates.

RESULTS

Conventional MR Imaging Findings Evaluation

One patient with KS had midline brain abnormalities (partial corpus callosum agenesia) (Fig 1*A*), and 1 had diffuse multiple sclerosis–like white matter abnormalities (Fig 1*B*).

On FLAIR images, nonspecific white matter signal abnormalities (1–20 punctuate hyperintensities) were observed in 15/45 patients (33%; mean age, 35.3 years; age range, 15–55 years); age did not differ between patients with and without white matter hyperintensities ($P = .07$). Similarly, the presence of obesity (7/45), hypertension (0/45), and cardiopathy (0/45) did not differ between these 2 subgroups.

One patient had small cortical abnormalities in the right superior frontal and inferior temporal gyri, consistent with sequelae of a known previous head trauma. One patient had a right intra/extrameatal acoustic nerve schwannoma (20 × 14 mm), with no significant mass effect on the pons (Fig 1*C*).

Quantitative MR Imaging Analysis

The 3 patients with partial agenesis of the corpus callosum, diffuse multiple sclerosis–like white matter lesions, and age younger than 12 years were excluded from quantitative analyses. Forty-two patients with KS were, therefore, considered for subsequent analyses (mean age, 30.6 years; range, 15–55 years).

Voxel-Based Morphometry

The total amount of gray and white matter did not differ between patients with KS and controls (gray matter, 919 ± 132 mL versus 949 ± 108 mL; white matter, 677 ± 091 mL versus 710 ± 081 mL, respectively) by using as covariates age, total intracranial volume, and site of MR imaging.

Patients with KS showed, compared with controls, 2 almost symmetric clusters of significant white matter volume decrease in the frontal basal regions (Montreal Neurological Institute [MNI] coordinates: −16, 26, −26 and 14, 32, −28; *P* value family-wise error–corrected, respectively, <.001 and .002), 2 almost symmetric clusters of significant gray matter volume increase in the frontal basal regions (MNI coordinates: 16, 38, −12 and −16, 34, −12; *P* value family-wise error–corrected, .001), and 2 almost symmetric clusters of significant gray matter volume decrease in the frontal basal regions (MNI coordinates: −10, 32, −24 and 12, 26, −18; *P* value family-wise error–corrected <.001) by using as covariates age, total intracranial volume, and site of MR imaging. As shown in Fig 2, these regions were very close to the olfactory sulci. Patients with KS did not show clusters of significant white matter volume increase compared with controls.

Sulcation, Curvature, and Cortical Thickness Whole-Brain Analyses

Significant differences between male patients with KS and controls are shown in the Table and Fig 2, in particular in the following manner:

By sulcation analysis, the sulcal depth was reduced at the level of the olfactory sulci and increased at the level of the medial orbital-frontal sulci in patients with KS.

By curvature analysis, patients with KS presented with a decreased curvature in the olfactory sulcus and a sharper curvature close to the medial orbital-frontal sulcus, bilaterally.

By cortical thickness analysis, patients with KS had thicker cortices than controls in a region corresponding to the olfactory sulcus, bilaterally. In the left hemisphere, 2 small areas of decreased cortical thickness were found at the level of the medial and lateral orbital-frontal sulci, the larger close to the olfactory sulcus.

Tract-Based Spatial Statistics Analysis

TBSS whole-brain analysis showed no differences between patients with KS and controls regarding fractional anisotropy, mean diffusivity, radial diffusivity, and axial diffusivity.

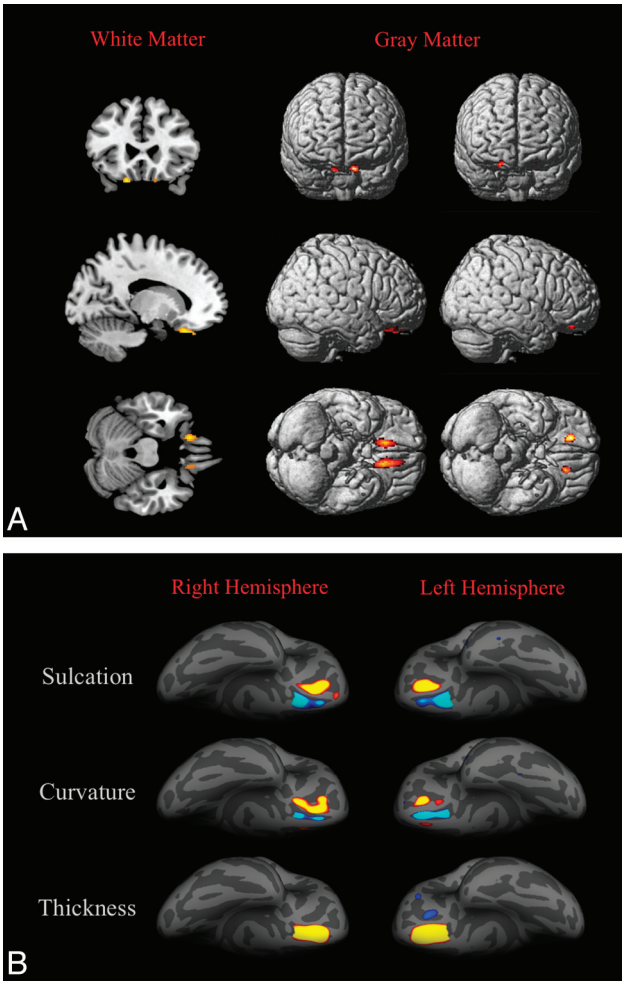

FIG 2. 3D-T1-based whole-brain analyses on 42 patients with Kallmann syndrome versus 23 controls. *A*, Voxel-based morphometry findings. Clusters of significantly decreased white matter volume (colored areas in the multiplanar reconstructions in the first column) were detected exclusively and symmetrically in the posterior portion of the medial orbital-frontal gyrus close to the olfactory sulcus; no regions of increased white matter volume were detected in our sample. Clusters of significantly decreased (second column) and increased (third column) gray matter volume are shown as colored cortical areas in the volume-rendering technique images within or close to the olfactory sulci. *B*, Sulcation, curvature, and thickness findings. Colored areas represent increased (yellow-red) and decreased (blue) values in patients with KS. Almost all differences are clustered within the olfactory sulci and the neighboring cortex of the rectus and medial orbital-frontal gyri.

DISCUSSION

The present study showed that patients with KS display surface cortical variations and gray and white matter volume changes, which clustered symmetrically in the frontal basal regions, close to the olfactory bulbs (gyrus rectus, medial orbital-frontal gyrus).

Changes in the frontal basal regions have been consistently described in the rhinencephalon and contiguous cerebral cortical and bone structures by pathology,[5,6] conventional MR imaging,[7-14] and CT studies in patients with KS.[15] Increased volume of the corticospinal tracts and corpus callosum has been also depicted by conventional MR imaging,[28] suggesting the involvement of brain structures beyond the basal forebrain, though these findings have not been confirmed in larger series.[7,17] A single MR imaging study formerly applied VBM to investigate gray and white matter volume in male patients with KS, detecting changes in several areas outside the basal forebrain, namely regions of increased gray matter volume (precentral gyrus bilaterally, left middle occipital and middle frontal gyri), decreased gray matter volume (right parahippocampal gyrus), increased white matter volume (left cuneus and right subcallosal gyrus), and decreased white matter volume (left superior frontal gyrus, right medial frontal gyrus, left frontal lobe subgyral and left insula).[17] In our VBM whole-brain analysis, gray and white matter changes appeared fairly symmetric and limited to the frontal basal regions. White matter volume changes (ie, decrease of white matter volume) were found exclusively in small subcortical areas of the medial orbital-frontal gyri close to the olfactory sulci. Similarly, VBM analysis disclosed small symmetric and contiguous areas of increased and decreased gray matter volume in the frontal basal regions close to the olfactory sulcus. The striking relationship between white and gray matter changes seems to suggest that these changes embody a fairly localized cortical-subcortical abnormal architectural development. Moreover, because all parenchymal changes are very close to the olfactory sulcus, they are most likely induced by the rhinencephalon hypo-/aplasia.

Except for these areas, by VBM analysis, cerebral gray and white matter did not differ between patients with KS and healthy controls. Similarly, TBSS analysis did not reveal any significant difference between patients with KS and controls, revealing that the ultrastructure of the white matter is preserved despite significant forebrain cortical changes. Nonetheless, KS genetic heterogeneity does not allow the exclusion of white matter hypertrophic or degenerative phenomena in specific subgroups of patients with KS because a strict genotypic/MR imaging phenotypic correlation requires a larger sample. Actually, no pathologic study reported brain parenchyma abnormalities in patients with KS, even though histologic data are very scarce. Peripheral axonal degeneration due to the absence of the olfactory bulbs has been shown in the olfactory mucosa,[29] but concomitant significant processes of axonal degeneration within the brain are not supported by VBM and TBSS findings.

Differences from previous MR imaging studies may be due to several issues, among them, the heterogeneity of the phenotypic spectrum of brain anomalies in KS or a different methodologic approach. The size of our study sample and the spatial coherence between gray/white matter volume changes and the well-known disease-related abnormalities of the olfactory sulcus seem to support the findings of the present study.

Consistently, the whole-brain curvature and sulcation analyses showed symmetric cortical abnormalities strictly confined to the frontal basal cortical regions (gyri recti and medial orbital-frontal gyri). Olfactory sulcus abnormalities were expected because the reduction in depth and length of the olfactory sulcus at gross pathology and conventional MR imaging evaluation is a known morphologic feature of the brain in patients with KS.[7-12] Olfactory sulcus abnormalities have been associated with embryogenic olfactory bulb–inducted processes.[10,11,30,31] In patients with KS, the aplasia/hypoplasia of the olfactory bulbs is associated with an ipsilaterally decreased depth of the olfactory sulcus, which might turn medially, opening anteriorly into the interhemi-

Cortical areas >40 mm² with significant differences between patients with Kallmann syndrome and controls by sulcation, curvature, and cortical thickness analyses

Hemisphere	Size (mm²)		Local Maximum, Talairach X	Y	Z	FDR Threshold	Cerebral Region
Sulcation							
Right	394.05	↓	11.2	13.8	−14.9	3.3429	Olfactory sulcus and contiguous cortex of the rectus gyrus
Right	325.72	↑	16.4	28.7	−23.7	3.3429	Medial orbital-frontal gyrus
Left	518.07	↓	−9.8	16.0	−15.4	3.3159	Olfactory sulcus and contiguous cortex of the rectus gyrus
Left	252.41	↑	−19.6	33.2	−17.3	3.3159	Medial orbital-frontal gyrus
Curvature							
Right	372.85	↑	14.4	32.3	−25.3	3.4704	Medial orbital-frontal gyrus
Right	77.61	↓	11.7	16.6	−14.2	3.4704	Olfactory sulcus
Right	44.71	↓	11.5	37.9	−19.1	3.4704	Olfactory sulcus
Left	196.94	↓	−11.6	38.7	−20.0	3.4704	Olfactory sulcus
Left	114.79	↑	−19.6	32.7	−14.9	3.4704	Medial orbital-frontal gyrus
Thickness							
Right	568.97	↑	−14.1	30.7	−19.2	3.3834	Olfactory sulcus and contiguous cortex of the rectus and medial orbital-frontal gyri
Left	686.38	↑	13.7	33.4	−23.3	3.2803	Olfactory sulcus and contiguous cortex of the rectus and medial orbital-frontal gyri
Left	78.39	↓	12.7	48.6	33.5	3.2803	Medial orbital-frontal sulcus
Left	40.54	↓	45.2	−62.3	36.9	3.2803	Lateral orbital-frontal gyrus

Note:— ↑ indicates that patients with KS showed increased sulcation, curvature, and cortical thickness; ↓, patients with KS showed decreased sulcation, curvature, and cortical thickness; FDR, false discovery rate.

spheric fissure.[7] Indeed, as shown in Fig 2, the olfactory sulcus presented with decreased sulcation and curvature, while the medial orbital-frontal sulcus showed a "compensatory-like" increased sulcation and curvature. The concomitant changes of the contiguous orbital-frontal regions seem to highlight a more extensive effect of the olfactory bulbs on forebrain morphogenesis. Most interesting, patients with KS display increased cortical thickness very close to VBM, sulcation, and curvature forebrain anomalies, suggesting that olfactory bulb–induction failure might act not only on the sulcal but also on the structural organization of the cortex.

Regional gray matter increase has been associated with the absence of a sulcus,[32] though so far no study investigated the correlation between cortical thickness and sulcation abnormalities, to our knowledge. We might speculate that a less deep sulcus results in an abnormal regional gray matter volume and cortical thickness as a consequence of overcrowding neurons migrated to this region. Alternatively, gray matter volume and cortical thickness changes might result from cortical functional differences between patients with KS and controls. The orbital-frontal cortex is deeply involved not only in olfaction (odor identification and olfactory memorization) but also in integrating emotion into cognition within decision-making processes.[33] KS is clinically characterized by the absence or reduction of olfaction, whereas few data are available on cognitive functioning and psychiatric risk, though schizophrenic disorders have been anecdotally reported among patients with KS.[22,23] Nonetheless, the primary and secondary olfactory cortices correspond to piriform and periamygdalar cortices and the posterior orbital-frontal gyrus and insula, all areas that in our study did not present with gray matter and cortical thickness changes. Moreover, none of our patients presented with a history of overt psychiatric disease, even though a specific neuropsychological and psychiatric assessment was not performed. Focused neurocognitive studies are warranted to investigate the presence of basal forebrain function impairment due to the above-mentioned morphologic and structural brain changes.

Finally, the changes observed in our study might be at least partly ascribed to hormonal differences between patients with KS and controls. Most of KS phenotypic features (hypogonadism, small penis, sexual secondary characteristics) are due to low testosterone levels during infancy and adolescence, which could also induce a feminine brain development. Sex brain dimorphism includes brain size, white and gray matter volume and regional cortical thickness changes.[34-36] This study did not reveal significant differences in brain size between patients with KS and controls. Moreover, sex- and testosterone-related brain differences do not seem to involve the medial orbital-frontal basal regions, thus restraining the direct role of hormonal dysfunction in determining the morphologic pattern observed in patients with KS. Longitudinal studies on patients with KS enrolled before hormone replacement therapy will help clarify the effects of testosterone in postnatal brain development, even though the effect of hormone milieu on prenatal and early brain development phases will remain difficult to unravel.

Because KS is a disease due to mutation of genes that are involved in neuronal migration,[37] patients with KS have been previously reported to present with midline head and brain abnormalities, such as cleft palate, corpus callosum dysgenesis, and holoprosencephaly.[6,38,39] These abnormalities have been thoroughly mentioned in studies on patients with KS.[7,10,40] Nonetheless, brain MR imaging evaluation of our large sample revealed corpus callosum partial agenesis in only 1/45 patients with KS (2.2%), thus supporting the observation by Quinton et al[7] that patients with KS mostly do not present significant intracranial midline abnormalities. A biased inclusion of syndromic patients

in the initial case series[6] might explain the difference with more recent larger samples. On the other hand, holoprosencephalic patients might be underdiagnosed as also being affected by hypogonadotropic hypogonadism and hypoanosmia due to their shorter life expectancy and overwhelming clinical issues.

Among our patients with KS, 15 (33%) showed small nonspecific punctuate FLAIR hyperintensities; 1 showed diffuse multiple sclerosis–like white matter lesions; and 1, an acoustic nerve schwannoma. These findings should be considered incidental unless otherwise demonstrated.

Even though these multimodality MR imaging analyses were applied to a large homogeneous sample of patients with KS with a strictly uniform MR imaging protocol (same scanner, same sequence parameters, and so forth), this study presents some limits. We evaluated KS-related brain MR imaging changes only in males, and further studies are warranted to confirm our findings in female patients with KS. Moreover, the genetic heterogeneity of our sample and its still ongoing molecular characterization did not allow investigating a precise genotypic/MR imaging correlation. Finally, because this was a cross-sectional study with almost no pediatric patients with KS, we could not investigate the brain changes related to aging or the effects of sex hormone deprivation and subsequent replacement on brain development.

The enrollment of specific subgroups, subdivided according to genetics, sex, age, ancillary clinical features (eg, the presence of mirror movement and psychiatric disorders), and treatment will help define more precisely the specific brain changes in KS.

CONCLUSIONS

This MR imaging study on a large group of male patients with KS showed significant brain changes specifically involving the gyri recti and the contiguous medial orbital-frontal regions. Even though further validation is warranted, curvature, sulcation, cortical thickness, gray/white matter volume, and bone changes in patients with KS point toward a profound structural and morphologic involvement of the basal forebrain that is far more consistent than a simple hypoplasia of the olfactory sulcus, driven by the olfactory bulbs. Future studies on the cognitive and psychiatric domains will define the clinical impact of these morphologic and structural brain changes.

APPENDIX

Members of the Kallmann Syndrome Neurological Study Group were the following: Arianna D'Errico, "Federico II" University, Napoli, Italy; Giancarlo Ottaviano, University of Padova, Padova, Italy; Elena Cantone, "Federico II" University, Napoli, Italy; Chiara Briani, University of Padova, Padova, Italy; Nella A. Greggio, Azienda Ospeddaliera, University of Padova, Padova, Italy; Silvia Rizzati, University of Padova, Padova, Italy; Marco Rossato, University of Padova, Padova, Italy; Eugenio De Carlo, University of Padova, Padova, Italy; Elvira Napoli, Medicanova Diagnostic Center, Battipaglia, Italy; Gianfranco D'Agosto, Medicanova Diagnostic Center, Battipaglia, Italy; Giangennaro Coppola, University of Salerno, Salerno, Italy.

Disclosures: Renzo Manara—*UNRELATED: Payment for Lectures (including service on Speakers Bureaus)*: BioMarin, *Comments*: lecture on mucopolysaccharidosis type 6 (600 Euro).

REFERENCES

1. Seminara SB, Hayes FJ, Crowley WF Jr. **Gonadotropin-releasing hormone deficiency in the human (idiopathic hypogonadotropic hypogonadism and Kallmann's syndrome): pathophysiological and genetic considerations.** *Endocr Rev* 1998;19:521–39
2. Kallmann FJ, Schonfeld WA, Barvera SE. **The genetic aspects of primary eunuchoidism.** *Am J Ment Defic* 1944;48:203–36
3. Schwanzel-Fukuda M, Bick D, Pfaff DW. **Luteinizing hormone-releasing hormone (LHRH)-expressing cells do not migrate normally in an inherited hypogonadal (Kallmann) syndrome.** *Brain Res Mol Brain Res* 1989;6:311–26
4. Okubo K, Sakai F, Lau EL, et al. **Forebrain gonadotropin-releasing hormone neuronal development: insights from transgenic medaka and the relevance to X-linked Kallmann syndrome.** *Endocrinology* 2006;147:1076–84
5. Maestre de San Juan A. **Falta total de los nervios olfactorios con anosmía en un individuo en quien existia una atrofía congénita de los testículos y miembro viril.** *Siglo Medico* 1856;131–211
6. De Morsier G. **Studies in cranio-encephalic dysraphia. I. Agenesia of the olfactory lobe (lateral telencephaloschisis) and of the callous and anterior commissures (median telencephaloschisis); olfactogenital dysplasia** [in French]. *Schweiz Arch Neurol Psychiatr* 1954;74:309–61
7. Quinton R, Duke VM, de Zoysa PA, et al. **The neuroradiology of Kallmann's syndrome: a genotypic and phenotypic analysis.** *J Clin Endocrinol Metab* 1996;81:3010–17
8. Birnbacher R, Wandl-Vergesslich K, Frisch H. **Diagnosis of X-recessive Kallmann syndrome in early infancy: evidence of hypoplastic rhinencephalon.** *Eur J Pediatr* 1994;153:245–47
9. Truwit CL, Barkovich AJ, Grumbach MM, et al. **MR imaging of Kallmann syndrome, a genetic disorder of neuronal migration affecting the olfactory and genital systems.** *AJNR Am J Neuroradiol* 1993;14:827–38
10. Vogl TJ, Stemmler J, Heye B, et al. **Kallman syndrome versus idiopathic hypogonadotropic hypogonadism at MR imaging.** *Radiology* 1994;191:53–57
11. Yousem DM, Turner WJ, Li C, et al. **Kallmann syndrome: MR evaluation of olfactory system.** *AJNR Am J Neuroradiol* 1993;14:839–43
12. Knorr JR, Ragland RL, Brown RS, et al. **Kallmann syndrome: MR findings.** *AJNR Am J Neuroradiol* 1993;14:845–51
13. Koenigkam-Santos M, Santos AC, Versiani BR, et al. **Quantitative magnetic resonance imaging evaluation of the olfactory system in Kallmann syndrome: correlation with a clinical smell test.** *Neuroendocrinology* 2011;94:209–17
14. de m Freitas P, Carvalho S, Ribeiro F, et al. **Neuroradiology of Kallmann's syndrome** [in Portuguese]. *Acta Med Port* 2001;14:123–26
15. Maione L, Benadjaoud S, Eloit C, et al. **Computed tomography of the anterior skull base in Kallmann syndrome reveals specific ethmoid bone abnormalities associated with olfactory bulb defects.** *J Clin Endocrinol Metab* 2013;98:E537–46
16. Ueno H, Yamaguchi H, Katakami H, et al. **A case of Kallmann syndrome associated with Dandy-Walker malformation.** *Exp Clin Endocrinol Diabetes* 2004;112:62–67
17. Koenigkam-Santos M, Santos AC, Borduqui T, et al. **Whole-brain voxel-based morphometry in Kallmann syndrome associated with mirror movements.** *AJNR Am J Neuroradiol* 2008;29:1799–804
18. Costa-Barbosa FA, Balasubramanian R, Keefe KW, et al. **Prioritizing genetic testing in patients with Kallmann syndrome using clinical phenotypes.** *J Clin Endocrinol Metab* 2013;98:E943–53
19. Dale AM, Fischl B, Sereno MI. **Cortical surface-based analysis. I. Segmentation and surface reconstruction.** *Neuroimage* 1999;9:179–94
20. Fischl B, Sereno MI, Dale AM. **Cortical surface-based analysis. II: inflation, flattening, and a surface-based coordinate system.** *Neuroimage* 1999;9:195–207
21. Fischl B, Dale AM. **Measuring the thickness of the human cerebral cortex from magnetic resonance images.** *Proc Natl Acad Sci U S A* 2000;97:11050–55

22. Vagenakis GA, Hyphantis TN, Papageorgiou C, et al. **Kallmann's syndrome and schizophrenia.** *Int J Psychiatry Med* 2004;34:379–90
23. Verhoeven WM, Egger JI, Hovens JE, et al. **Kallmann syndrome and paranoid schizophrenia: a rare combination.** *BMJ Case Rep* 2013; 2013: pii: bcr2012007387
24. Oldfield RC. **The assessment and analysis of handedness: the Edinburgh inventory.** *Neuropsychologia* 1971;9:97–113
25. Ashburner J, Friston KJ. **Voxel-based morphometry: the methods.** *Neuroimage* 2000;11(6 pt 1):805–21
26. Maldjian JA, Laurienti PJ, Kraft RA, et al. **An automated method for neuroanatomic and cytoarchitectonic atlas-based interrogation of FMRI data sets.** *Neuroimage* 2003;19:1233–39
27. Smith SM, Nichols TE. **Threshold-free cluster enhancement: addressing problems of smoothing, threshold dependence and localisation in cluster inference.** *Neuroimage* 2009;44:83–98
28. Krams M, Quinton R, Ashburner J, et al. **Kallmann's syndrome: mirror movements associated with bilateral corticospinal tract hypertrophy.** *Neurology* 1999;52:816–22
29. Schwob JE, Szumowski KE, Leopold DA, et al. **Histopathology of olfactory mucosa in Kallmann's syndrome.** *Ann Otol Rhinol Laryngol* 1993;102:117–22
30. Abolmaali ND, Hietschold V, Vogl TJ, et al. **MR evaluation in patients with isolated anosmia since birth or early childhood.** *AJNR Am J Neuroradiol* 2002;23:157–64
31. Nguyen AD, Pelavin PE, Shenton ME, et al. **Olfactory sulcal depth and olfactory bulb volume in patients with schizophrenia: an MRI study.** *Brain Imaging Behav* 2011;5:252–61
32. Buda M, Fornito A, Bergström ZM, et al. **A specific brain structural basis for individual differences in reality monitoring.** *J Neurosci* 2011;31:14308–13
33. Bechara A, Damasio H, Damasio AR. **Emotion, decision making and the orbitofrontal cortex.** *Cereb Cortex* 2000;10:295–307
34. Sacher J, Neumann J, Okon-Singer H, et al. **Sexual dimorphism in the human brain: evidence from neuroimaging.** *Magn Reson Imaging* 2013;31:366–75
35. Witte AV, Savli M, Holik A, et al. **Regional sex differences in grey matter volume are associated with sex hormones in the young adult human brain.** *Neuroimage* 2010;49:1205–12
36. Im K, Lee JM, Lee J, et al. **Gender difference analysis of cortical thickness in healthy young adults with surface-based methods.** *Neuroimage* 2006;31:31–38
37. Bonomi M, Libri DV, Guizzardi F, et al, for the Idiopathic Central Hypogonadism Study Group of the Italian Societies of Endocrinology and Pediatric Endocrinology and Diabetes. **New understandings of the genetic basis of isolated idiopathic central hypogonadism.** *Asian J Androl* 2012;14:49–56
38. Parr JH. **Midline cerebral defects and Kallmann's syndrome.** *J R Soc Med* 1988;81:355–56
39. Gibby OM, Rayner PHW, West RJ, et al. **Short stature due to median craniocephalic dysraphia with nasal encephalocoele**. In: *Proceedings of the 1st Meeting of the British Endocrine Society*, 1982; Abstract 98:48
40. Dodé C, Hardelin JP. **Kallmann syndrome**. *Eur J Hum Genet* 2009; 17:139–46

NeuroImage 104 (2015) 52–58

Contents lists available at ScienceDirect

NeuroImage

journal homepage: www.elsevier.com/locate/ynimg

Brain anatomical substrates of mirror movements in Kallmann syndrome☆

R. Manara [a,*,1], A. Salvalaggio [b,1], V. Citton [c], V. Palumbo [d], A. D'Errico [e], A. Elefante [e], C. Briani [b], E. Cantone [f,g], G. Ottaviano [h], M.T. Pellecchia [i], N.A. Greggio [j], L. Weis [c], G. D'Agosto [k], M. Rossato [m], E. De Carlo [m], E. Napoli [k], G. Coppola [n], F. Di Salle [a], A. Brunetti [e], G. Bonanni [l], A.A. Sinisi [d], A. Favaro [o]

[a] Neuroradiology, Dept. of Medicine and Surgery, University of Salerno, Italy
[b] Neurology, Dept. of Neurosciences, University of Padova, Italy
[c] IRCCS S. Camillo, Venezia, Italy
[d] Dept. of Clinical and Experimental Medicine and Surgery, Endocrinology and Medical Andrology Section, Second University of Napoli, Italy
[e] Neuroradiology, Dept. of Scienze Biomediche Avanzate, Federico II University, Napoli, Italy
[f] Ent. Section, Dept. of Neurosciences, "Federico II" University, Napoli, Italy
[g] Dept. of Molecular and Cellular Biology and Pathology, "Federico II" University, Napoli, Italy
[h] Otolaryngology Section, Dept. of Neurosciences, University of Padova, Italy
[i] Neurology, Dept. of Medicine and Surgery, University of Salerno, Italy
[j] UOS di Endocrinolgia Pediatrica e Adolescentologia, D.A.I.S. per la Salute della Donna e del Bambino, Azienda Ospedaliera — University of Padova, Italy
[k] Medicanova, Diagnostic Center, Battipaglia (SA), Italy
[l] Unità di Endocrinologia, Dept. of Medicine (DIMED), University of Padova, Italy
[m] Clinica Medica III, Dept. of Medicine (DIMED), University of Padova, Italy
[n] Child and Adolescent Neuropsychiatry, University of Salerno, Italy
[o] Psychiatry, Dept. of Neurosciences, University of Padova, Italy

ARTICLE INFO

Article history:
Accepted 29 September 2014
Available online 6 October 2014

Keywords:
Kallmann syndrome
Mirror movements
MRI
Brain
Motor cortex

ABSTRACT

Among male patients affected by Kallmann syndrome, a genetically determined disease due to defective neural migration leading to hypogonadropic hypogonadism and hypo/anosmia, about 40% present the peculiar phenomenon of mirror movements, i.e. involuntary movements mirroring contralateral voluntary hand movements. Several pathogenic hypotheses have been proposed, but the ultimate neurological mechanisms are still elusive. The aim of the present study was to investigate brain anatomical substrates of mirror movements in Kallmann syndrome by means of a panel of quantitative MRI analyses. Forty-nine male Kallmann syndrome patients underwent brain MRI. The study protocol included 3D-T1-weighted gradient echo, fluid attenuated inversion recovery and diffusion tensor imaging. Voxel-based morphometry, sulcation, curvature and cortical thickness analyses and tract based spatial statistics were performed using SPM8, Freesurfer and FSL. All patients underwent a complete physical and neurological examination including the evaluation of mirror movements (according to the Woods and Teuber criteria).

Kallmann syndrome patients presenting with mirror movements (16/49, 32%) displayed the following brain changes: 1) increased gray matter density in the depth of the left precentral sulcus behind the middle frontal gyrus; 2) decreased cortical thickness in the precentral gyrus bilaterally, in the depth of right precentral sulcus and in the posterior portion of the right superior frontal gyrus; and 3) decreased fractional anisotropy in the left hemisphere involving the temporal lobe and peritrigonal white matter. No differences were shown by cortical curvature and sulcation analyses.

The composite array of brain changes observed in Kallmann syndrome patients with mirror movements likely represents the anatomical–structural underpinnings leading to the peculiar derangement of the complex circuitry committed to unilateral hand voluntary movements.

☆ All authors read and approved the final manuscript.

* Corresponding author at: Neuroradiology, University of Salerno, Via S. Allende 1, Baronissi 89081 (SA), Italy. Fax: +39 0498213673.
E-mail addresses: rmanara@unisa.it (R. Manara), salvalaggio.a@gmail.com (A. Salvalaggio), valentinacitton@gmail.com (V. Citton), dott.vincenzopalumbo@hotmail.it (V. Palumbo), ariannaderrico@gmail.com (A. D'Errico), andrea.elefante@unina.it (A. Elefante), chiara.briani@unipd.it (C. Briani), elenacantone@libero.it (E. Cantone), giancarlo.ottaviano@unipd.it (G. Ottaviano), mpellecchia@unisa.it (M.T. Pellecchia), greggio@pediatria.unipd.it (N.A. Greggio), luca.weis@ospedalesancamillo.net (L. Weis), g.dagosto@istitutodam.it (G. D'Agosto), marco.rossato@unipd.it (M. Rossato), eugedicarlo@tiscali.it (E. De Carlo), elvinapoli@libero.it (E. Napoli), gcoppola@unisa.it (G. Coppola), fdisalle@unisa.it (F. Di Salle), brunetti@unina.it (A. Brunetti), guglielmo.bonanni@unipd.it (G. Bonanni), antonioagostino.sinisi@unina2.it (A.A. Sinisi), angela.favaro@unipd.it (A. Favaro).

[1] These authors equally contributed to the study and should be considered first authors.

http://dx.doi.org/10.1016/j.neuroimage.2014.09.067
1053-8119/

Introduction

Kallmann syndrome (KS) is a rare inherited disorder clinically characterized by the association of hypogonadropic hypogonadism and hypo/anosmia (Kallmann et al., 1944). At conventional brain imaging, KS patients are featured by olfactory bulb hypo/aplasia and typical forebrain and anterior skull base morphological changes (Quinton et al., 1996; Maione et al., 2013). Among male KS patients, about 40% (Quinton et al., 2001) present with a peculiar phenomenon consisting of insuppressible involuntary movements that mirror voluntary contralateral hand movements (mirror movements, MMs) (see online video). Though MMs have been anecdotally reported in FGFR1 or CHD7 gene mutations (Koenigkam-Santos et al., 2010; Costa-Barbosa et al., 2013), MMs are predominantly detected in KS patients with KAL1 or, with minor frequency, PROK2/PROKR2 mutations (Quinton et al., 2001; Costa-Barbosa et al., 2013). KAL1 mutations also result in more severe reproductive phenotype while PROK2 and PROKR2 mutations are associated with variable reproductive impairment, thus highlighting a striking genotypic–phenotypic correlation (Costa-Barbosa et al., 2013).

Although MMs in KS have usually scarce clinical impact, their existence is intriguing as they unveil a genetically determined derangement of the complex circuitry committed to planning and execution of unilateral voluntary hand movement. Mild MMs are considered a physiological phenomenon before the age of 10, likely as a result of an incomplete brain myelination (Beaulé et al., 2012). Non physiological MMs have been reported in congenital (e.g. KS, Klippel–Feil disease, congenital cerebral palsy, corpus callosum agenesis, Joubert syndrome) (Farmer et al., 1990, 2004; Mayston et al., 1997; Kuhtz-Buschbeck et al., 2000; Ferland et al., 2004) and acquired conditions (Parkinson's disease, corticobasal syndrome, essential tremor, focal hand dystonia, Creutzfeld–Jakob disease, Huntington disease, stroke) (Poisson et al., 2013; Espay et al., 2005; Park et al., 2009; Chollet et al., 1991), thus highlighting the heterogeneous spectrum of diseases that might present this phenomenon. So far, the main pathogenic hypotheses of MM are: 1) abnormal persistence of the ipsilateral cortico-spinal tract, 2) abnormal interhemispheric transcallosal inhibition between the two motor cortices and/or 3) functional alteration of motor planning and motor execution (Galléa et al., 2011). All these mechanisms should entail morphological, volumetric or ultrastructural brain changes such as cervical spine neuroschisis, corpus callosum volume reduction due to defective transcallosal inhibitory fibers, or cortical–subcortical gray matter structure abnormalities.

Indeed, despite the early and rich description of MM since the 1930s (Bauman, 1932; Guttmann et al., 1939), the underlying neurological pathogenic mechanisms remain elusive and likely differ according to the associated disease. In KS, several authors suggest an involvement of the cortico-spinal tract (Conrad et al., 1978; Cox et al., 2012) mostly because cortico-spinal tract abnormalities have been observed in other inherited disorders, such as Klippel–Feil disease and Joubert syndrome, or the involvement of transcallosal networks based on the increased detection of midline abnormalities in KS (e.g. corpus callosum agenesis). The evidence for both hypotheses is however scarce (Koenigkam-Santos et al., 2008, 2010; Krams et al., 1999).

In the last two decades, a few MRI studies investigated more closely the anatomical and functional underpinnings of MM in KS, challenging some of the previous hypotheses. By means of conventional MRI, KS patients presenting with MM (KSMM+ patients) did not show hypertrophic or hypoplasic corpus callosum compared to KS patients without MM (KSMM−) (Quinton et al., 1996). Voxel-based morphometry (VBM) showed bilateral cortico-spinal tract hypertrophy in KSMM+ patients (Krams et al., 1999) that was not confirmed in a subsequent study on a larger series (Koenigkam-Santos et al., 2008). In contrast, the same cohort showed magnetization transfer ratio (MTR) and T2 relaxation time changes within the white matter of some portions of the right cortico-spinal tract suggesting possible ultrastructural white matter abnormalities coexisting with the MM phenomenon (Koenigkam-Santos et al., 2010). Functional studies puzzled the pathogenic MM hypotheses showing bilateral cortical activation during unilateral voluntary hand movement, thus advocating a more complex brain involvement (Krams et al., 1997; Leinsinger et al., 1997).

On a large KS cohort, we recently showed with novel MRI techniques (including VBM, cortical thickness, curvature, sulcation and DTI based analyses), that KS patients present with specific structural forebrain cortical changes consistent with a localized profound derangement of cortex development (Manara et al., 2014). In the present study, besides all the abovementioned techniques, we applied MRI-based analyses focused on the motor cortical and subcortical brain structures to investigate whether KSMM+ patients show specific brain anatomical and ultrastructural changes able to shed light on the intriguing phenomenon of MM.

Materials and methods

Subjects

Forty-nine male patients older than 14 years (mean-age 29.9 years; range: 15–55) affected with KS underwent brain MRI (e-Table in supplemental data). All patients met the diagnostic criteria for KS based on clinical findings and smell analysis (hypogonadotropic hypogonadism and hypo/anosmia). Forty-four patients (patients #1–44) also participated in a previous MRI study on brain changes in KS patients compared to healthy controls (Manara et al., 2014).

All KS patients underwent a complete physical and neurological examination including the evaluation of handedness (according to the Edinburgh Handedness Inventory; Oldfield, 1971) and the evaluation of MM according to the Woods and Teuber criteria (Woods and Teuber, 1978). In particular MM were scored as follows: 0 (absent); 1 (barely discernible but repetitive movements); 2 (either slight but sustained movement or stronger but briefer repetitive movement); 3 (strong and sustained repetitive movement); 4 (movement equal to that observed in the intended hand).

Subjects were divided into two groups: KS patients with MM ≥ 2 (KSMM+), KS patients without MM (KSMM−). Patients with MM $= 1$ were excluded from either the KSMM+ and KSMM− subgroups as this MM score might be observed also in normal subjects.

The study was approved by the local Ethics Committee and written informed consent was obtained from patients or their parents.

MRI acquisition

All MRI scans were performed in two centers (University Hospital of Padova and Medicanova Diagnostic Center, Battipaglia, Salerno) equipped with the same 1.5 T MRI scanner (Achieva, Philips Medical Systems, Best, the Netherlands) with a standard quadrature head coil. The MRI study protocol included:

- 3D T1-weighted imaging (repetition time/echo time: 20/3.8 ms; flip angle: 20°; slice thickness: 1 mm, acquired pixel size: 1 × 1 mm; reconstructed pixel size: 0.66 × 0.66 mm; acquisition matrix 212 × 210; reconstructed matrix 320 × 320; acquisition-time: about 7 min);
- Fluid-attenuated inversion-recovery (FLAIR, repetition time/echo time/inversion time: 10,000/140/2800 ms; echo train length: 53; flip angle: 90°; slice thickness: 5 mm; interslice gap: 0.5 mm; acquisition pixel: 0.90 × 1.15 mm; reconstructed pixel: 0.9 × 0.9 mm; acquisition-time: 3 min 20 s);
- Diffusion tensor images (DTI) were acquired with a single-shot echo planar diffusion weighted imaging (repetition time/echo time: 11114/80 ms; acquisition matrix: 112 × 110, echo train length: 59; reconstructed matrix: 128 × 128; acquisition pixel: 2 × 2 mm; reconstructed pixel: 1.75 × 1.75 × 2 mm, SENSE p reduction: 2; slice thickness: 2 mm without gap; number of excitations: 2;

acquisition-time: 12 min 24 s). The axial sections covered the whole brain including the cerebellum. The diffusion sensitizing gradients were applied along 32 non-collinear gradient encoding directions with maximum b = 800 s/mm^2. One additional image without diffusion gradients (b = 0 s/mm^2) was also acquired.

No patients required sedation during MRI acquisition.

Image processing

Data processing of volumetric images and diffusion tensor imaging

The imaging processing methods are presented in extenso in the online supplementary material.

We utilized the optimized VBM protocol (DARTEL) available in the Statistical Parametric Mapping software (SPM8, www.fil.ion.ucl.ac.uk/spm) (Ashburner and Friston, 2000). For statistical analyses, the parametric *t*-test as implemented by SPM8 was applied, using age, total intracranial volume and lateralization as covariates of no interest. Results for gray matter were considered significant for $p < 0.05$ cluster-based FWE-corrected. Statistical analyses were first performed in the whole-brain and then in the left and right motor and premotor cortices as regions of interest (ROI). Masks for motor and premotor cortices to be used for ROI analyses were obtained with the MarsBaR tool for SPM.

All 3DT1 weighted data were processed by Freesurfer (http://surfer.nmr.mgh.harvard.edu/) to derive quantitative estimates of sulcation, curvature and cortical thickness. The sulcation conveys information on how far a particular surface vertex point is from a hypothetical "mid surface" that exists between the sulci and gyri. The curvature conveys information on the curvature (not distance) at a specific vertex point. The higher the value (negative or positive), the sharper the curve. The color conveys the sign, and is just an arbitrary choice. Sulcation, curvature and cortical thickness were estimated for the whole brain (Dale et al., 1999; Fischl et al., 1999; Fischl and Dale, 2000) and in those brain areas in which a significant difference emerged in analyzing gray matter volumes. Group analysis was performed using GLM models, including age as a nuisance variable. Results were considered significant for $p < 0.05$ FDR-corrected.

Using the automated segmentation procedure implemented by the Freesurfer software, we obtained volumes of subcortical nuclei (caudate, putamen, thalamus, pallidum) and corpus callosum (divided into 5 sections). With this method, each voxel in the MRI volume was automatically assigned a neuroanatomical label, based on probabilistic information estimated automatically from a manual training set (Fischl et al., 2002).

All DTI data were preprocessed by means of the Oxford Center for Functional MRI of the Brain (FMRIB)'s Diffusion Toolbox (FDT) within FMRIB's Software Library (FSL; http://www.fmrib.ox.ac.uk/fsl) (Smith et al., 2004). The Trait-Based Spatial Statistics method has been used (for details see supplementary materials). For group comparisons concerning fractional anisotropy (FA) and diffusivity values (mean, radial, and axial diffusivity; MD, RD and L1), data were fed into the voxel-wise statistical analysis which was based on nonparametric permutation testing (5000 permutations) to account for multiple comparison corrections across space (Smith and Nichols, 2009) combined with the threshold-free cluster enhancement procedure (TFCE). Age and sites of MRI scan acquisition were entered into the analysis as covariates.

As some of the theories on MM pathogenesis include changes in the structure of the cortico-spinal tract or corpus callosum, TBSS analysis was also restricted to these structures by applying dedicated masks taken from the JHU white-matter tractography atlas (Mori et al, 2005) as implemented by FSL.

Results

The study group (e-Table 1) consisted of 16 KSMM+ patients (mean-age 33.8 years; age-range 16–48), 29 KSMM− patients (mean-age 28.0 years; age-range 15–55) and four patients with MM = 1. MM = 1 patients were not considered in subsequent MRI analyses.

Seven KS patients were left-handed; three of them were KSMM+, four were KSMM− ($p = 0.69$, Fisher's exact test).

One KSMM− patient presented with midline brain abnormalities and one KSMM− patient showed striking multiple sclerosis-like white matter lesions. These two patients were excluded from 3D-T1 and DTI based analyses to avoid the interference of malformative or acquired factors on the quantitative parenchymal and morphological evaluation.

Five KS patients (two KSMM+, and three KSMM−) were excluded from TBSS analysis because of DTI protocol deviation (longer repetition time).

Therefore, 43 patients (16 KSMM+) underwent analyses of 3D-T1 data (VBM, cortical thickness, sulcation, curvature), and 38 (14 KSMM+) underwent also DTI analysis (TBSS).

Voxel-based morphometry (VBM)

The total amount of gray and white matter did not differ between KSMM+ and KSMM−: gray matter = 0.907 ± 0.143 mL vs 0.951 ± 0.132 mL; white matter = 0.686 ± 0.094 mL vs 0.687 ± 0.099 mL, respectively.

By whole brain analysis no gray or white matter density differences were found between subgroups. By hypothesis-driven gray matter ROI analysis (motor and premotor areas), KSMM+ showed a single cluster of significantly increased gray matter density in the depth of the left precentral sulcus behind the middle frontal gyrus (cluster size 37 voxels, peak MNI coordinates −32, 4, 46) compared to KSMM− (see Fig. 1A). In addition, the analysis of hypothesis-driven white matter ROI (cortico-spinal tract and corpus callosum) did not reveal significant differences.

Automated segmentation analyses of corpus callosum and subcortical nuclei.

Compared to KSMM−, KSMM+ showed a slightly increased volume in the medium-posterior region of the corpus callosum ($p = 0.029$, adjusted for total intracranial volume) but the difference was not significant after correction for multiple comparisons.

In addition, KSMM+ patients disclosed a volume decrease of the globus pallidus, bilaterally (left: $p = 0.043$, adjusted for total intracranial volume, uncorrected for multiple comparison, Bonferroni threshold for significance $p = 0.006$; right: $p = 0.052$, adjusted for total intracranial volume, uncorrected for multiple comparison, Bonferroni threshold for significance $p = 0.006$); no other significant differences were found among subcortical gray matter structures.

Sulcation, curvature and cortical thickness whole brain analyses

Regarding curvature and sulcation analyses, there were no differences between KSMM+ and KSMM−.

By whole brain cortical thickness analysis, a few areas of decreased thickness were detected in the precentral gyrus bilaterally, in the depth of the right precentral sulcus and in the posterior portion of the right superior frontal gyrus (Fig. 1B and Table 1). The cortical thickness did not differ between KS subgroups in the region of gray matter volume increase.

Tract based spatial statistics analysis (TBSS)

The analysis did not reveal any significant difference between KSMM+ and KSMM− regarding MD, RD and L1. In contrast, KSMM+ presented several clusters of decreased FA in the left hemisphere (Fig. 1C and Table 2) involving the temporal lobe and peritrigonal white matter. Notably, TBSS analysis did not reveal any significant difference at the level of the cortico-spinal tract and the corpus callosum.

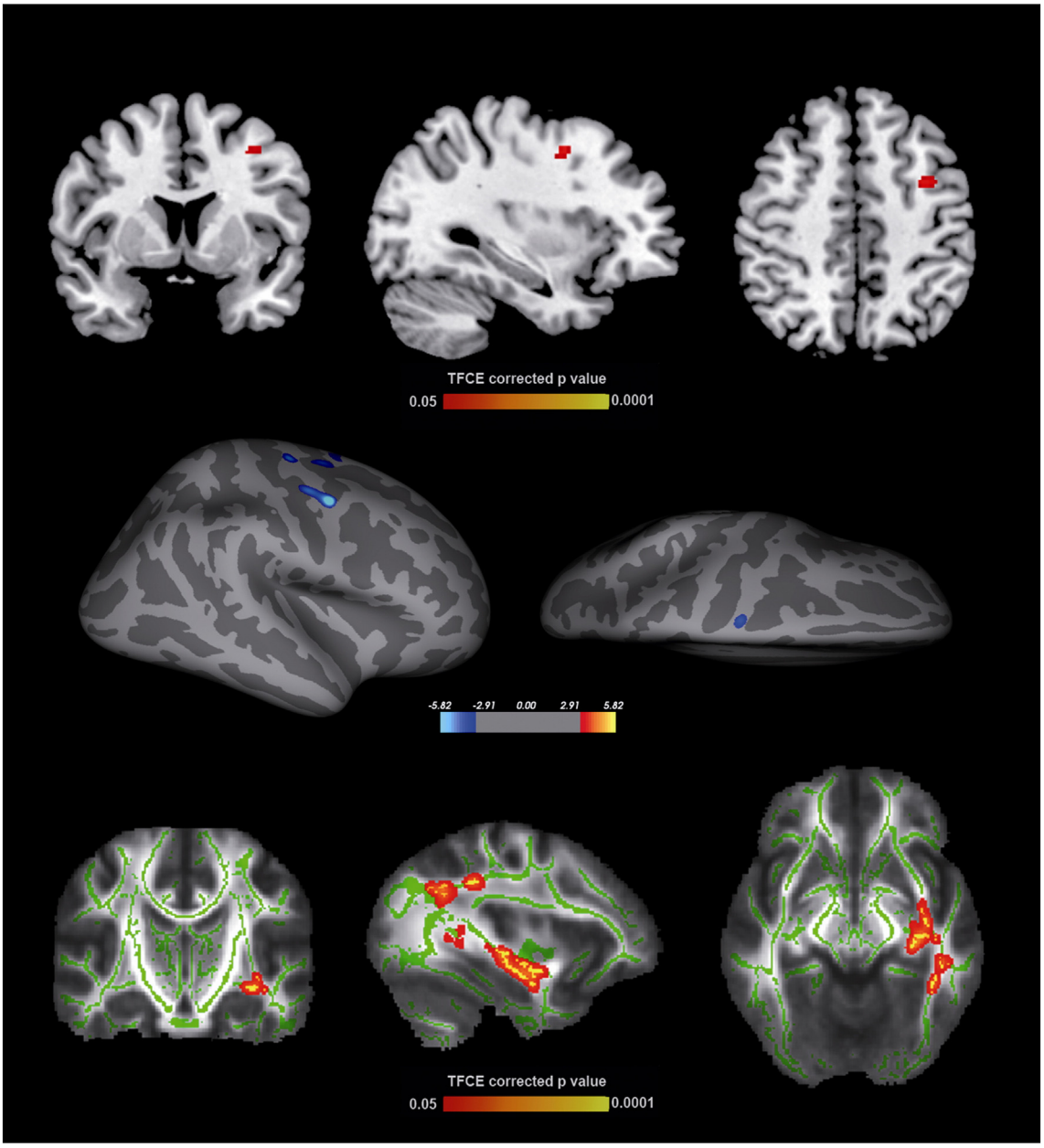

Fig. 1. Anatomical and structural brain changes in Kallmann syndrome patients presenting with mirror movements compared to Kallmann syndrome patients without mirror movements. A) Whole brain voxel-based morphometry analysis showing a cluster of increased gray matter density (red area) in the depth of the left precentral sulcus behind the middle frontal gyrus in Kallmann syndrome patients with mirror movements. B) Whole brain analysis showing areas of decreased cortical thickness located in the precentral and superior frontal cortex (blue areas) of Kallmann syndrome patients with mirror movements. There were no areas of increased cortical thickness. C) Whole brain tract based spatial statistics analysis revealing several clusters of decreased fractional anisotropy in the left hemisphere (yellow-red areas) of Kallmann syndrome patients with mirror movements; the cortico-spinal tracts were not involved. Mean, radial and axial diffusivity did not differ between Kallmann syndrome subgroups.

Table 1
Cortical areas > 30 mm^2 with significant differences between Kallmann syndrome patients with mirror movements and Kallmann syndrome patients without mirror movements by cortical thickness analysis.

Hemisphere	Size (mm^2)		Local maximum, Talairach			FDR threshold	Cerebral region
			X	Y	Z		
Left	36.79	↓	−17.1	−21.5	72.1	4.46487	Precentral
Right	200.06	↓	47.2	−3.2	47.7	3.57396	Precentral
Right	66.10	↓	31.8	−19.8	67.1	3.57396	Precentral
Right	69.38	↓	22.1	−9.6	52.4	3.57396	Precentral
Right	57.97	↓	22.9	0.2	63.0	3.57396	Superiorfrontal

↓ = Kallmann syndrome patients with mirror movements showed decreased cortical thickness.

Table 2
Clusters of significant fractional anisotropy (FA) differences between Kallmann syndrome patients with mirror movements and Kallmann syndrome patients without mirror movements by TBSS analysis.

Hemisphere	Size (voxel)		Local maximum, Talairach		
			X	Y	Z
Left	1096	↓	−33	−16	−11
Left	845	↓	−32	−53	27
Left	152	↓	−25	−59	27
Left	37	↓	−26	−68	24
Left	30	↓	−29	−59	−1

↓ = Kallmann syndrome patients with mirror movements showed decreased FA values.

Discussion

The present study showed that KS patients with MM phenomenon have distinctive cortical and subcortical changes, mostly in regions involved in motor function (globus pallidus and both primary and secondary motor areas) by VBM and cortical thickness analyses. As the neural anatomical and functional underpinnings of MM have not yet been completely understood and several pathogenic hypotheses have been proposed (Galléa et al., 2011), we will discuss which theory best fits with the presence of MM in KS, according to the literature and our findings.

(i) Abnormal persistence of the ipsilateral cortico-spinal tract

In Klippel–Feil disease, the absence of the pyramidal decussation of the cortico-spinal tract has been –shown both by pathologic (Gunderson and Solitare, 1968) and imaging studies (Royal et al., 2002). Nonetheless, the lack of cortico-spinal tract decussation leads to voluntary movements ipsilaterally to the activated cortex and does not justify by itself the presence of contralateral MM unless other still unidentified brain and/or spine anomalies coexist. Pathologic evidence of decussation abnormalities has not been reported in other pathologic conditions presenting with congenital MM. Moreover, abnormal cortico-spinal tract decussation is not supposed to be present in acquired MM disorders (e.g. Parkinson disease, Creutzfeldt–Jakob disease, stroke) (Cox et al., 2012) thus suggesting different pathogenic mechanisms and anatomical basis in different conditions.

Cortico-spinal tract hypertrophy in KSMM+ vs KSMM− was reported by Krams et al (1999) but subsequent VBM analysis on larger KS cohorts did not confirm these findings (Koenigkam-Santos et al., 2008 and the present study). Higher magnetization transfer ratio was observed in the pyramidal decussation of KS vs healthy controls, but no difference was found when comparing KSMM+ vs KSMM−, thus weakening its role in MM pathogenesis (Koenigkam-Santos et al., 2010). The same study revealed unilateral significantly decreased magnetization transfer ratio in the right internal capsule posterior limb and in the right cerebral peduncle together with an increased T2 relaxation time in the right internal capsule posterior limb, despite the presence of bilateral MM. These findings suggested the presence of primary or secondary structural cortico-spinal tract abnormalities consistent with axonal fiber microstructural disarrangement or damage, and the authors solicited DTI analysis to better characterize cortico-spinal tract white matter abnormalities. However, the present study, which included TBSS DTI analysis, did not identify ultrastructural abnormalities at cortico-spinal tract level not supporting cortico-spinal tract abnormalities as the anatomical substrate of MM. Therefore, other mechanisms acting at the cortical or spinal levels should have a role in generating MM in KS.

(ii) Abnormal inter-hemispheric inhibition between the two motor cortices

Unilateral voluntary movements require the suppression of the contralateral primary motor cortex by means of complex transcallosal inhibitory pathways. The absence of these inhibitory mechanisms in KSMM+ might be revealed by morphological and ultrastructural changes of corpus callosum. Studies on corpus callosum in KS have however produced contradictory findings. Corpus callosum underdevelopment has been reported in the seminal study by De Morsier (De Morsier, 1954) and it was claimed to be a typical feature of KS. This finding was not confirmed in subsequent larger series (Quinton et al., 1996) and even in our KS cohort only one patient presented with partial agenesia of corpus callosum. Interestingly, this patient did not present the MM phenomenon. Early studies in the late 90s detected both corpus callosum normal size or hypertrophy in KSMM+ patients (Quinton et al., 1996; Krams et al., 1999) thus leaving unresolved the issue on the role of corpus callosum in the genesis of MM. In a large cohort of KS patients, magnetization transfer ratio was found to be bilaterally decreased in the splenium of the corpus callosum and T2 relaxation time resulted to be increased in the left splenium of the corpus callosum, thus suggesting significant ultrastructural abnormalities in the posterior corpus callosum (Koenigkam-Santos et al., 2010). Moreover, the abovementioned magnetization transfer ratio and T2 relaxation time changes were restricted to the splenium, i.e. the portion of the corpus callosum that connects cortical areas that should not be significantly involved in voluntary movements. In the same cohort, VBM analysis did not reveal any change in corpus callosum white matter density (Koenigkam-Santos et al., 2008). Our study confirmed the latter finding on a larger cohort (no significant VBM white matter differences between KSMM+ and KSMM− patients). In contrast to previous studies, by TBSS analyses we did not find significant ultrastructural changes, as FA, MD, RA and L1 did not differ in corpus callosum both between KS patients and controls (Manara et al., 2014) or between KSMM+ and KSMM− patients.

(iii) Functional alteration of motor planning and motor execution

Unilateral voluntary movement requires a complex multistep activity which encompasses cortical activation and inhibition of both the primary and secondary motor cortices. Functional imaging studies disclosed an abnormal recruitment of both motor cortices in patients with MM while performing unilateral voluntary hand movements (Krams et al., 1997; Leinsinger et al., 1997).

In the present study we applied a panel of structural quantitative MRI analyses aimed at identifying subtle gray matter abnormalities in KSMM+ patients. A previous VBM study did not detect significant gray matter density changes between KSMM+ and KSMM− patients (Koenigkam-Santos et al., 2008). In contrast, VBM analysis in our KS cohort showed a cluster of increased gray matter density in the depth of the precentral sulcus. Interestingly, this area corresponds to the border between the left primary motor cortex and the contiguous premotor cortex, an area that is crucial for motor planning and execution control. The detection of this cluster in the present study might be due to several factors including the increased sample size and the exclusion from analysis of patients with age <14 years and with subtle or uncertain MM, such as those with score = 1. On the other hand, the dominant role of the left hemisphere might explain this asymmetric finding, which could represent both an anatomical substrate of MM or a secondary cortex rearrangement.

According to the other analyses applied in this study and specifically investigating cortical abnormalities, KSMM+ did not show sulcation or curvature abnormalities that could unveil an impaired developmental gyrification of motor areas, as occurs in the forebrain of KS patients (Manara et al., 2014). In contrast, this study revealed areas of decreased cortical thickness strikingly localized in the precentral gyri and in the contiguous secondary motor cortex in the left hemisphere. The areas in the motor cortical strip are located slightly inferior-laterally to the precentral hook that is usually identified with the hand representation of the motor homunculus (Yousry et al., 1997). Interestingly, the sole task-related fMRI image during voluntary finger tapping in a KSMM+ patient present in the literature seems to display bilateral motor cortex activation slightly inferior-lateral to the precentral hook (Leinsinger et al., 1997). If this observation is just a coincidence or reflects a true relocation of cortical motor areas slightly inferior-lateral to the precentral hook (thus locating the thickness changes exactly within the motor hand cortex) will be unraveled only by associating cortical thickness and functional imaging studies in an adequate KSMM+ cohort.

Interestingly, cortical areas presenting with thickness changes are relatively close to the area of increased gray matter density. These findings might appear conflicting (increased gray matter volume without cortical thickness changes and decreased cortical thickness without gray matter volume changes and, above all, areas of decreased cortical thickness close to a region of increased gray matter volume) but they

likely reflect a rather complex cortical reorganization as a possible anatomical substrate of MM. As KS is secondary to an abnormal migration of neurons from the olfactory placode to the hypothalamus (Schwanzel-Fukuda et al., 1989) involving also neurons of the forebrain (Manara et al., 2014), we might hypothesize that an analogous process involves the primary and secondary motor cortices. In particular, a subpopulation of inhibitory neurons might fail to reach the cortex causing a morphological relative decrease of cortical thickness and a functional lack of suppression of the physiological contralateral activation.

Two other extra-cortical findings have to be considered while discussing the abovementioned cortical changes. First, the trend of volume reduction of the globus pallidus observed in KSMM+ patients underlines the concomitant profound involvement of the extrapiramidal motor circuit in the phenomenon of mirror movement. Whether these changes are primitive or secondary to the motor dysfunction is unclear, but they seem to strengthen the link between mirror movements and those conditions where the basal ganglia are primarily involved (Poisson et al., 2013; Espay et al., 2005; Park et al., 2009). Second, though the association is weak and needs to be confirmed, the selective volume increase of the medium-posterior portion of the corpus callosum in KSMM+ patients seems to highlight the role of the cortex-to-cortex connectivity in the pathogenesis of MM.

All these data need validation but, more importantly, warrant further implementation with functional studies investigating the integrity of the motor neural network and the effective connectivity among cortical and subcortical structures.

Structural changes outside the motor circuitry in KSMM + patients

Previous quantitative MRI studies showed ultrastructural and volumetric differences between KSMM+ and KSMM− patients in regions not strictly involved in motor function (e.g. increased T2 relaxation time in the left frontal lobe and left corpus callosum splenium, decreased magnetization transfer ratio in the frontal lobe and corpus callosum splenium bilaterally and increased left parahippocampal white matter density) (Koenigkam-Santos et al., 2008, 2010). These data suggested a brain involvement in KSMM+ patients that spreads beyond the areas of motor function possibly related to the MM phenomenon. By whole brain VBM, we did not confirm white matter density changes in a larger cohort. Nonetheless, TBSS analysis disclosed several large clusters of increased FA in the left hemisphere. The lack of significant changes in MD, L1 and RA in the same regions seems to indicate that these changes are due to increased fiber crossing without concomitant significant myelin or axonal derangement. As the MM phenomenon is genetically linked to KAL1 and, less frequently, to PROK2/PROKR2 mutations (Quinton et al., 2001; Costa-Barbosa et al., 2013), we might infer that the involvement of these specific genes might determine other concomitant brain changes. Indeed, KAL1 mutations seem to be associated with a more severe impairment of a reproductive phenotype, thus a potential influence of early hormonal deficiency on this neurological pathway development might be hypothesized. As the left hemisphere has a key role in language functions and no data are available in the literature on language performance in KSMM+ patients, neuropsychological studies are warranted to investigate specific subtle cognitive alterations among KS subgroups.

Limits of the study

The phenomenon of mirror movement likely involves several aspects of brain anatomy (neurons, axons, cortical structure, white matter bundle anatomy) that are best studied with different neuroimaging techniques (VBM, TBSS, etc.). Each technique is not able by itself to evaluate exhaustively all the possible brain changes. VBM detects gray and white matter density changes, but does not provide any information about white matter ultrastructural or cortical developmental changes, that might coexist and contribute to the mirror movement phenomenon. Similarly, TBSS investigates the integrity of specific white matter bundles but might not detect concomitant hyper-/hypotrophy of the same structures, while cortical thickness changes do not necessarily identify concomitant regional gray matter density abnormalities. All these neuroimaging analyses apply different analytic strategies for multiple comparisons thus providing a non-uniform method for investigating brain structures. Moreover, we did not apply an overall correction for multiple comparisons, as it would have been extremely conservative with the risk of increasing the number of false negatives. In addition, we focused on the presence/absence of mirror movements in this disease, without taking into account the underlying genetics. Hypothetically, different gene mutations might imply different mechanisms leading to mirror movements, even among KS patient subgroups. This study likely represent a first step towards a more precise characterization of the significant anatomical underpinnings underlying the phenomenon of mirror movements in Kallmann syndrome but further studies applying selected analysis and genetically specific KS patient subgroups are needed to validate or enrich our findings.

Conclusions

The results of our multimodality MRI study revealed a composite array of brain changes in KSMM+ that might represent the anatomical substrate of the mirror movement phenomenon in Kallmann syndrome. Regarding the theories present in the literature our data: 1) seem to contrast the hypothesis of cortico-spinal tract abnormalities, 2) do not support the existence of abnormal transcallosal inhibitory pathways, and 3) sustain the presence of a rather complex motor (primary and secondary) cortical and subcortical (globus pallidus) reorganization that warrants focused functional studies to unravel the fascinating phenomenon of mirror movements.

Supplementary data to this article can be found online at http://dx.doi.org/10.1016/j.neuroimage.2014.09.067.

Conflict of interest

All authors report no disclosures.

References

Ashburner, J., Friston, K.J., 2000. Voxel-based morphometry—the methods. NeuroImage 11 (6 Pt. 1), 805–821.
Bauman, G.I., 1932. Klippel–Feil syndrome. JAMA 98, 129–132.
Beaulé, V., Tremblay, S., Théoret, H., 2012. Interhemispheric control of unilateral movement. Neural Plast. 2012, 627816.
Chollet, F., DiPiero, V., Wise, R.J., Brooks, D.J., Dolan, R.J., Frackowiak, R.S., 1991. The functional anatomy of motor recovery after stroke in humans: a study with positron emission tomography. Ann. Neurol. 29 (1), 63–71.
Conrad, B., Kriebel, J., Hetzel, W.D., 1978. Hereditary bimanual synkinesis combined with hypogonadotropic hypogonadism and anosmia in four brothers. J. Neurol. 218, 263–274.
Costa-Barbosa, F.A., Balasubramanian, R., Keefe, K.W., Shaw, N.D., Al-Tassan, N., Plummer, L., et al., 2013. Prioritizing genetic testing in patients with Kallmann syndrome using clinical phenotypes. J. Clin. Endocrinol. Metab. 98 (5), E943–E953.
Cox, B.C., Cincotta, M., Espay, A.J., 2012. Mirror movements in movement disorders: a review. Tremor Other Hyperkinet Mov. 2 (pii: tre-02-59-398-1).
Dale, A.M., Fischl, B., Sereno, M.I., 1999. Cortical surface-based analysis. I. Segmentation and surface reconstruction. NeuroImage 9 (2), 179–194.
De Morsier, G., 1954. Études sur les dysraphies crânio-encephaliques. I. Agénésie des lobes olfactifs (télencéphaloschizis latéral) et des commissures calleuse et antérieure (télencéphaloscizis median). La dysplasie olfacto-génitale. Schweiz. Arch. Neurol. Psychiatr. 74, 309–361.
Espay, A.J., Li, J.Y., Johnston, L., Chen, R., Lang, A.E., 2005. Mirror movements in parkinsonism: evaluation of a new clinical sign. J. Neurol. Neurosurg. Psychiatry 76 (10), 1355–1358.
Farmer, S.F., Ingram, D.A., Stephens, J.A., 1990. Mirror movements studied in a patient with Klippel–Feil syndrome. J. Physiol. 428, 467–484.
Farmer, S.F., Harrison, L.M., Mayston, M.J., Parekh, A., James, L.M., Stephens, J.A., 2004. Abnormal cortex–muscle interactions in subjects with X-linked Kallmann's syndrome and mirror movements. Brain 127 (Pt 2), 385–397.
Ferland, R.J., Eyaid, W., Collura, R.V., Tully, L.D., Hill, R.S., Al-Nouri, D., et al., 2004. Abnormal cerebellar development and axonal decussation due to mutations in AHI1 in Joubert syndrome. Nat. Genet. 36 (9), 1008–1013.
Fischl, B., Dale, A.M., 2000. Measuring the thickness of the human cerebral cortex from magnetic resonance images. Proc. Natl. Acad. Sci. U. S. A. 97 (20), 11050–11055.

Fischl, B., Sereno, M.I., Dale, A.M., 1999. Cortical surface-based analysis. II: inflation, flattening, and a surface-based coordinate system. NeuroImage 9 (2), 195–207.
Fischl, B., Salat, D.H., Busa, E., Albert, M., Dieterich, M., Haselgrove, C., et al., 2002. Whole brain segmentation: automated labeling of neuroanatomical structures in the human brain. Neuron 33, 341–355.
Galléa, C., Popa, T., Billot, S., Méneret, A., Depienne, C., Roze, E., 2011. Congenital mirror movements: a clue to understanding bimanual motor control. J. Neurol. 258 (11), 1911–1919.
Gunderson, C.H., Solitare, G.B., 1968. Mirror movements in patients with the Klippel–Feil syndrome. Neuropathologic observations. Arch. Neurol. 18 (6), 675–679.
Guttmann, E., Maclay, W.S., Stokes, A.B., 1939. Persistent mirror-movements as a heredofamilial disorder. J. Neurol. Psychiatry 2 (1), 13–24.
Kallmann, F.J., Schonfeld, W.A., Barvera, S.E., 1944. The genetic aspects of primary eunuchoidism. Am. J. Ment. Defic. 48, 203–236.
Koenigkam-Santos, M., Santos, A.C., Borduqui, T., Versiani, B.R., Hallak, J.E., Crippa, J.A., et al., 2008. Whole-brain voxel-based morphometry in Kallmann syndrome associated with mirror movements. AJNR Am. J. Neuroradiol. 29 (9), 1799–1804.
Koenigkam-Santos, M., de Castro, M., Versiani, B.R., Diniz, P.R., Santos, A.C., 2010. Kallmann syndrome and mirror movements: white matter quantitative evaluation with magnetic resonance imaging. J. Neurol. Sci. 292 (1–2), 40–44.
Krams, M., Quinton, R., Mayston, M.J., Harrison, L.M., Dolan, R.J., Bouloux, P.M., et al., 1997. Mirror movements in X-linked Kallmann's syndrome. II. A PET study. Brain 120 (Pt 7), 1217–1228.
Krams, M., Quinton, R., Ashburner, J., Friston, K.J., Frackowiak, R.S., Bouloux, P.M., et al., 1999. Kallmann's syndrome: mirror movements associated with bilateral corticospinal tract hypertrophy. Neurology 52 (4), 816–822.
Kuhtz-Buschbeck, J.P., Sundholm, L.K., Eliasson, A.C., Forssberg, H., 2000. Quantitative assessment of mirror movements in children and adolescents with hemiplegic cerebral palsy. Dev. Med. Child Neurol. 42 (11), 728–736.
Leinsinger, G.L., Heiss, D.T., Jassoy, A.G., Pfluger, T., Hahn, K., Danek, A., 1997. Persistent mirror movements: functional MR imaging of the hand motor cortex. Radiology 203 (2), 545–552.
Maione, L., Benadjaoud, S., Eloit, C., Sinisi, A.A., Colao, A., Chanson, P., et al., 2013. Computed tomography of the anterior skull base in Kallmann syndrome reveals specific ethmoid bone abnormalities associated with olfactory bulb defects. J. Clin. Endocrinol. Metab. 98 (3), E537–E546.
Manara, R., Salvalaggio, A., Favaro, A., Palumbo, V., Citton, V., Elefante, A., et al., 2014. Brain changes in Kallmann syndrome. Am. J. Neuroradiol. 30 (PMID:24788131).
Mayston, M.J., Harrison, L.M., Quinton, R., Stephens, J.A., Krams, M., Bouloux, P.M., 1997. Mirror movements in X-linked Kallmann's syndrome. I. A neurophysiological study. Brain 120 (Pt 7), 1199–1216.
Mori, S., Wakana, S., Nagae-Poetscher, L., Zijl, P.V., 2005. MRI Atlas of Human White Matter. Elsevier, Amsterdam, The Netherlands.
Oldfield, R.C., 1971. The assessment and analysis of handedness: the Edinburgh inventory. Neuropsychologia 9 (1), 97–113.
Park, I.S., Song, I.U., Lee, S.B., Lee, K.S., Kim, H.T., Kim, J.S., 2009. Mirror movements and involuntary homolateral limb synkinesis in a patient with probable Creutzfeldt–Jakob disease. Clin. Neurol. Neurosurg. 111 (4), 380–383.
Poisson, A., Ballanger, B., Metereau, E., Redouté, J., Ibarolla, D., Comte, J.C., et al., 2013. A functional magnetic resonance imaging study of pathophysiological changes responsible for mirror movements in Parkinson's disease. PLoS One 8 (6), e66910.
Quinton, R., Duke, V.M., de Zoysa, P.A., Platts, A.D., Valentine, A., Kendall, B., et al., 1996. The neuroradiology of Kallmann's syndrome: a genotypic and phenotypic analysis. J. Clin. Endocrinol. Metab. 81 (8), 3010–3017.
Quinton, R., Duke, V.M., Robertson, A., Kirk, J.M., Matfin, G., de Zoysa, P.A., et al., 2001. Idiopathic gonadotrophin deficiency: genetic questions addressed through phenotypic characterization. Clin. Endocrinol. 55 (2), 163–174.
Royal, S.A., Tubbs, R.S., D'Antonio, M.G., Rauzzino, M.J., Oakes, W.J., 2002. Investigations into the association between cervicomedullary neuroschisis and mirror movements in patients with Klippel–Feil syndrome. Am. J. Neuroradiol. 23 (4), 724–729.
Schwanzel-Fukuda, M., Bick, D., Pfaff, D.W., 1989. Luteinizing hormone-releasing hormone (LHRH)-expressing cells do not migrate normally in an inherited hypogonadal (Kallmann) syndrome. Brain Res. Mol. Brain Res. 6, 311–326.
Smith, S.M., Nichols, T.E., 2009. Threshold-free cluster enhancement: addressing problems of smoothing, threshold dependence and localisation in cluster inference. NeuroImage 44 (1), 83–98.
Smith, S.M., Jenkinson, M., Woolrich, M.W., Beckmann, C.F., Behrens, T.E.J., Johansen-Berg, H., et al., 2004. Advances in functional and structural MR image analysis and implementation as FSL. NeuroImage 23 (S1), 208–219.
Woods, B.T., Teuber, H.L., 1978. Mirror movements after childhood hemiparesis. Neurology 28 (11), 1152–1157.
Yousry, T.A., Schmid, U.D., Alkadhi, H., Schmidt, D., Peraud, A., Buettner, A., et al., 1997. Localization of the motor hand area to a knob on the precentral gyrus. A new landmark. Brain 120, 141–157.